Progress in Oceanography 91 (2011) 410–436

Contents lists available at ScienceDirect

Progress in Oceanography

journal homepage: www.elsevier.com/locate/pocean

Biogenic carbon flows through the planktonic food web of the Amundsen Gulf (Arctic Ocean): A synthesis of field measurements and inverse modeling analyses

Alexandre Forest [a,b,*], Jean-Éric Tremblay [b], Yves Gratton [a], Johannie Martin [b], Jonathan Gagnon [b], Gérald Darnis [b], Makoto Sampei [b], Louis Fortier [b], Mathieu Ardyna [c], Michel Gosselin [c], Hiroshi Hattori [d], Dan Nguyen [e], Roxane Maranger [e], Dolors Vaqué [f], Cèlia Marrasé [f], Carlos Pedrós-Alió [f], Amélie Sallon [c,g], Christine Michel [g], Colleen Kellogg [h], Jody Deming [h], Elizabeth Shadwick [i], Helmuth Thomas [i], Heike Link [c], Philippe Archambault [c], Dieter Piepenburg [j]

[a] Institut National de la Recherche Scientifique – Eau Terre Environnement, Québec, Canada G1K 9A9
[b] Québec-Océan, Département de biologie, Université Laval, Québec, Canada G1V 0A6
[c] Institut des sciences de la mer, Université du Québec à Rimouski, Rimouski, Québec, Canada G5L 3A1
[d] Tokai University, Minamisawa, Minamiku, Sapporo, Hokkaido 005-8601, Japan
[e] Département de sciences biologiques, Université de Montréal, Montréal, Québec, Canada H3C 3J7
[f] Institut de Ciències del Mar (CSIC), E-08003 Barcelona, Spain
[g] Freshwater Institute, Fisheries and Oceans Canada, Winnipeg, Manitoba, Canada R3T 2N6
[h] University of Washington, Seattle, WA 98195-2192, USA
[i] Department of Oceanography, Dalhousie University, Halifax, Nova Scotia, Canada B3H 4J1
[j] Mainz Academy of Sciences, The Humanities and Literature, c/o Institute for Polar Ecology, University of Kiel, 24148 Kiel, Germany

ARTICLE INFO

Article history:
Received 22 December 2010
Received in revised form 24 May 2011
Accepted 25 May 2011
Available online 6 June 2011

ABSTRACT

Major pathways of biogenic carbon (C) flow are resolved for the planktonic food web of the flaw lead polynya system of the Amundsen Gulf (southeast Beaufort Sea, Arctic Ocean) in spring-summer 2008. This period was relevant to study the effect of climate change on Arctic marine ecosystems as it was characterized by unusually low ice cover and warm sea surface temperature. Our synthesis relied on a mass balance estimate of gross primary production (GPP) of 52.5 ± 12.5 g C m^{-2} calculated using the drawdown of nitrate and dissolved inorganic C, and a seasonal *f*-ratio of 0.64. Based on chlorophyll *a* biomass, we estimated that GPP was dominated by phytoplankton (93.6%) over ice algae (6.4%) and by large cells (>5 μm, 67.6%) over small cells (<5 μm, 32.4%). Ancillary *in situ* data on bacterial production, zooplankton biomass and respiration, herbivory, bacterivory, vertical particle fluxes, pools of particulate and dissolved organic carbon (POC, DOC), net community production (NCP), as well as selected variables from the literature were used to evaluate the fate of size-fractionated GPP in the ecosystem. The structure and functioning of the planktonic food web was elucidated through inverse analysis using the mean GPP and the 95% confidence limits of every other field measurement as lower and upper constraints. The model computed a net primary production of 49.2 g C m^{-2}, which was directly channeled toward dominant calanoid copepods (i.e. *Calanus hyperboreus* 20%, *Calanus glacialis* 10%, and *Metridia longa* 10%), other mesozooplankton (12%), microzooplankton (14%), detrital POC (18%), and DOC (16%). Bacteria required 29.9 g C m^{-2}, a demand met entirely by the DOC derived from local biological activities. The ultimate C outflow comprised respiration fluxes (82% of the initial GPP), a small sedimentation (3%), and a modest residual C flow (15%) resulting from NCP, dilution and accumulation. The sinking C flux at the model limit depth (395 m) supplied 60% of the estimated benthic C demand (2.8 g C m^{-2}), suggesting that the benthos relied partly on other C sources within the bottom boundary layer to fuel its activity. In summary, our results illustrate that the ongoing decline in Arctic sea ice promotes the growth of pelagic communities in the Amundsen Gulf, which benefited from a ~80% increase in GPP in spring-summer 2008 when compared to 2004 – a year of average ice conditions and relatively low GPP. However, 53% of the secondary production was generated within the microbial food web, the net ecological efficiency of zooplankton populations was not particularly high (13.4%), and the quantity of biogenic C available for trophic export remained low (6.6 g C m^{-2}). Hence it is unlikely that the increase in lower food web productivity, such as the one observed in our study, could support new harvestable fishery resources in the offshore Beaufort Sea domain.

* Corresponding author at: Québec-Océan and Takuvik Joint Laboratory, Département de biologie, Université Laval, Québec, Canada G1V 0A6. Tel.: + 1 418 656 5917; fax: +1 418 656 2339.
E-mail addresses: alexandre.forest@takuvik.ulaval.ca, alforest@videotron.ca (A. Forest).

0079-6611/$ - see front matter © 2011 Elsevier Ltd. All rights reserved.
doi:10.1016/j.pocean.2011.05.002

1. Introduction

Resolving the structure and function of pelagic food webs is crucial to our comprehension and modeling of ocean productivity and of the impact of environmental changes on the flows of energy, nutrients and organic matter (Barange et al., 2010 and chapters therein). A holistic view of Arctic marine systems is particularly needed since high-latitude northern ecoregions are at the forefront of changes in climatic forcing, hydrology, biodiversity, and biogeochemical–ecological interactions (ACIA, 2005; Carmack and Wassmann, 2006; Wegner et al., 2010; Carmack and McLaughlin, 2011; Wassmann et al., 2011). By the end of this century, Arctic marine ecosystems will likely have shifted to a new steady-state induced by the combined effects of sea surface warming (Perovich et al., 2008; Steele et al., 2008), the declining extent, thickness and age of sea ice (Wang and Overland, 2009; NSIDC, 2011), changes in the timing of seasonal ice growth and melt (Markus et al., 2009), altered storm tracks and increased poleward heat transport (Wu et al., 2010), intensified river discharge and freshwater storage (White et al., 2007; Proshutinsky et al., 2009), permafrost thawing and more intense coastal erosion (Frey and McClelland, 2009; Jones et al., 2009), increased bottom ice-scouring in shallow shelf areas (Conlan and Kvitek, 2005), earlier and enhanced ocean acidification due to increased CO_2 uptake in response to sea ice retreat (Bates and Mathis, 2009; Steinacher et al., 2009) and linked to the low buffer capacity of cold water (Thomas et al., 2007), as well as an expected – but still difficult to evaluate – increased inflow of warm Pacific and Atlantic waters (Shimada et al., 2006; Dmitrenko et al., 2008; Polyakov et al., 2011). Ecological thresholds associated with environmental transitions in the Arctic Ocean may potentially impact a large variety of organisms ranging from plankton to apex predators (e.g. Arrigo et al., 2008; Moore and Huntington, 2008; Li et al., 2009), as well as the circum-Arctic residents that rely on fisheries and/or marine mammal resources for food or economic growth (Hovelsrud et al., 2008). Yet, synoptic investigations on the consequences of rapid environmental changes on Arctic marine ecosystem processes and services still remain only a minor component of the global change literature (Hoegh-Guldberg and Bruno, 2010; Wassmann et al., 2011).

Arctic pelagic food webs are usually characterized by a low diversity within which biomass is typically dominated by a few species (e.g. Fuhrman et al., 2008; Kosobokova and Hirche, 2009; Degerlund and Eilertsen, 2010). This is the consequence of the harsh conditions prevailing in the Arctic Ocean, such as subzero water temperature and a marked seasonality in solar irradiance and food supply, which caused the development of specialized plankton species (e.g. Falk-Petersen et al., 2009; Gradinger et al., 2010; Søreide et al., 2010). Surprisingly, the large gradient in physical conditions and habitats that promotes specialization can also increase diversity and could, for example, explain the greater richness of phytoplankton species in Canadian Arctic waters relative to the two other oceans boarding Canada (Archambault et al., 2010). Despite severe light limitation during winter months, annual primary production (PP) in seasonally ice-free Arctic and Subarctic seas is ultimately determined by the upward supply of inorganic nitrogen to the euphotic zone (Tremblay and Gagnon, 2009). However, few field studies have attempted to quantify the fate and the partitioning of PP-derived organic C flows into key ecosystem components (e.g. Tremblay et al., 2006b; Olli et al., 2007; Rysgaard and Glud, 2007; Sejr et al., 2007). Such an analysis provides values to parameterize the utilization of organic C in numerical models that rely on structural and mechanistic information to propose scenarios on the nature of food web interactions under various physical conditions (e.g. Soetaert and van Oevelen, 2009). Two concerted efforts to review the structure and function of pan-Arctic marine food webs have been presented in special issues of *Progress in Oceanography* edited by Paul Wassmann and published in 2006 and 2011. But the geographical and temporal scopes were not as balanced as initially planned (Wassmann, 2006) or summarizations from intensive investigations (e.g. from the International Polar Year (IPY) 2007–2008) were not available yet (Wassmann, 2011). In particular, studies on the Beaufort Sea ecosystem were at that point restricted to the nearshore environment and its linkages to terrestrial C sources (Dunton et al., 2006). Hence, one of our objectives is to add perspective by documenting the offshore marine-dominated Beaufort Sea domain.

Here, we synthesize information on major planktonic and benthic food web components of the central Amundsen Gulf (area with a bottom depth >250 m, Fig. 1) during the winter-to-summer transition in 2008. Sampling was performed during the Circumpolar Flaw Lead (CFL) system study that involved the overwintering of the CCGS *Amundsen* in the Beaufort Sea during IPY 2007–2008, an achievement representing the first time an icebreaker has overwintered in the Arctic Ocean while remaining mobile (Barber et al., 2010). This study period was of particular relevance for anticipating the effect of global warming on Arctic marine systems as spectacular records in sea ice decline have been measured in 2007–2008 (NSIDC, 2011). In the southeast Beaufort Sea, the sea ice minima of 2007–2008 resulted in a substantial boost in PP due to the synergistic effect of sustained upwelling-favorable winds and open water (Tremblay et al., submitted for publication). A consequence of the increase in PP was the enhanced recruitment and growth of key mesozooplankton species (Forest et al., 2011; Tremblay et al., submitted for publication). In turn, increased biological activities fueled the active community of bacteria that subsists in the region throughout the winter due to allochthonous dissolved matter inputs (Garneau et al., 2008; Nguyen and Maranger, 2010). In summary, the central Amundsen Gulf ecosystem in 2008 was set up for the respiration of most of the PP-derived organic C and a modest fraction of it remained for vertical export or transfer to higher trophic levels. This paper exposes the details of this story and its implications with respect to regional comparison of Arctic marine ecosystems and biogeochemical C fluxes in the context of current environmental changes. Our main objective is to resolve and quantify the pathways of biogenic C flow in the pelagic food web of the central Amundsen Gulf in spring-summer 2008. The synthesis relies on mass balance estimates of new and gross PP, ancillary *in situ* data on phytoplankton dynamics, bacterial production, zooplankton biomass and respiration, herbivory and bacterivory rates, vertical particle fluxes, benthic C demand, pools of particulate and dissolved organic C, and by an inverse modeling analysis used to maximize the field measurements.

1.1. Study area

The Amundsen Gulf is a large channel (~400 km length × ~170 km width) that connects the southeast Beaufort Sea to the Canadian Archipelago (Fig. 1). The seasonal sea ice cover begins to form in October near the coast and by late December is usually consolidated over the region (Galley et al., 2008). In early April, a landfast ice bridge typically forms (~60% of the time over 1980–2007) directly south of Banks Island up to the continent (CIS, 2007). The sea ice retreat has typically begun in early June when winds and/or surface circulation push sea ice away from the Gulf. This generates the opening of the so-called Cape Bathurst polynya complex that can be considered as a recurrent widening of the circumpolar flaw lead system (Barber and Massom, 2007; Barber

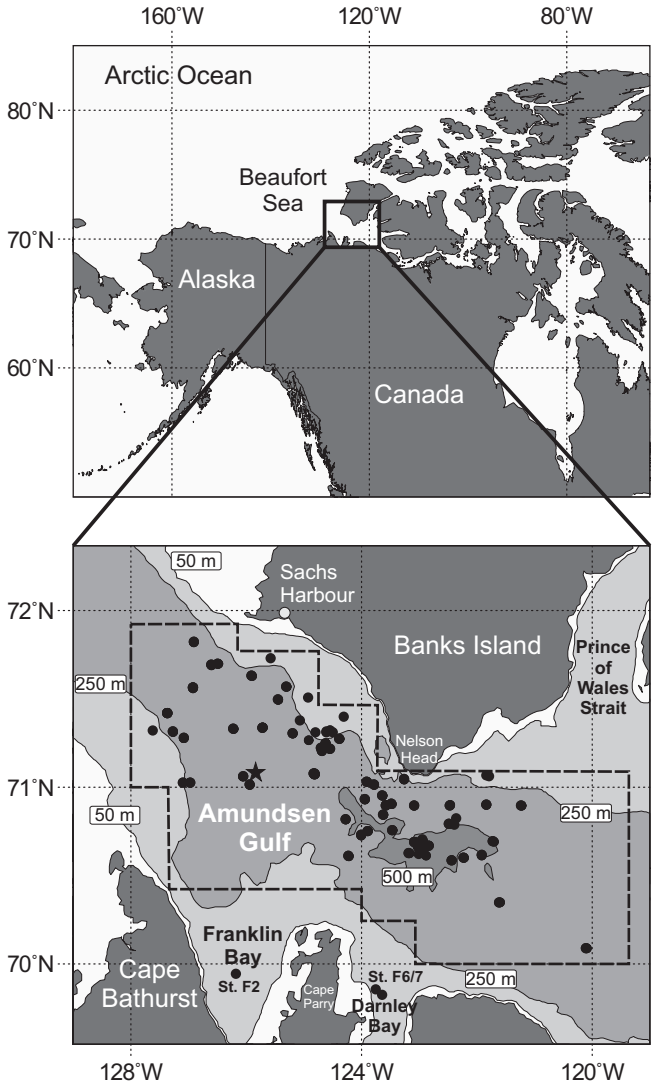

Fig. 1. Location and coarse bathymetry of the Amundsen Gulf region in the southeast Beaufort Sea (Arctic Ocean) with the position of the sampling stations (small black circles) used to estimate the fate of primary production in the pelagic food web from February to August 2008. The star corresponds to a mooring station where a sequential sediment trap has been deployed at 100 m depth. The dashed polygon delineates the area over which daily percent ice cover was extracted from Special Sensor Microwave Imager (SSM/I) archives over the study period. The detail and list of variables measured at all the sampling stations is given in the Appendix A.

et al., 2010). Simplified water masses in the Amundsen Gulf comprise the relatively fresh Polar mixed layer (salinity of ~29–31, 0–50 m depth), the Pacific halocline and its winter-summer components derived from Bering Sea waters (~31–33, ~50–200 m), and deep waters of Atlantic origin (~34.4–34.8, >220 m) (Lanos, 2009; Jackson et al., 2010; Lansard et al., submitted for publication). Ocean circulation in the region is variable and not fully resolved yet (Barber et al., 2010). Surface water is generally influenced by the anti-cyclonic Beaufort Gyre and enters the Amundsen Gulf near Banks Island and exits near Cape Bathurst (Lanos, 2009). Below the surface (>50 m), circulation is usually dominated by the eastward Beaufort Undercurrent that brings waters of both Pacific and Atlantic origin into the Amundsen Gulf (Barber et al., 2010).

A remote sensing analysis of the period 1998–2004 indicated that total annual PP rates varied from 90 to 175 g C m^{-2} in the Cape Bathurst polynya (Arrigo and van Dijken, 2004), but such values are possibly over-estimated by a factor of up to ca. four due to the use of ocean color algorithms not validated locally (Mustapha and Larouche, 2008). Conversely, satellite imagery could also underestimate PP since it does not include contributions from under-ice algae (Gosselin et al., 1997) or from the subsurface chlorophyll maximum (Martin et al., 2010). Accordingly, only *in situ* measurements of PP rates derived from incubation experiments (Brugel et al., 2009) or from nutrient drawdown (Simpson et al., 2007) appear to be suitable to estimate the PP in the Cape Bathurst polynya.

2. Material and methods

2.1. Spatial–temporal focus

The southeast Beaufort Sea is a complex study area with strong bathymetric gradients and important spatial–temporal variability in its physical, biogeochemical and biological properties (e.g. Darnis et al., 2008; Galley et al., 2008; Morata et al., 2008; Simpson et al., 2008; Juul-Pedersen et al., 2010; Sampei et al., 2011). In the present work, it was thus crucial to delineate a specific working framework into which homogeneity could be assumed throughout the study period. Hence, we chose to limit our model of biogenic C flows to the central Amundsen Gulf (defined as the area between 120 and 128°W with a bottom depth >250 m; Fig. 1). This environment is increasingly recognized as being dominated by marine autochthonous processes (Morata et al., 2008; Forest et al., 2010; Magen et al., 2010) in contrast to the adjacent Mackenzie Shelf and slope (O'Brien et al., 2006; Forest et al., 2007; Thomas et al., submitted for publication). Additionally, it has been shown that the zooplankton population assemblage in the central Amundsen Gulf (250–537 m) is statistically similar across the region (Darnis et al., 2008). Our spatial focus corresponds to the region that was sampled most intensively during the IPY–CFL System Study 2007–2008 (Barber et al., 2010) and excludes the episodic burst of productivity observed in adjacent Franklin and Darnley bays (e.g. Mundy et al., 2009; Tremblay et al., submitted for publication), which could not be adequately incorporated into our biogenic C budget.

2.2. Sea ice conditions, water column profiles and light

Time-series of daily sea ice concentrations (% of coverage) were acquired from the 85 GHz channel of the Special Sensor Microwave Imager (SSM/I) located onboard the DMSP satellite. Daily maps were processed by the Ifremer-CERSAT Team (http://cersat.ifremer.fr/fr/data/discovery/by_parameter/) using the daily brightness temperature maps from the National Snow and Ice Data Center (Maslanik and Stroeve, 1999). The Artist Sea Ice algorithm developed at University of Bremen (Germany) was used to process daily sea ice concentration maps at 12.5 km resolution (Kaleschke et al., 2001). For the period of February–August 2008, sea ice concentration data were extracted from the ice maps within a multi-faceted polygon box delineating the whole sampling station area (Fig. 1). In this manner, coastal sectors, such as the Franklin and Darnley bays, were excluded from the ice concentration time-series.

A rosette oceanographic profiler equipped with a conductivity–temperature–depth system (CTD, Seabird SBE-911+) and a fluorometer (Seapoint) was deployed at each sampling station (Fig. 1, Appendix A). The CTD data were calibrated and verified following the Unesco Technical Papers (Crease, 1988). Water samples were taken on board for salinity calibration using a Guildline Autosal salinometer (resolution <0.0002, precision ±0.002). The

fluorescence data from the fluorometer were calibrated against *in situ* chlorophyll *a* (chl *a*) concentrations (obtained as described in Section 2.3.3) using station-specific linear regressions ($r^2 > 0.8$, $p < 0.01$, $n > 5$ for all equations).

Downwelling photosynthetically active radiation (PAR, 400–700 nm) was measured at 10 min intervals with a LI-COR 2 pi sensor (LI-190SA) located on the deck in an area protected from potential shading. Underwater irradiance profiles performed with a PNF-300 2 pi radiometer (Biospherical Instruments) were used to determine the depth of the euphotic zone (Z_{EU}, 0.2% of surface irradiance). This percentage was chosen based on Tremblay et al. (2009) who observed that most of the chl *a* fluorescence in Canadian Arctic waters are observed between 0.2% and 5% of surface irradiance. A Secchi disk (Holmes, 1970) was also deployed prior to water collection to approximate the depth of the euphotic zone and guide sampling. But in the end, Z_{EU} was determined from the vertical attenuation of incident PAR measured with the PNF-300 radiometer.

2.3. Carbon pools, nutrients and primary production

2.3.1. Pools of dissolved and particulate carbon

The concentration of dissolved inorganic carbon (DIC) throughout the water column was measured at 20 stations from February to early August 2008 (Appendix A). Samples were collected from 12-L Niskin-type bottles (OceanTest Equipment) mounted on the rosette system, poisoned with a solution of supersaturated $HgCl_2$ to stop biological activity, and stored at 4 °C in the dark before analysis. All samples were analyzed on board by coulometric titration using a VINDTA 3C (Versatile Instrument for the Determination of Titration Alkalinity, Marianda). Full details of the analytical methods for the measurement of DIC are given in Shadwick et al. (2011). Estimates of net community production (NCP) were obtained from the February–August time-series found in Shadwick et al. (2011). The NCP rates were computed on the basis of monthly changes in DIC using a two-box model comprised of surface (0–50 m depth) and subsurface (>50 m) values within the area delimited by 122–126°W and 70–71.5°N (i.e. central Amundsen Gulf). This inorganic C budget accounted for horizontal and vertical advection, air–sea exchange of CO_2, freshwater input from river runoff and ice melt, and biological processes were used as closing term (Shadwick et al., 2011). In our work, the NCP rates constrained a residual C flux from the planktonic community over the whole water column. We did not attempt to perform a direct comparison between the NCP rates from the DIC budget and our PP values derived from nutrient drawdown because of a discrepancy in the delimitation of the surface layer. The surface NCP rates from Shadwick et al. (2011) were calculated in the 0–50 m water layer, whereas our surface PP values were estimated in the 0–80 m in order to fully include the layer of elevated chl *a* biomass (see Section 2.3.2 and Fig. 2).

Standing stocks of dissolved organic carbon (DOC) and total particulate carbon (TPC) were measured at 10 and 12 stations over the study period, respectively (Appendix A). Samples were collected at depths of 50% and 15% surface irradiance, at the depth of maximum chl *a* fluorescence (Z_{CM}), and at 100 m depth. Water subsample replicates (1000 mL) were filtered through Whatman GF/F glass fiber filters (nominal pore of 0.7 μm, precombusted at 450 °C for 5 h). Filters intended for the determination of TPC were dried at 60 °C for 24 h and analyzed on a Costech ECS 4010 CHN analyzer. In the Amundsen Gulf, particulate organic carbon (POC) is typically equal to 91% TPC (Juul-Pedersen et al., 2008; Forest et al., 2010) so this percentage was used when POC values were preferred to TPC for constraining the biogenic C budget. Filtrate samples for the determination of DOC were collected in 5 mL glass storage vials with Teflon-lined caps previously cleaned following Burdige and Homstead (1994) and acidified to pH ~ 2 with 25% H_3PO_4 (10 μl mL^{-1}). The samples were kept at 4 °C in the dark until analysis with a Shimadzu TOC-5000A according to Whitehead et al. (2000) and Mundy et al. (2010). Certified reference materials for DOC measurements were provided by D.A. Hansell and W. Chen from the Rosenstiel School of Marine and Atmospheric Science, University of Miami, Florida.

2.3.2. Nutrient inventories, nitrate drawdown and new primary production

Nutrient samples were collected at standard depths (Martin et al., 2010) using 12-L Niskin-type bottles mounted on the rosette system at almost all stations (Appendix A). Water samples were filtered through a 5 μm polycarbonate membrane filter housed in an in-line filter holder directly connected to the outlet spigot of the Niskin-type bottle (Tremblay et al., 2008). Samples were dispensed into acid-cleaned (10% HCl), 15 mL polypropylene tubes (Sarstedt Inc.) rinsed thoroughly with the seawater sample. The use of 5 μm filters allowed gravity filtration and minimized sample handling and contamination. Water samples were stored at 4 °C in the dark and analyzed within a few hours of collection. Concentrations of nitrate [NO_3^-], nitrite [NO_2^-], and silicic acid [$Si(OH)_4$] were measured onboard with a Bran and Luebbe Auto-Analyzer 3 (AA3) using standard colorimetric methods (Grasshoff et al., 1999). Ammonium concentration [NH4] was determined manually with the sensitive fluorometric method of Holmes et al. (1999). Details of the analytical procedures can be found in Simpson et al. (2008) and Martin et al. (2010). Linear regressions of [NO_3^-] against [DIC] and [$Si(OH)_4$] were performed with samples taken above 80 m depth (average Z_{EU}) and only for [NO_3^-] > 1.0 μm to avoid potential biases caused by greater analytical error at low nutrient concentrations (Simpson et al., 2008) and by DIC or $Si(OH)_4$ overconsumption once NO_3^- is exhausted (see Tremblay et al., 2008).

Vertical integration of water-column nutrients to compute inventory changes (mmol m^{-2}) over time is usually performed down to the depth of maximum winter concentrations (e.g. Hoppema et al., 2000). Here we chose to integrate nutrients down to 80 m as this depth corresponded roughly to the inferior limit of the nitracline, matched the average Z_{EU} in spring-summer, and contained the layer of elevated chl *a* fluorescence throughout the study period (see Section 3.1, Figs. 2 and 3). Nutrient inventories were computed from polynomial integration algorithms based on vertical profiles of nutrient concentrations at 10–12 sampling depths in the upper 120 m. In the absence of surface samples, we assumed that water was well mixed down to the first sample depth and that nutrient concentrations were uniform within this layer. Nutrient inventories at each station were corrected for freshwater dilution by multiplying every inventory by the ratio of salt content above 80 m at that particular station to the mean salt content above 80 m for all the stations. This method was valid as the mean salt content for all the stations (32.1) corresponded to the approximate salt content <80 m at the end of winter (32.5).

The drawdown of NO_3^- was calculated following a method adapted from Simpson et al. (2007). This procedure was used to obtain a cumulative rate of NO_3^--based new PP for the whole productive season. This method estimates the drawdown using the difference (i.e. consumption) between the maximum and minimum NO_3^- inventories calculated with a four-parameter logistic curve fit derived from the time-series of NO_3^- inventories in the surface layer and corrected for freshwater dilution. The new PP rate was then estimated using the DIC:NO_3^- depletion ratio (mol:mol) recorded *in situ* in the 0–80 m water layer and assuming an

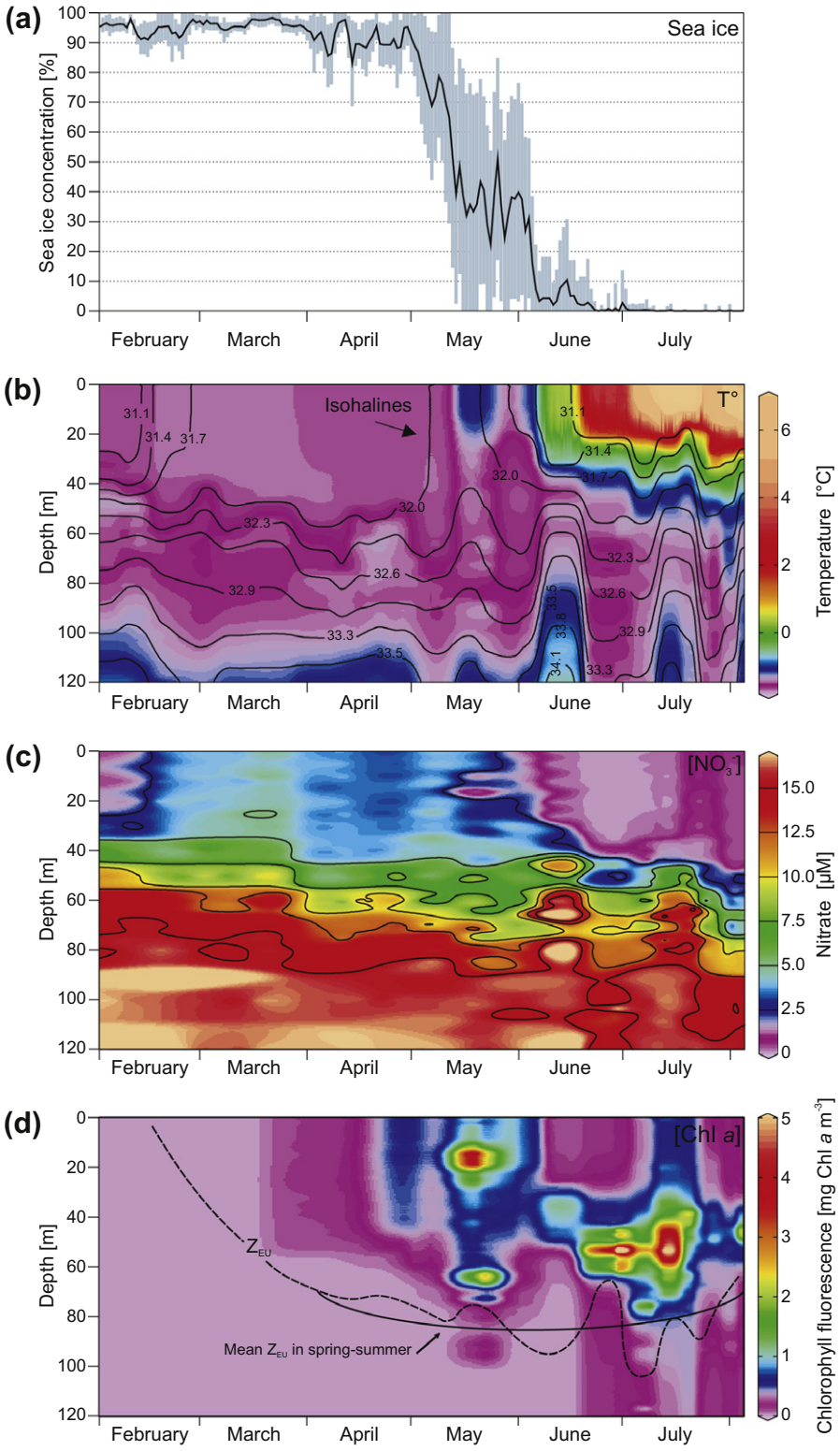

Fig. 2. Time-series from February to early August 2008 of (a) daily sea ice concentration (mean ± standard deviation) over the whole area encompassing the sampling stations in the central Amundsen Gulf (dashed polygon in Fig. 1), (b) water temperature (color) and salinity contours (isolines) in the upper 120 m water layer, (c) nitrate concentration as measured *in situ*, and (d) chlorophyll fluorescence and depth of the euphotic zone (Z_{EU}, 0.2% of surface irradiance). The fluorescence data were calibrated against *in situ* chlorophyll concentrations. The mean Z_{EU} contour in panel (d) delimits the depth of the vertical integration (80 m) of nitrate concentrations used to establish our time series of nitrate inventory and estimate seasonal new production (Table 1).

overall 6.5% NO_3^- uptake by bacteria as a typical percentage for the Amundsen Gulf ecosystem (Simpson et al., 2007). Since this method makes use of the DIC:NO_3^- depletion ratio calculated without taking into account the possible additional DIC uptake in late summer (Tremblay et al., 2008; Shadwick et al., 2011), the new PP estimated here should be considered the most parsimonious value, in accord with our inverse analysis methodology (see Section 2.7).

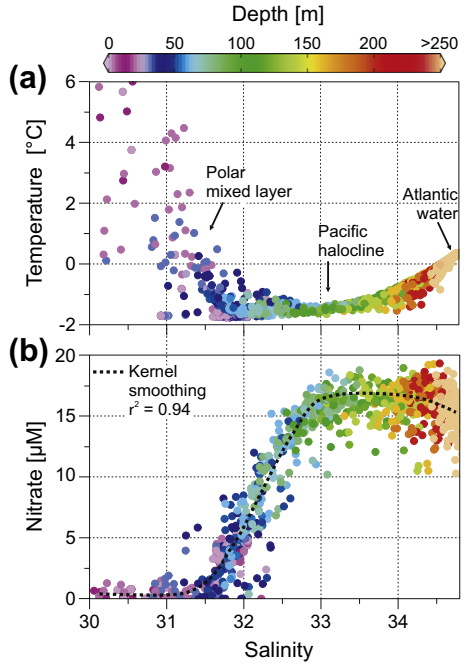

Fig. 3. Diagrams of (a) water temperature vs. salinity, and (b) nitrate vs. salinity, for all the stations used in the present study (see Fig. 1 and Appendix A for details). Only the temperature and salinity data recorded at the depths where nutrients have been sampled are presented. The main water masses that occupy the Amundsen Gulf region are shown in panel (a).

2.3.3. f-Ratios, gross primary production and size-fractions of primary producers

Uptake rates of NO_3^-, NH_4^+ (and urea after mid-July) by phytoplankton (>0.2 µm) were measured at the Z_{CM} at 11 selected stations over the study period (Appendix A) using the classical ^{15}N-labeling method of Dugdale and Goering (1967) as described in Tremblay et al. (2006b). From late April to early July, incubations (>4 h) were performed at various PAR intensities in an interior laboratory of constant cold temperature (~0 °C). The uptake rates at the Z_{CM} for this time-window were then calculated using the absolute PAR values measured at the Z_{CM}. After mid-July, incubations were done on the ship deck under simulated environmental conditions of temperature and light, so that assimilation rates for samples collected at the Z_{CM} were directly obtained. All samples were analyzed for ^{15}N isotopic ratios using a mass spectrometer (Thermo Finnigan Delta V Advantage) in the continuous-flow mode (ConFlo III) equipped with a Costech ECS 4010 CHNSO analyzer. At each station, the contribution of NO_3^- uptake to total N uptake (NO_3^- and NH_4^+, plus urea after mid-July) was used to estimate the *f*-ratio as defined by Dugdale and Goering (1967). An average seasonal *f*-ratio was calculated by giving weights to each of the 11 estimated *f*-ratios in proportion to the amount of chl *a* biomass measured in concomitance (see below). The mean seasonal (total) gross primary production (GPP) was then estimated by dividing the cumulative NO_3^--based new PP converted in C units (see Section 2.3.2) by the average *f*-ratio obtained through chl *a* biomass weighting.

Size-fractions (0.7–5 µm and >5 µm) of ice algae and phytoplankton were obtained from chl *a* biomass measurements (3 February–3 August) and/or simulated *in situ* production assays (28 June–3 August) (Appendix A). Before mid-March, chl *a* biomass in the water column was measured at 3–4 interval depths above 100 m. From mid-March to May, chl *a* biomass of ice algae was obtained from the melting of the bottom 10 cm of replicate ice cores as described in Brown et al. (2011). From mid-March to August, chl *a* biomass and PP in the upper water column were measured at seven optical depths (including Z_{CM}). Duplicate subsamples (500 mL) for the determination of chl *a* were filtered onto Whatman GF/F filters and onto Nuclepore polycarbonate membrane filters (5 µm). Following a 24 h extraction in 90% acetone at 4 °C in the dark without grinding, chl *a* concentrations were measured using a Turner Designs 10-AU fluorometer (Parsons et al., 1984). PP was estimated using the ^{14}C-uptake method (Knap et al., 1996; Gosselin et al., 1997). Two light and one dark 500 mL Nalgene polycarbonate bottles were filled with seawater from each light level and inoculated with 20 µCi of $NaH^{14}CO_3$. The dark bottle contained 0.5 mL of 0.02 M 3-(3,4-dichlorophenyl)-1,1-dimethyl urea in order to calculate the passive ^{14}C incorporation by phytoplankton (Legendre et al., 1983). The bottles containing the ^{14}C were incubated for 24 h under simulated *in situ* conditions in a deck incubator with running surface seawater (Garneau et al., 2007). At the end of incubation, half of each bottle was filtered onto Whatman GF/F filters and onto Nuclepore membrane filters (5 µm). Each filter was placed in a borosilicate scintillation vial, acidified with 200 µl of 0.5 N HCl, and left to evaporate overnight under the fume hood to remove any ^{14}C that had not been incorporated (Lean and Burnison, 1979). After this period, 10 mL of Ecolume (ICN) scintillation solution was added to each vial. The activity of each sample was determined using a Packard Tri-Carb 2900 TR liquid scintillation counter. Chl *a* biomass and PP of small and large cells (0.7–5 µm and >5 µm) were discriminated using results from the two size-fraction filters. Size-fractionated chl *a* biomass was transformed into POC biomass using the POC:chl *a* conversion factor obtained here (see Section 3.2.1). The proportion of small and large cells, as estimated from phytoplankton and ice algal biomass, was applied to the seasonal GPP value to estimate the contribution of the two size-fractions to total PP.

2.4. Dynamics of heterotrophic plankton

2.4.1. Mesozooplankton

Mesozooplankton were sampled at 19 stations (Appendix A) using vertical samplers equipped with flowmeters and Nitex plankton nets of 200 µm mesh size (0.5-m^2 Kiel Hydrobios or 1-m^2 metal frame). The sampling gear was deployed vertically from 10 m off the bottom to the surface. Mesozooplankton samples were condensed and preserved in seawater solution poisoned with borax-buffered 4% formaldehyde for further taxonomic count. Samples for taxonomy were rinsed with freshwater and fractionated on 1000 and 177 µm mesh sieves to separate large and small organisms. The two size fractions were divided with a Folsom-type splitter and known aliquots were resuspended in distilled water. From each sub-sample, approximately 300 animals were counted and identified to species or to the lowest possible taxonomical level. The Arctic species *Calanus glacialis* and the Pacific Subarctic *C. marshallae* that may co-occur in the region (Frost, 1974) were pooled in a single taxon due to lack of certainty in their differentiation (Seuthe et al., 2007; Darnis et al., 2008).

The abundance of dominant calanoid copepods (*Calanus hyperboreus*, *C. glacialis* and *Metridia longa*) was converted into C-units using the specific C-prosome length equations of Forest et al. (2011). Other mesozooplankton taxa were transformed into C-biomass according to Hopcroft et al. (2005) and assuming a 50% C-content. The production of copepods was estimated using their *in situ* C-biomass multiplied by empirical growth rates calculated as a function of chl *a* concentration, surface layer temperature, and the individual C-content of each stage/species (Hirst and Bunker, 2003). The production of other filter- and mucous-feeder

species considered in the present budget (i.e. *Limacina helicina*, *Oikopleura* sp., *Fritillaria* sp., and *Boroecia maxima*) was calculated according to Huntley and Lopez (1992) accounting for zooplankton biomass and mean surface layer temperature.

Herbivory rates by dominant calanoid copepods were estimated using the gut fluorescence technique (Hattori and Saito, 1997) at six stations over the study period (Appendix A). Gut evacuation rates were obtained through shipboard incubation experiments in late July 2008 using natural filtered seawater (Whatman GF/F). Mesozooplankton subsamples from the incubations were collected and quickly frozen at −80 °C at 0, 5, 15, 30, 45, and 60 min to follow changes in gut pigment content over time. Gut evacuation rates obtained in late July were corrected for temperature using a Q_{10} of 2.21 (Dam and Peterson, 1988) and applied to copepod samples for which chl *a* gut content and abundance were measured between late April and early August. The concentration of chl *a* in sorted individual copepods (stages CIII–VI, in triplicate samples whenever possible) was determined with a fluorometer (Turner Design, 10-AU) in a dim-light room after 24 h pigment extraction by DMF (N,N-dimethyl formamide) using the acidification method of Parsons et al. (1984). Herbivory rates in terms of C-units were estimated using the C-to-chl *a* relationship obtained in the present study.

The enzymatic activity of the electron-transfer-system (ETS) of mesozooplankton was determined following Båmstedt (2000) at 16 stations between February and July 2008 (Appendix A). For each ETS assay, live zooplankton samples were fractionated with a 1000 μm mesh sieve and the 200–1000 μm and >1000 μm size-classes were homogenized directly with an INT (*p*-iodonitrotetrazolium violet) reagent. The homogenates were incubated for 1 h at 40 °C after which the reaction was stopped by adding a quench solution (50% formalin and 50% phosphoric acid). A blank of INT reagent received the same treatment. One mL of chloroform/methanol (2:1 by volume) was added and mixed before the sample was centrifuged at 3000 rpm for 4 min. The lower phase was made up to 3 mL by adding methanol before a second centrifugation was carried out. The reaction color was measured at 475 nm against the blank. ETS activity was converted to respiration rate using a relationship between ETS assays and *in vitro* measurements of respiration on zooplankton assemblages. For each *in vitro* experiment, live zooplankton of the two size-classes were gently introduced in sealed glass bottles (473 mL capacity), filled with filtered seawater, and incubated for 24–36 h in darkness at 0 °C. Dissolved oxygen concentration was measured with a Clark-type polarographic electrode. After verification of the state of the incubated animals, the ETS activity of the zooplankton size fractions was determined.

2.4.2. Microzooplankton

Carbon flow through nano- and microzooplankton (hereafter referred as microzooplankton) was based on two distinct datasets in order to cover the full size range of 2–200 μm: (1) copepod nauplii of 50–200 μm; and (2) protozoans of 0.2–5 μm and >5 μm. Copepod nauplii were sampled at 17 stations with an external 10 cm diameter Nitex net of 50 μm mesh size attached to the 1-m^2 square metal frame used to collect mesozooplankton (as described above, see also Appendix A). Samples for taxonomy were preserved in seawater solution poisoned with borax-buffered 4% formaldehyde. After filtration on a 50 μm mesh sieve, the whole sample was rinsed with distilled water and all organisms present were identified to the lowest taxonomical level. The abundance of copepod nauplii was converted into biomass according to the set of equations relating length and width to C-content of crustacean nauplii given in Nozais et al. (2001) and assuming an elliptical shape. The biomasses of nauplii were further transformed into production rates using empirical growth rates (Hirst and Bunker, 2003) calculated the same way as copepodites and adult copepods (see Section 2.4.1).

Samples for the estimation of size-fractionated heterotrophic nanoflagellate (HNF) biomass (0.2–5 μm and >5 μm) in the surface layer were collected at 12 stations during CFL 2007–2008 (Appendix A). Alongside the HNF biomass measurements, bacterial production and bacterivory rates by heterotrophic protozoans were also assessed experimentally. An exhaustive description of the grazing experimental setup and methodological procedures can be found in Vaqué et al. (2008). The conversion factors of Menden-Deuer and Lessard (2000) were used to transform HNF counts into C biomass. The biomass of ciliates was not determined in 2008 and has been assumed to be equal to 9.4 ± 3.3% of the total HNF biomass as previously recorded in the region in spring (Vaqué et al., 2008). A minimal bound of herbivory and detritivory rate by protozoans was estimated considering that bacterial ingestion represented only 14% of the total C demand by large (>5 μm) HNF and ciliates (Vaqué et al., 2008).

2.4.3. Bacterioplankton

From February to July 2008, vertical profiles of bacterial production (BP) (5–7 depths from surface to bottom, including Z_{CM}) were obtained at 14 stations (Appendix A) using the ^{3}H-leucine incorporation method (Smith and Azam, 1992). Water samples (1.2 mL) were dispensed in triplicate into clean 2 mL microcentrifuge tubes pre-loaded with 50 μl ^{3}H-leucine (115.4 Ci $mmol^{-1}$, Amersham) to produce a final leucine concentration of 10 nM (Garneau et al., 2008). Samples were incubated in the dark at *in situ* temperature for ca. 4 h. Incorporated leucine was collected by microcentrifugation after precipitation by trichloroacetic acid (TCA) and centrifugation. Tubes were filled with 1.25 mL liquid scintillation cocktail (ScintiVerse, Fisher Scientific) and radioactivity was measured using a Packard Liquid Scintillation Analyzer Tri-Carb 2900 TR scintillation counter. Rates of leucine incorporation were corrected for radioactivity adsorption using TCA killed controls and converted to BP using two conversion factors: 0.9 and 1.5 kg C per mol of ^{3}H-leucine (Garneau et al., 2008). Vertical profiles of bacterial production were integrated over the water column using standard trapezoidal integration.

Extracellular enzyme activity (EEA) by bacterioplankton (cell-free and cell-attached) was estimated at three stations in June–July (Appendix A) on particles (>1 μm) collected at Z_{CM}, 50, 100 m depth, and close to the seafloor (~12 m above bottom) using large-volume *in situ* pump filtration or water samples collected with the rosette system using an in-line filtration setup (see Kellogg and Deming (2009) for details). EEA represents the sum of the protease and carbohydrase exoenzymatic activities as calculated using two fluorogenic substrate analogs: L-leucine 7-amido-4-methylcoumarin (leucine aminopeptidase) and 4-methylumbelliferyl-β-D-glucoside (β-glucosidase). In our biogenic C budget, EEA rates (μg C m^{-3} d^{-1}) were used (1) to estimate the bacterial degradation of detritus to DOC (Kellogg et al., 2011) and (2) to constrain an exudation/lysis flow from bacteria to DOC combining the exoenzymatic DOC excretion from bacteria and assuming that 7–52% of BP can be potentially lost to DOC through viral lysis (Wilhelm and Suttle, 1999).

2.5. Long- and short-term sampling of vertical particle fluxes

An automated sediment trap was deployed at 104 m depth (Technicap PPS 3/3 cylindrico-conical trap, 0.125 m^2 aperture, 24 cups, aspect ratio of 4.0) on mooring CA08 (star in Fig. 1) to collect settling particles from November 2007 to July 2008 (Appendix A). The long-term sediment trap was prepared following the JGOFS protocols (Knap et al., 1996). Sample cups were filled with filtered seawater (Whatman GF/F) adjusted to final salinity of 36 with

NaCl. Borax-buffered formalin was added as a preservative (5% v/v). After retrieval, sample cups were put aside for 24 h to allow particles to settle. Zooplankton swimmers were removed from the samples with a 1-mm sieve and by handpicking under a stereomicroscope. Sediment trap sub-samples were filtered in two triplicates through pre-weighed GF/F filters (25 mm, pre-combusted at 450 °C for 3 h). A first subset of triplicates was analyzed for total particulate carbon (TPC) whereas the second subset was exposed for 12 h to concentrated HCl fumes to remove the inorganic C fraction. Samples were analyzed on a Perkin Elmer 2400 Series II or on a Leeman Lab CEC 440 to measure POC, TPC and particulate organic nitrogen (PON) fluxes.

Short-term particle interceptor traps (Sallon et al., in press) were deployed at ca. 50, 100, and 150 m depth, at five stations in June and July (Appendix A). Short-term traps were filled with filtered seawater (0.22 μm, Millipore Durapore membrane filters) collected below 200 m depth to create a dense layer within the traps. Short-term traps were deployed for ~24 h, in accordance with the JGOFS protocols (Knap et al., 1996) with recommendations by Gardner (2000). Zooplankton swimmers were removed from the samples as described above. Subsamples from the short-term traps were filtered onto pre-combusted Whatman GF/F filters, dried for 24 h at 60 °C onboard the ship, and latter analyzed for the determination of TPC on a Costech ECS 4010 CHN analyzer. For each short-term trap profile, the scaling exponent (b) in the depth-dependent power law relationship of vertical flux attenuation in the water column (using 100 m as the reference depth) was calculated following Primeau (2006).

2.6. Benthic carbon demand estimates

Benthic C demand and POC content of sediments were assessed at 11 sites in the Amundsen Gulf region from April to August 2008 (Appendix A). At each station, five round sub-cores (10 cm diameter × 20 cm depth) and three surface samples (0–2 cm) were taken from one large sediment core collected with a USNEL box corer (50 cm × 50 cm × 40 cm). Surface samples were frozen at −20 °C for the later determination of POC content using dried and acidified sub-samples processed with an elemental analyzer Costech ECS 4010. The sub-cores were incubated onboard to measure sediment oxygen demand (SOD) in a dark and temperature controlled room (2–4 °C), applying the protocol described in Renaud et al. (2007). The sediment sub-cores were carefully topped with bottom-near water collected at the same station, saturated with oxygen in order to avoid suboxic conditions during the incubation, and let acclimated for 6–8 h. At the beginning of the incubations, these cores were hermetically closed to avoid bubbles. During the incubations, the water phase was kept homogenous by a magnetic stirring device, and speed was regulated to avoid resuspension. Dissolved oxygen concentration in the overlying water phase was measured periodically at 4–8 h with a non-invasive optical probe (Fibox 3 LCD, PreSens, Germany). The incubations were stopped when oxygen saturations had declined by approximately 20% (i.e., after 24–48 h). Gross estimates of benthic C demand were calculated from the linear oxygen decrease in the incubation cores, using a respiration coefficient of 0.8, a net growth efficiency of 0.3 and an assimilation efficiency of 0.8 (Brey, 2001). These values are considered as valid proxies of short-term pelagic–benthic fluxes that vary on the scale of days to weeks (Renaud et al., 2008). The decrease of benthic C demand with water depth was modeled using a log–log function.

2.7. Carbon flow and budget: an inverse modeling approach

Biogenic C flows in the planktonic system of the Amundsen Gulf were resolved using the inverse modeling method of Vézina and Platt (1988) as described in Niquil et al. (2006) and Richardson et al. (2006). The computation and graphical output of the food web solution was produced using a Matlab routine adapted from a code kindly provided by Georges Jackson, leader of the Ecosystem Modeling Group at the Texas A&M University (http://oceanz.tamu.edu/~ecomodel/). This approach was chosen over a conventional mass balance budget in order to estimate the C flows not measured *in situ* (under-determinacy problem). This analysis can be described as a 4-step methodology (*sensu* Grami et al., 2008): (1) the inverse model is defined by selecting the C flows that will be considered as possible within the food web; (2) a set of mass balance linear relations was constructed so that the sum of flows was equal to the sum of the outflows for each model compartment; (3) several biological constraints based on field measurements and vital rates from the literature provided upper and lower bounds so that computed flows were the most realistic; and (4) the unique final solution was the one which had the smallest sum of squared flows, that is the least complex explanation for the system. The resulting model describes the planktonic food web structure and functioning for the entire study period in terms of C fluxes. For more details on the model rationale and components, see Appendix B.

3. Results

3.1. Sea ice conditions, water column profiles and light

The mean daily sea ice concentration in the central Amundsen Gulf in 2008 remained above 90% in February and March, but episodic decreases down to ~81% were recorded throughout April (Fig. 2a). Sea ice concentrations declined sharply from ~90% in early May to ~5% in early June. During this period, the standard deviation of daily sea ice concentrations was particularly high across the sampling area. Except for small-dispersed ice floes, the central Amundsen Gulf was virtually clear of ice by early June. The temperature and salinity (T/S) diagram constructed for the study period (Fig. 3a) was consistent with the layering of water masses previously reported for the area (Lanos, 2009). Winter mixing homogenized the surface layer down to ~50 m depth, but isohalines remained relatively stable over time below this depth (Fig. 2b). Upward displacements of salinity contours were detected at ice break-up, at mid-June and in mid-July (Fig. 2b) in concomitance with lenses of high nitrate concentration detached from deeper water (Fig. 2c). Relatively low salinity water near the surface and increasing stratification were recorded from mid-May to August, consistent with the period of sea ice melting (Fig. 2b). Temperature in the surface layer remained below 0 °C until early June and increased rapidly over the summer (Figs. 2b and 3a). Maximum sea surface temperature (<25 m depth) was reached in July, with values up to ~7–8 °C around 11 and 21 July. Between ~50 m and at least 250 m depth, water temperature remained below 0 °C throughout the study period (Fig. 3a).

In spring-summer 2008, the depth of the euphotic zone (Z_{EU}, 0.2% of surface irradiance) ranged from 54 to 108 m, with an average depth of 80 m (Fig. 2d). Chl *a* fluorescence in the upper water column raised above nil values in late April but increased substantially only when sea ice concentrations crossed the 50% threshold in mid-May (Fig. 2d). The depth of the chlorophyll maximum (Z_{CM}) in May was located at ~15 m, but a second lens of increased fluorescence was detected at ~65 m, probably as a result of rapid aggregation and sinking of phytoplankton during the bloom. Following a period of relatively low fluorescence (<1 mg chl a m^{-3}) in the first half of June, the biomass of chl *a* increased again and developed as a subsurface chlorophyll maximum (SCM, up to ~5 mg chl a m^{-3}) at ca. 55 m depth until late July. The intensity

of the SCM was high and its vertical extent especially large (~40 m) around 8–12 July when the isohalines (Fig. 2b) were pushed upward in the water column.

3.2. Carbon pools, nutrients and primary production

3.2.1. Pools of dissolved and particulate carbon

From February to August 2008, monthly changes in DIC inventory in the surface and subsurface waters in the central Amundsen Gulf yielded a cumulative NCP rate of 19.5 g C m^{-2} (Table 1) when vertically-integrated over the two layers (i.e. 0–50 m and >50 m depth, respectively). However, the standard deviation associated with this average value for the whole water column was high (±13.3 g C m^{-2}), indicating that the error of biological activity into the inorganic C budget that propagated from spatial variability and uncertainties in advection, air–sea exchange and freshwater input was high. The linear regression of DIC vs. NO_3^- for samples collected above 80 m (average Z_{EU}) yielded a depletion C:N ratio of 6.9 (Fig. 4a), close to the Redfield C:N proportion of 6.6.

The time-series of DOC inventory in the 0–100 m interval revealed a strong background of DOC concentration (~80–95 g C m^{-2}) that apparently remained unused (Fig. 5a). Interestingly, no marked increase in DOC concentration was recorded from April to early August, except in mid-July when it rose by ~50% (up to 133 g C m^{-2}) and rapidly declined to background values before the end of the month. Inventory of TPC in the upper water column (Fig. 5b) followed a pattern similar to the chl *a* fluorescence time-series (Fig. 2d). Compared to an average background of ~5 g C m^{-2}, marked increases in TPC up to 24 and 18 g C m^{-2} were recorded in mid-May and early July, respectively. When assuming a 91% POC in TPC, a significant linear regression ($r^2 = 0.70$, $p < 0.0001$, $n = 54$) relating POC to *in situ* chl *a* fluorescence biomass provided a POC:chl *a* conversion factor of 59.3 ± 5.4 (g:g).

3.2.2. Nutrient inventories, nitrate drawdown and new primary production

From February to August 2008, NO_3^- accounted for 97.4% of the total inorganic nitrogen pool ($NO_3^- + NO_2^-$). Since the contribution of NO_2^- was low and that no clear pattern was observed in its vertical and temporal distributions (not shown), we decided not to use [NO_2^-] in our estimate of new PP. In contrast, [NO_3^-] was tightly related ($r^2 = 0.94$) to salinity as visualized through the optimal Kernel-density function (Epanechnikov) presented in Fig. 3b. The time-series of NO_3^- inventories corrected for dilution in the euphotic zone (0–80 m) showed unusually high values in mid-June and mid-July (Fig. 6a) as a result of the episodic upward displacements of isohalines and lenses of high [NO_3^-] (Fig. 2b and c). A meticulous inspection of the nutrient vertical profiles during these events revealed that the sporadic upward excursion of high-NO_3^- contours did not reinject any substantial NO_3^- stocks that would have remained in the stratified upper water column (Fig. 2b and c). Accordingly, we excluded these outliers from the four-parameter logistic regression fit in order to calculate the actual NO_3^- consumption over our study period (Fig. 6a). Since the NO_3^- drawdown continued until near-exhaustion in the euphotic zone (Fig. 2c and d), we assumed that our methodology accounted for the further

Table 1
Calculated values (means ± 95% confidence level) for the period of February to August 2008 in the central Amundsen Gulf: net community production (NCP) in the surface (0–50 m depth) and subsurface (>50 m) water layers, consumed NO_3^- inventory above the depth of the euphotic zone (Z_{EU}, ~80 m) and corrected for freshwater dilution and bacterial uptake, DIC:NO_3^- consumption ratio above Z_{EU}, NO_3^--based new production above Z_{EU}, seasonal *f*-ratio at the depth of the chlorophyll maximum (Z_{CM}, ~15–60 m), total gross primary production (GPP), fraction of large and small cells as estimated from the biomass of ice algae and phytoplankton, and export POC flux at mean Z_{EU}. Please note that these values are derived directly from field measurements and not from the inverse modeling analysis.

Net community production (0–50 m)[a]	47.0 ± 18.8 g C m^{-2}
Net community production (>50 m)[a]	−27.5 ± 5.5 g C m^{-2}
Total NO_3^- consumed (0–80 m)	432.7 ± 103.3 mmol m^{-2}
DIC:NO_3^- consumption ratio (0–80 m)	6.91 ± 0.14 (mol:mol)
New primary production (0–80 m)[b]	33.5 ± 8.0 g C m^{-2}
Seasonal *f*-ratio at Z_{CM} (~15–60 m)	0.64 ± 0.15
Total gross primary production (0–80 m)	52.5 ± 12.5 g C m^{-2}
Fraction of cells >5 μm (0–80 m)[c]	67.6 ± 7.0 %
Fraction of cells <5 μm (0–80 m)[c]	32.4 ± 7.0 %
Export POC flux at mean Z_{EU} (80 m)	5.0 ± 1.5 g C m^{-2}

[a] Adapted from Shadwick et al. (2011).
[b] Corrected for a 6.5% nitrate uptake by bacteria.
[c] Include the contribution of both ice algae and phytoplankton cells.

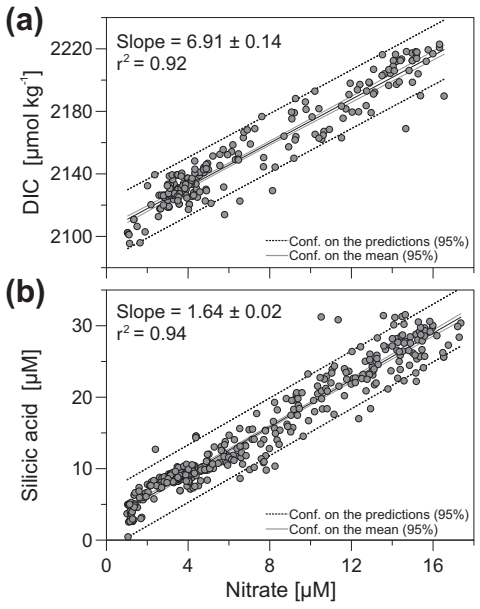

Fig. 4. Linear regressions of (a) dissolved inorganic carbon (DIC) against nitrate, and (b) silicic acid against nitrate, for samples taken at all the stations where these variables were collected (see Appendix A for details). Only the values measured at and above 80 m depth (mean depth of the euphotic zone) and for which nitrate concentrations were greater than 1.0 μm were used.

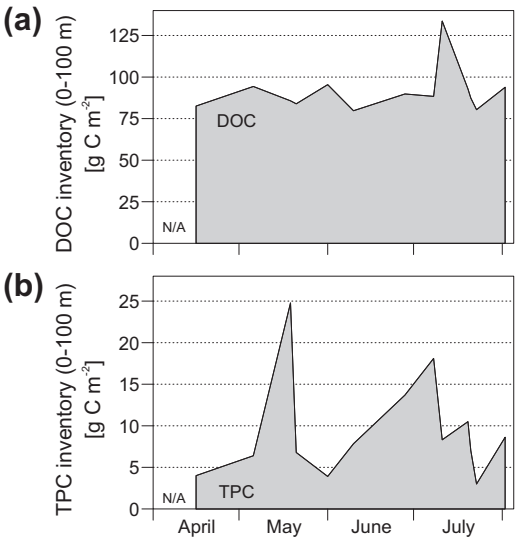

Fig. 5. Inventories of (a) dissolved organic carbon (DOC) and (b) total particulate carbon (TPC) within the 0–100 m water layer from April to early August 2008. N/A: not available.

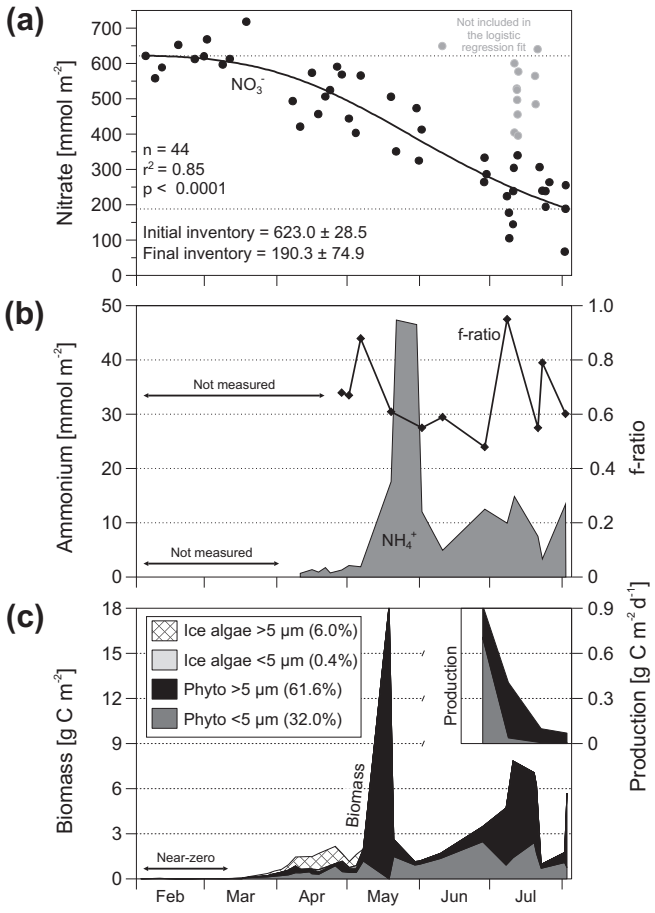

Fig. 6. Time-series of (a) nitrate inventories integrated over the 0–80 m surface layer (euphotic zone, Z_{EU}, 0.2% of surface irradiance) and corrected for freshwater dilution, (b) ammonium inventories corrected and integrated the same way, and *f*-ratios measured at the chlorophyll maximum (Fig. 2d), and (c) size-fractionated ice algal biomass (March–May) in the bottom 10 cm of sea ice as well as phytoplankton biomass (February–August) and total phytoplankton production (June–August) integrated down to Z_{EU}. Primary production rates were estimated at only four stations in the central Amundsen Gulf in 2008 (see Appendix A). The unusually high nitrate inventories recorded during the episodic upward displacement of isohalines in mid-June and mid-July (Fig. 2b and c) were not used within the logistic regression fit of nitrate consumption (see Section 3.2.2 for details).

NO_3^- consumption following these episodic events. The amount of total NO_3^- consumed was thus estimated by calculating the difference between the initial and final inventories from February to early August (432.7 ± 103.3 mmol m^{-2}) and the NO_3^--based new PP (33.5 ± 8.0 g C m^{-2}) was computed accordingly (Table 1). According to the logistic equation, roughly 50% of the NO_3^- consumption in the euphotic zone during our study period was already achieved before late May. The linear regression of *in situ* [$Si(OH)_4$] against [NO_3^-] for samples collected above 80 m (average Z_{EU}) provided a drawdown molar ratio of 1.64 (Fig. 4b).

Inventories of NH_4^+ in the upper water column were close to zero in April, but dramatically increased in the second half of May (up to ~50 mmol m^{-2}, Fig. 6b) following the development of the surface (~15 m) spring bloom (Fig. 2d). Similar to the chl *a* fluorescence pattern, NH_4^+ inventories decreased rapidly in early June and increased again to intermediate values (~15 mmol m^{-2}) in late June and July. High concentrations of NH_4^+ (0.3–1.0 µm) were typically observed just below the chlorophyll maximum (i.e. from approximately ~50–70 m depth over the spring-summer period, not shown), suggesting a link between grazing activities occurring in the lowest portion of the euphotic zone and NH_4^+ recycling.

3.2.3. *f*-Ratios, gross primary production and size-fractions of primary producers

In spring-summer, the discrete *f*-ratios calculated at Z_{CM} oscillated between 0.48 and 0.95 (Fig. 6b), with the maximal ratio being observed when the intense SCM around 10 July was recorded (Fig. 2b). The computation of a seasonal average *f*-ratio (0.64) enabled us to estimate the total GPP (52.5 ± 12.5 g C m^{-2}) for our study period (Table 1). Our seasonal *f*-ratio was relatively high, but it was comparable with a previous study of spring-summer primary productivity in the Beaufort Sea (*f*-ratio of 0.67; Carmack et al., 2004). The overall biomass of primary producers was dominated by phytoplankton (93.6%) over ice algae (6.4%) (Fig. 6c). From March to early May, ice algae contributed as much as phytoplankton to total biomass, confirming their surmised role in the CO_2 drawdown detected over April (Shadwick et al., 2011); but the rapid ice melt in May prevented ice algae to further develop across our study area (i.e. dashed polygon in Fig. 1). The biomass of primary producers integrated over the course of the study was dominated at 67.6% by cells >5 µm (Fig. 6c). The dominance of large cells was particularly strong in ice algal communities in April (94.0%), and at mid-May (100%) and around mid-July (~82%) for phytoplankton. In phytoplankton only, the biomass of large cells represented 65.8% of the total phytoplankton C pool. The few *in situ* PP assays performed revealed that the absolute contribution of small cells was high (~0.9 g C m^{-2} d^{-1}) in late June (Fig. 6c) when the lowest *f*-ratio was measured (Fig. 6b). The average fractions of small and large cells obtained through biomass measurements were used to partition the GPP into two size-fractions (Table 1).

3.3. Dynamics of heterotrophic plankton

3.3.1. Mesozooplankton

The estimated secondary production of copepods varied markedly over the spring-summer period (Fig. 7). In general, pronounced peaks in production (ca. ⩾20 mg C m^{-2} d^{-1}) were measured in May and in July. This bimodal pattern was particularly apparent for *C. hyperboreus*, a species for which 91% of the integrated production was due to stages CV and adult females (Table 2). The production of *C. glacialis* – dominated by stages CIV–V at 82% (Table 2) – remained relatively high in June and peaked around 10 July (38 mg C m^{-2} d^{-1}) when the SCM was the most intense (Fig. 2d). Due to a relatively low biomass in spring-summer, *C. glacialis* females represented a low fraction (4.3%) of the integrated secondary production for this species. After the peak of May and a dramatic decrease around 1 June, the production of *M. longa* was more uniform (~15 mg C m^{-2} d^{-1}) until the end of the sampling period (Fig. 7c). The production of *M. longa* was dominated by stages CV (38.6%) but the contribution of adult females and stages CIV were relatively similar (Table 2). The production of other copepod species was dominated by omnivorous cyclopoids and small calanoids (Table 2).

Rates of herbivory by the three dominant Arctic copepods estimated through gut pigment measurements peaked in May (ca. 150–300 mg C m^{-2} d^{-1}), following the phytoplankton production patterns (Fig. 2a–c). In all species, herbivory in early June decreased to near zero in accordance with the decline in chl *a* fluorescence (Fig. 2d) and phytoplankton biomass (Fig. 6c). Herbivory by *C. hyperboreus* peaked again in mid-July when the SCM was at its maximum intensity. Interestingly, herbivory by *C. glacialis* was relatively low in July (<50 mg C m^{-2} d^{-1}), indicating that this species was most likely relying on non-algal food resources to partly fuel its growth. Herbivory by *M. longa* in late June, July and early August remained at intermediate rates (~75 mg C m^{-2} d^{-1}), suggesting even and continuous ingestion of phytoplankton.

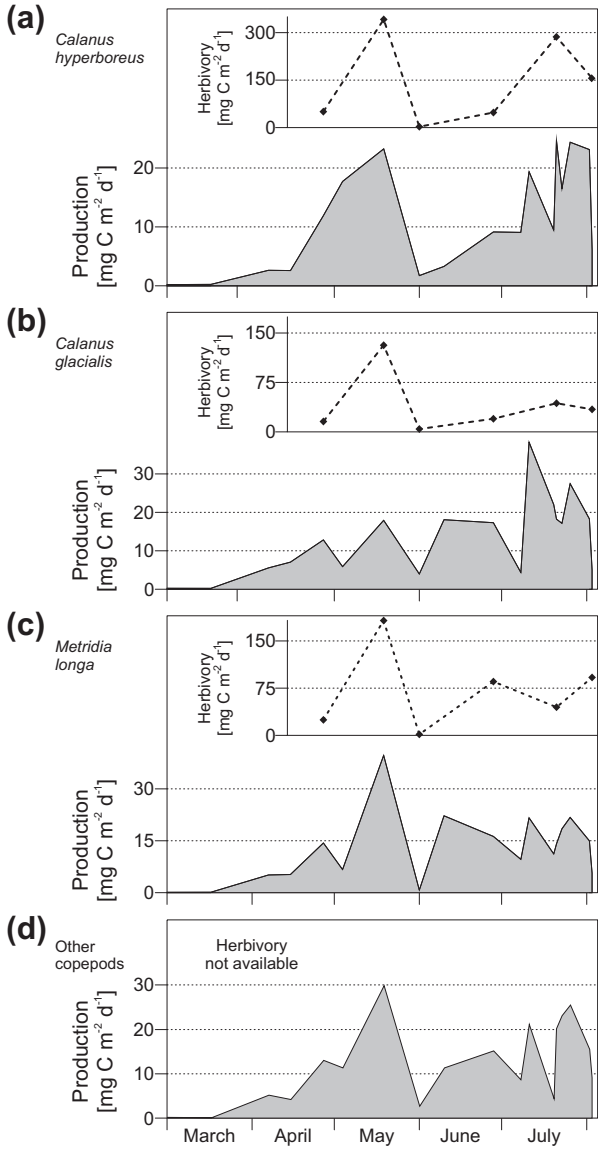

Fig. 7. Production and herbivory rates of: (a) *Calanus hyperboreus*, (b) *C. glacialis*, (c) *Metridia longa*, and (d) all other copepod species sampled in the central Amundsen Gulf from March to early August 2008. The productivity of copepods was estimated using *in situ* biomass measurements multiplied by empirical growth rates. Herbivory rates were calculated only for the three dominant calanoid species using the gut pigment technique combined with egestion rates. The detail of stage composition in dominant calanoids and species fraction in the other copepod group is given in Table 2.

Production of the pteropod, appendicularian and ostracod species considered in the present C budget and integrated for the entire study period (Fig. 8a) represented 5.6% of the total mesozooplankton secondary production as estimated from biomass measurements (~7.2 g C m^{-2}; as calculated upon Table 2 and Fig. 8a). Among these species, the mucous-feeder *L. helicina* clearly dominated the production (59%) over *Oikopleura* sp., *Fritillaria* sp., and *B. maxima* – except for the 19 May when no pteropod was found in the mesozooplankton sample (Fig. 8a).

Respiration rates of the whole mesozooplankton population were relatively high (ca. 25–140 mg C m^{-2} d^{-1}) over the sampling period, even prior to spring (Fig. 8b). Such high rates were related to high total mesozooplankton dry weight (DW) biomass (2.9–18.2 g DW m^{-2}) measured in the central Amundsen Gulf in 2008 (not shown). The average contribution of species >1000 μm to total respiration was 75% with a standard deviation of only ±6%. Respiration rates peaked (~140 mg C m^{-2} d^{-1}) around 10 July when both the SCM and sea surface temperature were at maximum intensity (Fig. 2b and c). The total integrated respiration rate estimated here can be considered as maximum, because the total respiration rates as calculated *in situ* with the ETS technique took into account all mesozooplankton species >200 μm (i.e. possibly including other species not considered in the present C model) and could comprise an unknown respiration fraction of old C reserves.

3.3.2. Microzooplankton

According to the empirical equations based on chl *a* availability, temperature and body length, the production of copepod nauplii was low (1–3 mg C m^{-2} d^{-1}) in winter, but dramatically increased in late April/early May (Fig. 9a), up to ~23 mg C m^{-2} d^{-1} as the spring bloom developed at mid-May (Fig. 2d). After a progressive decline during June, the naupliar production reached a second peak (~16 mg C m^{-2} d^{-1}) in late July. The production of copepod nauplii was overall dominated by cyclopoids (71%) over calanoids (29%).

Bacterivory rates by protozoans in the surface layer during 2007–2008 ranged from 0.14 to 1.43 mg C m^{-3} d^{-1} (Table 3). A significant linear relationship was found between BP measured during the experiments (Table 3) and bacterivory rates: bacterivory = 0.588 * BP + 0.0831, $r^2 = 0.72$, $p < 0.01$, $n = 10$. This relationship was used to estimate an average bacterivory rate cumulated for the study period as a function of BP in the water column (Fig. 9b). The integrated bacterivory estimate (2.2 ± 0.5 g C m^{-2}) was then used to constrain bacterial ingestion by protozoans in the inverse C flow model. The size-fractionated HNF biomass measured alongside the experiments revealed that large HNF cells dominated (84%) the integrated HNF biomass (Table 3). The fraction of HNF > 5 μm combined with an assumed 9.4 ± 3.3% biomass of ciliates enabled us to estimate reliable ranges for herbivory and detritivory by protozoans (13.0 ± 3.2 g C m^{-2}) throughout the study period, considering that bacterial ingestion would meet only 14% of their C demand (Vaqué et al., 2008; see Section 2.4.2).

3.3.3. Bacterioplankton

The two conversion factors linking C to ^{3}H-leucine provided minimum and maximum values of bacterial production (BP)

Table 2
Species-specific copepod production from February to August 2008 (detail from Fig. 7) as estimated from *in situ* biomass and empirical growth rates following Hirst and Bunker (2003).

	Calanus hyperboreus	*Calanus glacialis*	*Metridia longa*	Other copepod species	
CVI-♀	71.2%	4.3%	31.0%	*Oithona* sp.	26.4%
CVI-♂	0.4%	1.0%	7.6%	*Microcalanus* spp.	16.2%
CV	19.4%	53.8%	38.6%	*Triconia* sp.	15.2%
CIV	6.5%	27.7%	21.4%	*Pseudocalanus* spp.	13.6%
CIII	2.4%	12.8%	0.9%	*Paraeuchaeta* sp.	9.2%
CII	0.1%	0.3%	0.4%	*Cyclopina* sp.	3.5%
CI	0.1%	0.2%	0.2%	Others (⩽3% each)	15.9%
Total (g C m^{-2})	1.42 ± 0.35	1.78 ± 0.44	1.92 ± 0.48		1.67 ± 0.42

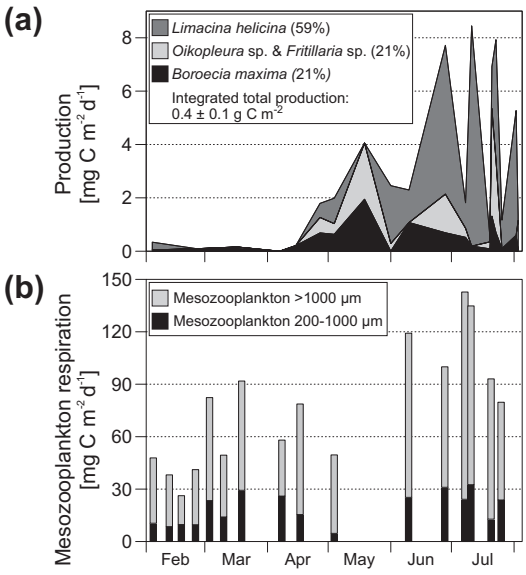

Fig. 8. Time-series of (a) production rates for the pteropod, appendicularian and ostracod species included in the present carbon flow model using *in situ* biomass data, and (b) measured respiration rates of the whole mesozooplankton community integrated over the water column (i.e. all species >200 µm divided into two size-fractions) as calculated using the technique based on the activity of the respiration Electron-transport-system (ETS).

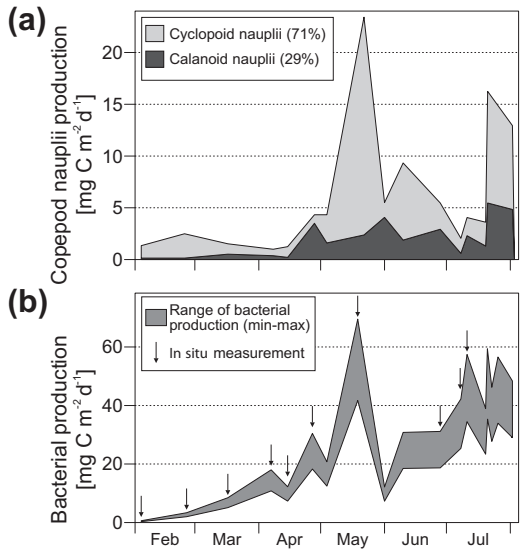

Fig. 9. Time-series of (a) copepod nauplii production as estimated using *in situ* biomass data, and (b) range of the bacterial production as calculated using incubation experiments (downward arrows) and as estimated using a multiple linear regression equation ($r^2 = 0.96$) linking bacterial production to temperature, chlorophyll concentration, and total mesozooplankton production (as an index of food web activities).

throughout the study period (Fig. 9b). Significant multiple linear relationships ($r^2 = 0.96$, $p < 0.0001$, $n = 11$) were found linking the range of experimentally-measured BP to mean temperature and chl *a* fluorescence in the surface layer (0–80 m) (cf. Garneau et al., 2008), as well as total mesozooplankton production (an index of food web activity). These relationships were used to estimate the range of BP during periods when discrete *in situ* measurements of BP were lacking, such as in early May, early June and after mid-July (Fig. 9b). The average BP rate estimated with the mean C-to-^{3}H-leucine conversion factor and integrated for the whole study period cumulated to 3.7 ± 0.9 g C m^{-2}.

Rates of bacterial extracellular enzyme activity (EEA) measured at discrete depths over the water column in June–July ranged from 53.4 to 1590 µg C m^{-3} d^{-1} (Table 4). The linear regression of EEA rates (µg C m^{-3} d^{-1}) against *in situ* POC concentrations (mg C m^{-3}) in the surface layer (⩽100 m) provided a significant relationship (EEA = 5.34 ∗ POC + 29.5, $r^2 = 0.83$, $p < 0.001$, $n = 9$). When used with a mean EEA rate of 84.6 ± 37.1 µg C m^{-3} d^{-1} for waters ⩾100 m (Table 4) this simple model enabled us to calculate a cumulated EEA value of 8.2 ± 2.2 g C m^{-2} for the entire productive season. Enzymatic excretion was further used with viral lysis estimates (7–52% of BP, see Section 2.4.3) to constrain an exudation/lysis C flow of 9.4 ± 3.1 g C m^{-2} from bacteria to DOC in the inverse model.

3.4. Vertical particle fluxes and benthic carbon demand

Organic carbon represented overall 95.6% of TPC fluxes across ~100 m depth at mooring CA08, in accord with the percentage measured by Juul-Pedersen et al. (2008) in the Beaufort Sea. Daily vertical POC fluxes remained very low (<4 mg C m^{-2} d^{-1}) until early May (Fig. 10a) and subsequently showed peaks in mid-May (18 mg C m^{-2} d^{-1}), mid-June (47 mg C m^{-2} d^{-1}) and late July (74 mg C m^{-2} d^{-1}). This sequence is in line with the results of Shadwick et al. (2011), who found two subsurface respiration peaks induced by increases in biologically mediated DIC in May and July 2008. The cumulated POC flux for the whole study period at 100 m depth amounted to 3.0 g C m^{-2}. The mean C:N ratio (mol:mol) of sinking particles was 7.1 ± 0.7, indicating that the material was of autochthonous marine origin.

Absolute daily rates of vertical POC fluxes measured with short-term drifting sediment traps in June–July were always higher (Fig. 10b) than the mean rates measured with the long-term trap in the corresponding interval (Fig. 10a). This discrepancy is essentially due to technical differences in the sampling gear (e.g. aspect ratio, aperture), deployment duration (hours vs. days), and spatial–temporal variability across the Amundsen Gulf region. Hence, average differences in flux measurements coupled with vertical attenuation coefficients (*b*) calculated on the basis of the short-term profiles (Fig. 10b) were applied to the average sinking POC fluxes estimated with the long-term trap in order to provide minimum and maximum bounds to total POC sedimentation at a mean depth of 395 m (i.e. the average bottom of all sampling stations, see Appendix A) within the inverse food web model (1.7 ± 0.5 g C m^{-2}). The same approach of applying a correction and the *b* coefficients to the average flux dataset was used to calculate a seasonal export POC flux of 5.0 ± 1.5 g C m^{-2} at the mean Z_{EU} (80 m depth) for the entire March–August period (Table 1). For convenience within the graphical output of the model, we did not permit direct sedimentation from zooplankton or phytoplankton but only from the detritus pool, which is connected to all pertinent plankton components.

The daily benthic C demand (mean ± standard error) ranged from 19.0 ± 1.5 to 46.4 ± 3.2 mg C m^{-2} d^{-1} across the stations in the central region of the Amundsen Gulf where sediment core sampling was performed from April to early August 2008 (Fig. 11). An increase in the benthic C demand was generally observed over the spring-summer transition when coastal regions were included in the analysis, but overall differences among sites were more pronounced than the seasonal variability (see Link et al. (2011) for details). In the central Amundsen Gulf, benthic C demand decreased significantly with water depth (ANCOVA: $F = 31.26$, $p < 0.01$), but did not differ significantly between ice-covered conditions in spring and open-water conditions in summer for the spatially distributed sites (ANCOVA: $F = 3.43$, $p = 0.07$). The log–log equation derived from the significant correlation ($r^2 = 0.62$, $p < 0.01$, $n = 11$) between daily benthic C demand and water depth

Table 3
Surface values (means ± standard deviation) of bacterial production, bacterivory rates and size-fractionated biomasses of heterotrophic nanoflagellates (HNF) recorded *in situ* at stations where grazing experiments (following Vaqué et al., 2008) were performed in the Amundsen Gulf region in 2007–2008. Stations F2, F6 and F7 were located in Franklin and Darnley bays (Fig. 1). No bacterivory measurements were performed in the central Amundsen Gulf from May to July 2008 (N/A: not available).

Date	Station ID	Latitude (°N)	Longitude (°W)	Bacterial production (mg C m^{-3} d^{-1})	Bacterivory rates (mg C m^{-3} d^{-1})	Biomass HNF <5 μm (mg C m^{-3})	Biomass HNF >5 μm (mg C m^{-3})
19-November-07	405	70°37.3′	123°00.1′	0.18 ± 0.07	0.28 ± 0.19	0.08 ± 0.07	0
2-December-07	D4	71°43.9′	125°33.8′	0.32 ± 0.25	0.14 ± 0.10	0.5 ± 0.25	3.54 ± 2.15
7-December-07	D5	71°18.8′	124°47.3′	0.95 ± 0.56	0.60 ± 0.44	0.6 ± 0.27	1.17 ± 0.45
29-December-07	D12	71°22.8′	125°04.1′	0.03 ± 0.19	0.18 ± 0.13	0.30 ± 0.23	1.14 ± 0.52
15-January-08	D17	71°30.6′	124°55.3′	0.25 ± 0.22	0.21 ± 0.13	0.46 ± 0.29	5.75 ± 2.19
18-February-08	D22	71°18.7′	124°29.8′	0.63 ± 0.33	0.19 ± 0.16	0.54 ± 0.24	2.89 ± 1.11
2-March-08	D27	70°47.5′	122°23.0′	0.31 ± 0.15	0.68 ± 0.34	0.60 ± 0.29	3.42 ± 1.51
27-March-08	D33	71°03.8′	121°47.2′	0.68 ± 0.32	0.17 ± 0.15	0.19 ± 0.02	3.61 ± 1.94
12-April-08	D38	71°14.7′	124°36.7′	1.17 ± 0.29	N/A	1.02 ± 0.18	6.07 ± 3.26
26-May-08	F2	69°56.8′	126°10.3′	N/A	N/A	0.52 ± 0.29	0.05 ± 0.02
2-June-08	F6	69°51.6′	123°45.1′	0.49 ± 0.30	0.41 ± 0.28	0.63 ± 0.31	0
9-June-08	F7	69°49.6′	123°37.9′	2.04 ± 0.42	1.43 ± 0.45	1.03 ± 0.53	0

Table 4
Extracellular enzyme activity (EEA) by bacterioplankton measured on particles (>1 μm) at Z_{CM} (depth of the chl *a* maximum), 50 m, 100 m, and close to the seafloor (~12 m above bottom) using water samples collected with a large-volume *in situ* pump or with the rosette system. The concentration of particulate organic carbon (POC) measured at the same depths as EEA is also given when available. N/A: not available.

Date	Sampling depth	EEA (μg C m^{-3} d^{-1})	EEA sampling gear	POC (mg C m^{-3})
10-June	Z_{CM}	764.1	Rosette	87.0
	50 m	234.0	Pump	40.8
	100 m	53.4	Pump	39.0
	Bottom	63.8	Rosette	N/A
28-June	Z_{CM}	1341.5	Rosette	205.1
	50 m	592.2	Pump	151.1
	100 m	57.1	Pump	27.8
	Bottom	115.8	Rosette	N/A
8-July	Z_{CM}	887.6	Pump	88.2
	50 m	1586.1	Pump	318.4
	100 m	133.2	Pump	51.1
	Bottom	N/A	N/A	N/A

enabled us to calculate a cumulated C demand of 2.8 g C m^{-2} at the boundary depth (395 m) of the C flow model for the entire spring-summer period (i.e. 124 days from 1 April to 3 August). The mean POC content in surface sediments was low (1.3 ± 0.5%), consistent with the low total POC sedimentation allowed within the inverse analysis (Table 5).

3.5. Carbon flow model

The biological variables used as lower and upper bounds for constraining the inverse food web model and obtained both from *in situ* field measurements and from the literature are detailed in Table 5. The structure and rationale of the model are presented in the Appendix B. The food web solution was based on the mean GPP of 52.5 g C m^{-2} that was divided into the production of small and large cells (32.4% and 67.6%, respectively) and assuming a contribution by both ice algae (~6%) and phytoplankton (~94%) (Fig. 6c). The GPP was further fractionated into the heterotrophic community (six components), pools of detritus and DOC, and a residual C flux (Fig. 12, Table 6). The model computed a net PP of 49.2 g C m^{-2}, which yields a ratio of export (*e*-ratio) at Z_{EU} (80 m depth) of only ≈10% when using the POC export flux estimated in 3.4 and shown in Table 1. The direct ingestion of the net PP by micro- and mesozooplankton yielded an exploitation efficiency of 66% (i.e. total ingestion of phototrophs by zooplankton divided by the amount of net PP), but the high turnover of biogenic C in the planktonic food web resulted into the retention of nearly 97% of the initial GPP in the water column (Fig. 12). Accordingly, the cumulated respiration fluxes dominated (82%) the ultimate C outflow, whereas the residual C flux and the total POC sedimentation flow represented 15% and 3% of the initial GPP, respectively. The vertical POC output from the inverse model (1.7 g C m^{-2}) was 1.1 g C lower than the mean benthic C demand (2.8 g C m^{-2}) estimated for the April–August period at the boundary depth of 395 m (see Section 3.4). Within the total respiration flux, bacteria were responsible for 45% of the outflow, mesozooplankton for 29%, microzooplankton for 18%, and phytoplankton for only 8%. Based on the C flows from the inverse analysis (Table 6), we calculated the main physiological parameters (see Appendix B for definitions) of the heterotrophic components (Table 7).

4. Discussion

4.1. Environmental setting and the control of primary production by climatic and oceanic forcings in the central Amundsen Gulf in spring-summer 2008

In September 2007, a dramatic record low in sea ice extent was reported over the Amerasian Arctic Ocean (NSIDC, 2011). In the southeast Beaufort Sea, the phase of seasonal ice expansion in the fall of 2007 was characterized by anomalously strong easterly winds that set the stage for unprecedented lead formation and ice mobility over the following winter (Barber et al., 2010). Solar heating due to reduced ice conditions in summer 2007 contributed additional heat to the ocean, which hindered ice growth during fall-winter (Perovich et al., 2008). As a result, the landfast ice bridge that typically forms in the Amundsen Gulf over March–April did not consolidate in spring 2008 and a rapid ice decline occurred in early May, roughly 1 month earlier than usual (Galley et al., 2008). It is thus likely that the combination of strong winds and open leads during winter 2007–2008 produced more convection and vertical mixing between the surface layer and the nutrient-rich waters of Pacific origin (Simpson et al., 2008; see also Fig. 2b and c). According to the pattern of isohalines (Fig. 2b), winter mixing in 2008 homogenized the surface layer down to at least 50 m depth in the central Amundsen Gulf. Such a stratum was ~45% deeper than what has been measured (~35 m depth) in the adjacent Franklin Bay during the Canadian Arctic Shelf Exchange Study (CASES) in 2003–2004 (Gratton, unpublished data) – a year of moderate winds, near-average ice concentrations and more stable ice cover (Galley et al., 2008; Forest et al., 2010; Tremblay et al., submitted for publication). In fact, the mixed-layer depth in late winter 2008 appeared to have reached at times a depth of ~70 m, roughly twice deeper than what has been measured during

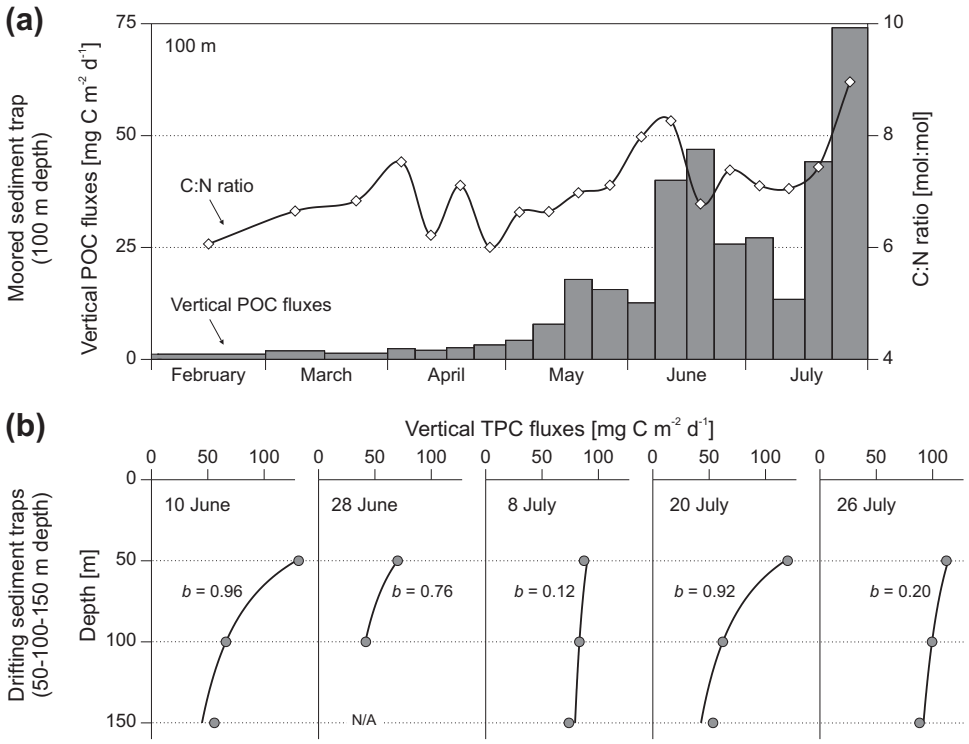

Fig. 10. Time-series of (a) vertical particulate organic carbon (POC) fluxes and molar C:N ratios (molar) measured with the sequential sediment trap deployed at ~100 m depth on mooring CA08 (star in Fig. 1), and (b) vertical fluxes of total particulate carbon (TPC) measured at ca. 50, 100 and 150 m depth with drifting short-term (<24 h) sediment traps. The vertical attenuation coefficients (b) of vertical TPC fluxes are given in panel (b). The locations of short-term deployments are given in the Appendix A. N/A: not available.

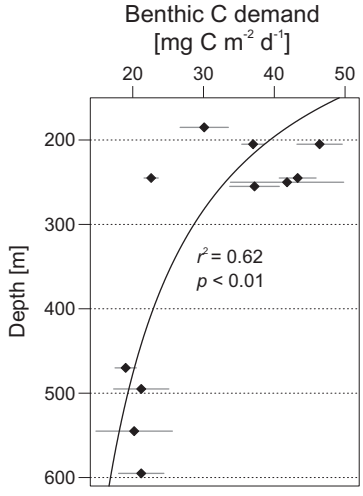

Station	Date	Latitude (°N)	Longitude (°W)	Depth (m)	Number of incubations
D37	10-Apr	71° 18.7'	124° 36.2'	245	5
D39	14-Apr	70° 49.5'	122° 21.2'	470	5
1020A	6-May	71° 01.7'	127° 05.3'	255	5
405B	19-May	70° 39.7'	122° 53.2'	495	4
405B	10-Jun	70° 40.0'	123° 00.6'	545	5
1200	27-Jun	71° 31.9'	124° 17.8'	205	5
D34	13-Jul	71° 04.2'	121° 49.4'	185	5
405	21-Jul	70° 42.4'	122° 56.3'	595	5
408	25-Jul	71° 19.4'	127° 36.3'	205	5
1020A	27-Jul	71° 01.7'	127° 05.3'	245	5
2011	2-Aug	71° 19.0'	124° 35.7'	250	5

Equation: $\text{Log(C demand)} = \frac{\text{Log(Depth)} - 3.955}{-1.002}$

Fig. 11. Exponential decrease of the benthic carbon demand with water depth in the central Amundsen Gulf. The log–log equation was used to estimate a cumulated carbon demand at the boundary depth (395 m) of the carbon flow model over the course of a 124-day productive period (April–August 2008). The exact dates and positions of sampling stations used to produce the plot are given at the right, since they did not entirely correspond to the stations listed in the Appendix A. The horizontal gray bars depict the standard error associated with each mean benthic carbon demand rate. See also Link et al. (2011) for more details and an in-depth analysis of the benthic carbon cycling during CFL 2008.

2004 (Nahavandian Isfahani, INRS-ETE, personal communication). Interestingly, the mean NO_3^--based new PP calculated in our study (33.5 g C m^{-2}) was nearly twice higher than the one estimated using a similar methodology and over the same seasonal window during CASES 2004 (16.6–17.9 g C m^{-2}; Simpson et al., 2007; Tremblay et al., 2008). Assuming a conservative f-ratio of 0.6 for the southeast Beaufort Sea (Carmack et al., 2004) yields a corresponding mean GPP rate of ~28.8 g C m^{-2} for 2004. Hence, the mean GPP estimated from the nutrient drawdown in the central Amundsen Gulf in spring-summer 2008 (Table 1) was approximately 80% higher than in 2004. Still, the increase in PP detected here was not as pronounced as in the coastal zone of the Beaufort Sea (<250 m isobath) where the new PP rate was at minimum 4-fold higher in 2007–2008 relative to 2003–2004, due to the

Table 5
List of the biological variables (mean primary production rates and minimum–maximum bounds for other trophic flows) used as constraints for reconstructing the food web flows using the inverse modeling approach (see Section 2.7).

Biological constraint	Units	Lower bound	Upper bound	Reference
Phototrophs				
Primary production by small cells (<5 μm)	g C m^{-2}	17.0		This study
Primary production by large cells (>5 μm)	g C m^{-2}	35.5		This study
Respiration by small and large cells	% of production	5	30	Vézina and Platt (1988)
Exudation/lysis from small and large cells to DOC	% of production	8	82	Gosselin et al. (1997), Klein et al. (2002)
Mesozooplankton				
Production of *Calanus hyperboreus*	g C m^{-2}	1.1	1.8	This study
Production of *Calanus glacialis*	g C m^{-2}	1.3	2.2	This study
Production of *Metridia longa*	g C m^{-2}	1.4	2.4	This study
Production of other mesozooplankton[a]	g C m^{-2}	1.6	2.5	This study
Herbivory by *Calanus hyperboreus*	g C m^{-2}	9.8	17.4	This study
Herbivory by *Calanus glacialis*	g C m^{-2}	2.8	5.1	This study
Herbivory by *Metridia longa*	g C m^{-2}	4.9	8.8	This study
Assimilation efficiency of mesozooplankton	%	60	80	Daly (1997), Frangoulis et al. (2010)
Gross growth efficiency of mesozooplankton	%	15	33	Straile (1997), Frangoulis et al. (2010)
Total respiration by mesozooplankton	g C m^{-2}	9.9	14.8	This study
Excretion/egestion from mesozooplankton to DOC	% of respiration	33	100	Vézina and Platt (1988)
Microzooplankton				
Production of copepod nauplii	g C m^{-2}	0.9	1.3	This study
Bacterivory by protozoans	g C m^{-2}	1.7	2.7	Vaqué et al. (2008); This study
Herbivory and detritivory by protozoans	g C m^{-2}	9.8	16.2	Vaqué et al. (2008), This study
Assimilation efficiency of microzooplankton	%	50	90	Vézina and Platt (1988)
Gross growth efficiency of microzooplankton	%	10	40	Straile (1997)
Excretion/exudation from microzooplankton to DOC	% of respiration	33	100	Vézina and Platt (1988)
Bacteria				
Production of bacteria	g C m^{-2}	2.8	4.6	This study
Exoenzymatic degradation of detritus by bacteria	g C m^{-2}	6.0	10.2	This study
Net growth efficiency of bacteria	%	7	25	del Giorgio and Cole (2000), Kirchman et al. (2009b)
Exudation and viral lysis from bacteria to DOC	g C m^{-2}	6.3	12.4	Wilhelm and Suttle (1999), This study
Other parameters				
Total POC sedimentation at 395 m	g C m^{-2}	1.2	2.2	This study
Net community production (whole water column)	g C m^{-2}	6.2	32.8	Shadwick et al. (2011)

[a] Other mesozooplankton comprise copepods other than the three dominant calanoids, as well as ostracods, appendicularians and mucus-feeder pteropods.

synergistic effect of persistent upwelling-favorable (i.e. north-easterly) winds and the steep topography (Williams and Carmack, 2008; Tremblay et al., submitted for publication). This spatial comparison indicates that despite the potential for enhanced vertical mixing, the central Amundsen Gulf remains a stratified area (cf. Lansard et al., submitted for publication). Such a characteristic is a consequence of its inherent offshore condition, but probably also of the residual anti-cyclonic circulation in the Gulf (Lanos, 2009), which is influenced by the Beaufort Gyre conveying a large amount of freshwater (Proshutinsky et al., 2009).

Wind-driven upwelling events in 2007–2008 have particularly boosted the PP associated with the landfast-ice (i.e. ice algae and under-ice phytoplankton), as observed in May and June in the Darnley and Franklin bays (Mundy et al., 2009; Brown et al., 2011; Tremblay et al., submitted for publication). However, measurements in these shallow areas were of coarse temporal resolution and could not be adequately included into our seasonal C budget of the planktonic food web. Nevertheless, three apparent upwelling events were detected in our offshore time-series, as surmised by the upward displacement of isohalines and NO_3^- contours at mid-May (less visible), mid-June and mid-July (Fig. 2b and c). Each of these events occurred shortly (<2 weeks) after episodes of north-easterly winds (20–40 km h^{-1}) that persisted for at least 5 days over the IPY–CFL study region (Tremblay et al., submitted for publication). Hence, we propose that what has been detected in the central Amundsen Gulf is not a consequence of local upwelling, but simply a reflection of the episodic south-eastward entrainment of deep water from the Beaufort Sea into the Amundsen Gulf (Lanos, 2009), as a consequence of the surface Ekman drift toward the north-west (cf. Williams and Carmack, 2008). These remotely-driven, transient uplifts in the nitracline during May and July were clearly associated with marked increases in chl *a* fluorescence (Fig. 2d) and in the proportion of large phytoplankton cells (Fig. 6c), whereas the apparent lack of similar effect in mid-June is likely an artifact linked to the lack of sampling in the central Amundsen Gulf from 11 to 27 June 2008 (see Appendix A). We assumed that our new PP rate compensated to some extent for this shortage of measurements, as our methodology integrated the NO_3^- deficit over the euphotic zone and throughout the productive season until near-exhausted nutrient stocks (cf. Hoppema et al., 2000). Therefore, we conclude that in addition to enhanced vertical mixing during winter, the so-called upwelling events in spring-summer have likely contributed to the increase in PP in the offshore zone of the Amundsen Gulf in 2008, when compared with the average PP rate measured in 2004. Indeed, more data accounting for the influence of inter-annual variability and spatial heterogeneity of sea ice and wind conditions on nutrient inventories are needed to establish a real trend in primary productivity in the region.

According to our NO_3^- drawdown equation (Fig. 6a), half of the cumulated new PP occurred from late March to May and the other half was mediated by the subsurface chlorophyll maximum (SCM) that developed in June–July. Phytoplankton biomass over March–April was low (Fig. 6c) and it is most probable that ice algae (Fig. 6c) and pelagic mixotrophic microorganisms (e.g. *Micromonas*-like picoprasinophytes; Lovejoy et al., 2007) began to deplete the surface NO_3^- inventory before the phytoplankton bloom recorded in May. A decrease in the pCO_2 has also been attributed

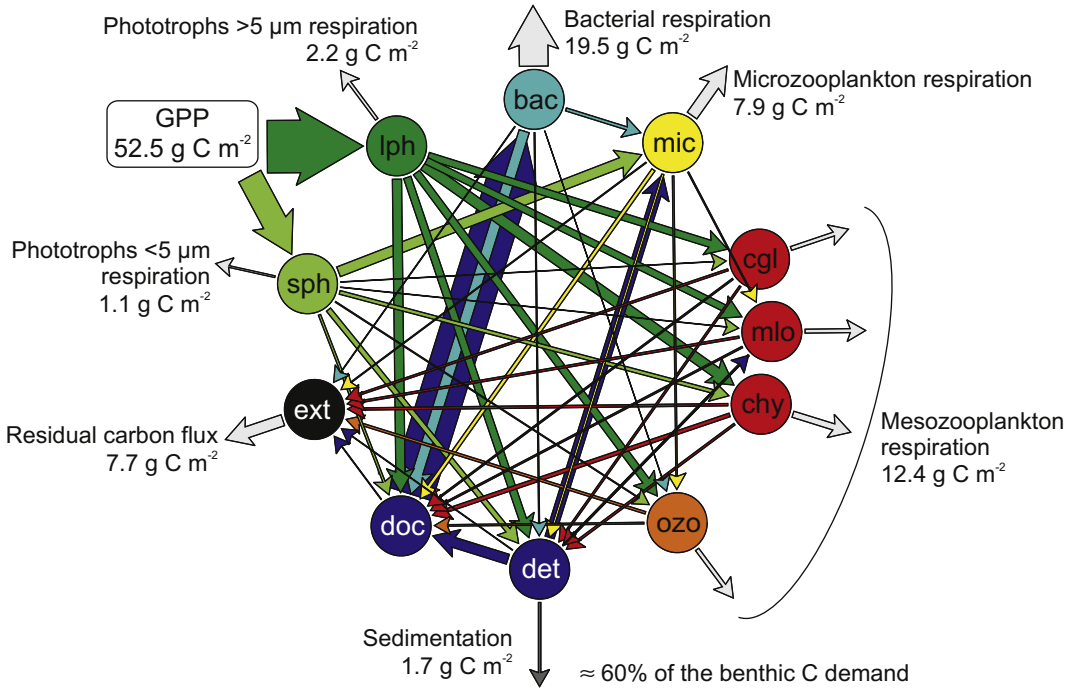

Fig. 12. Inverse modeling solution for the planktonic food web flows in the central Amundsen Gulf for the whole period of spring-summer 2008 (0–395 m depth). Arrow widths are proportional to the importance of each carbon flow between connected food web components as abbreviated as: GPP: gross primary production (i.e. total), sph: small phototrophs <5 µm, lph: large phototrophs >5 µm, bac: bacteria, mic: microzooplankton (i.e. protozoans and copepod nauplii), cgl: *Calanus glacialis*, mlo: *Metridia longa*; chy: *Calanus hyperboreus*, ozo: other mesozooplankton >200 µm, det: detrital particulate organic carbon, doc: dissolved organic carbon, ext: residual carbon flow). Please note that the contribution of both phytoplankton (93.6%) and ice algae (6.4%) is assumed to be included in the two phototroph compartments since GPP in our study is derived from the drawdown of NO_3^- and DIC in the upper water column (see Appendix B). Mesozooplankton were divided into four sub-categories to take into account the species-specific feeding strategies (see Section 2.7). The detail of all carbon flows is given in Table 6.

to the growth of ice algae over April–early May, but the uncertainty on this decline was large (Shadwick et al., 2011). Photosynthesis by picoprasinophytes probably corresponds to the passage of chl *a* fluorescence above nil values during March (Fig. 2d), but a reasonable maximum biomass for these small species before ice break-up appears to be only ~1.0 mg chl *a* m^{-2} (Lovejoy et al., 2007). By contrast, ice algal biomass in the central Amundsen Gulf in 2008 peaked around mid-April at ~1.2 g C m^{-2}, a value recorded as the ship drifted along with a large ice floe (Brown et al., 2011). This maximum ice-algal biomass is more than one order of magnitude lower than the C biomass of phytoplankton measured in the upper water column during the spring bloom of May (~18.2 g C m^{-2}, Fig. 6c). Actually, the biomass of phototrophs in our study (Fig. 6c) was largely dominated by phytoplankton (93.6%) over ice algae (6.4%). This supports that ice algae accounted for a minor fraction of total PP when averaged spatially across the study area and integrated temporally throughout the sampling period. Such low relative contribution of ice algae to PP is consistent with the chl *a* fluorescence time-series (Fig. 2d), within which the weak increase in late April probably corresponded to the release of ice algae as the ice cover ruptured (Fig. 2a). This was a period when the stable isotopic composition of phytoplankton and ice algae ($\delta^{13}C$, $\delta^{15}N$) was overlapping and highly variable (Forest et al., 2011). It is clear, hence, that uncertainties remain about the precise contribution of ice algae to total PP, as actual PP rates were not measured *in situ* on ice algae and phytoplankton before ice break-up (Appendix A). This is particularly true as the *f*-ratio of ice algal communities could be lower (e.g. ~0.34; Lee et al., 2008) than the one that has been used in the present study (0.64) to calculate the total GPP.

Long-lived SCMs (i.e. generally below 25 m depth) are widespread features in seasonally ice-free waters of the Canadian Arctic (Martin et al., 2010). The depth of the SCM in our study (~55 m, Fig. 2d) was greater than the usual depth (~30–40 m) associated with these features in the Amundsen Gulf (Martin et al., 2010), consistent with the deepening of the chlorophyll maximum in the Canada Basin observed over 2003–2008 (from 45 to 60 m depth; Jackson et al., 2010). During the CASES expedition in 2004, the SCM developed simultaneously with the ice break-up as a result of low initial NO_3^- inventories in the surface layer and persisted at least until early August (Tremblay et al., 2008). In 2008, the SCM in the central Amundsen Gulf developed in June (Fig. 2d) and was first characterized by a *f*-ratio of ~0.5 and small phytoplankton cells at ~74% (Fig. 6b and c). Such a large proportion of total GPP fueled by regenerated nutrients is consistent with heterotrophic activities and the peak NH_4^+ inventory generated in the wake of the superficial spring bloom. A shift toward high *f*-ratios (up to 0.95) and dominance of both PP and chl *a* biomass by large phytoplankton (>80%) occurred in early July as the SCM grew in intensity with the upward displacement of isohalines. This illustrated a prompt response by phytoplankton in the SCM to the sudden availability of high NO_3^- concentrations from intermediate Pacific-derived waters (Fig. 3). However, this transient event affected only the lower euphotic zone and did not restore late-winter concentrations at the surface (which would show in Fig. 6a). It boosted productivity of the existing SCM, whose NO_3^- consumption is adequately captured by the logistic model described in Section 3.2.2. The increase in the chl *a* fluorescence signal observed in the SCM in mid-July implies a high photosynthetic capacity despite its location in the lower portion of the euphotic zone (i.e. near 1% light level; cf. Tremblay et al., 2009; Martin et al., 2010). Diatoms and silicoflagellates were most likely the dominant phytoplankton species in the SCM – as well as during the spring bloom – since we found a tight relationship between $[Si(OH)_4]$ and $[NO_3^-]$ drawdown (Fig. 4b). Accordingly, the high depletion ratio

Table 6
Results of food web flows from the inverse modeling solution (Fig. 12). All flows are expressed in g C m^{-2}, which are integrated rates for the whole period of spring-summer 2008.

From	To	Flow (g C m^{-2})
Gross primary production	Phytoplankton <5 μm	16.961
Gross primary production	Phytoplankton >5 μm	35.549
Phototrophs <5 μm	Microzooplankton	7.024
Phototrophs <5 μm	*Calanus hyperboreus*	2.561
Phototrophs <5 μm	*Calanus glacialis*	0.216
Phototrophs <5 μm	*Metridia longa*	0.225
Phototrophs <5 μm	Other mesozooplankton	0.545
Phototrophs <5 μm	Detritus	3.555
Phototrophs <5 μm	Dissolved organic carbon	1.647
Phototrophs <5 μm	Respiration	1.187
Phototrophs >5 μm	*Calanus hyperboreus*	7.203
Phototrophs >5 μm	*Calanus glacialis*	4.859
Phototrophs >5 μm	*Metridia longa*	4.717
Phototrophs >5 μm	Other mesozooplankton	5.187
Phototrophs >5 μm	Detritus	5.160
Phototrophs >5 μm	Dissolved organic carbon	6.290
Phototrophs >5 μm	Respiration	2.133
Bacteria	Microzooplankton	2.158
Bacteria	Other mesozooplankton	0.110
Bacteria	Detritus	0.612
Bacteria	Dissolved organic carbon	7.210
Bacteria	Respiration	19.500
Bacteria	Residual flux (net production)	0.320
Microzooplankton	*Calanus glacialis*	1.164
Microzooplankton	*Metridia longa*	0.733
Microzooplankton	Other mesozooplankton	1.053
Microzooplankton	Detritus	1.558
Microzooplankton	Dissolved organic carbon	2.607
Microzooplankton	Respiration	7.900
Microzooplankton	Residual flux (net production)	0.563
Calanus hyperboreus	Detritus	1.388
Calanus hyperboreus	Dissolved organic carbon	2.518
Calanus hyperboreus	Respiration	4.296
Calanus hyperboreus	Residual flux (net production)	1.562
Calanus glacialis	Detritus	1.258
Calanus glacialis	Dissolved organic carbon	0.991
Calanus glacialis	Respiration	2.645
Calanus glacialis	Residual flux (net production)	1.345
Metridia longa	Detritus	1.161
Metridia longa	Dissolved organic carbon	1.050
Metridia longa	Respiration	2.703
Metridia longa	Residual flux (net production)	1.468
Other mesozooplankton	Detritus	1.391
Other mesozooplankton	Dissolved organic carbon	1.103
Other mesozooplankton	Respiration	2.756
Other mesozooplankton	Residual flux (net production)	1.673
Detritus	Microzooplankton	6.395
Detritus	*Metridia longa*	0.708
Detritus	Dissolved organic carbon	6.910
Detritus	Other mesozooplankton	0.027
Detritus	Sedimentation	1.654
Detritus	Residual flux (accumulation)	0.388
Dissolved organic carbon	Bacteria	29.910
Dissolved organic carbon	Residual flux (dilution)	0.416

measured in our study (1.64) was a good indicator of siliceous plankton growth at low irradiance (Tremblay et al., 2008). But the fact that it was slightly lower than during CASES (1.86) suggests that the SCM contributed less to total PP in 2008 than in 2004. Actually, the spring bloom in 2004 was a "flash" event that has been barely detected at ice break-up, as a result of the weak surface renewal of inorganic nutrients during winter 2003–2004 (Simpson et al., 2008; Tremblay et al., 2008).

4.2. Biotic regulation of trophic and downward carbon flows: influence of the high carbon demand by zooplankton and bacterial communities

In marine ecosystems, primary producers provide the initial organic C source, whereas consumers and decomposers determine its distribution and fate in the food web. The balance in the quantity of energy retained in the pelagic environment or transferred to the benthos depends primarily upon the degree of coupling between PP and heterotrophic plankton (Wassmann, 1998). Despite differences in their size and feeding strategies, zooplankton and microorganisms can be seen as an interacting functional unit that controls both trophic export and sinking losses (e.g. Steinberg et al., 2008). In the Amundsen Gulf in spring-summer 2008, the POC sedimentation modeled at the depth of 395 m amounted to 1.7 g C m^{-2} (only 3% of the initial GPP), a rate which accounted for ~60% of the estimated C demand of benthic communities. This discrepancy could be explained by uncertainties on vertical flux measurements (Buesseler et al., 2007), such as underestimation due to passively sinking copepods (Sampei et al., 2009b), or by variability in the timescale of C cycling in the sediment when compared to the pelagic (Rysgaard and Nielsen, 2006). A possible additional C source to the benthos in a trough-like environment such as the Amundsen Gulf might be cascading particles, i.e. lateral transport of organo-mineral aggregates or benthic algal POC within the bottom boundary layer of the slope (Feder et al., 1994; Thomsen, 1999; Rysgaard and Glud, 2007). However, sediment pigment concentrations did not suggest that lateral input was important in spring-summer 2008 (Link et al., 2011). The low fraction of downward C flow out of the pelagic food web computed here is nevertheless in accord with a recent multi-year study on vertical POC fluxes showing that only ~5% of the surface POC signal appears to reach 210 m depth in the area (Forest et al., 2010). Clearly, the general picture emerging from these results and from our synthesis illustrates that the pelagic food web in the central Amundsen Gulf leaves little for other components of the ecosystem (cf. Sallon et al., in press). This seems to be the case in most years, even when PP levels are unusually high like in 2008. The high retention is obviously induced by a high top-down pressure, a condition that is increasingly recognized in off-shelf Arctic environments (e.g. Olli et al., 2007). The challenge now is to identify the driving forces behind this condition. If the impact of environmental changes on the Amundsen Gulf dynamics is to be adequately understood and projected, the comprehension of key mechanisms governing food web function is needed. In particular, the fact that we estimated an export flux at Z_{EU} representing only ~10% of GPP (Table 1) suggests that the C demand of heterotrophs was especially high in 2008. High top-down pressure at the onset of PP in spring was presumably exerted by large populations of heterotrophic plankton in place beforehand. Such pre-conditioning of the ecosystem is likely to be the critical determinant of pelagic retention.

In autumn 2007, high recruitment of the key copepod species *C. glacialis* was detected on the Mackenzie Shelf and in the Franklin Bay, thanks to the abundant food resources available following the highly productive season of 2007 (Tremblay et al., submitted for publication; see also above). A high biomass of *C. glacialis*, as well as of the two other dominant calanoid copepods *C. hyperboreus* and *M. longa*, was subsequently measured in the Amundsen Gulf in January 2008 (up to 7.6 g C m^{-2}; Forest et al., 2011). This tendency for sustained secondary production obviously persisted over spring-summer 2008, as peaks in zooplankton production were generally detected in concomitance with the successive increases in chl *a* biomass. Peaks in the production of dominant calanoid copepods were also associated with the rapid moulting of young copepodite stages into older stages (Forest et al., 2011). Most importantly, the early spring bloom detected in May favored a steep increase in the production rate of all zooplankton species, including copepod nauplii (Figs. 7a–d, 8a and 9a). This response occurred despite the prevalence of sub-zero temperature throughout the upper water column (Fig. 2b), indicating that Arctic zooplankton are well adapted to their cold environment (e.g. Conover and Huntley, 1991). Herbivory in the three dominant calanoids reached

Table 7
Vital parameters of planktonic heterotrophs as obtained from the inverse food web solution (Fig. 12 and Table 6) and of the benthos as calculated upon Fig. 11 and according to Brey (2001). The definition of each parameter is given in the Appendix B. Please note that the secondary production of each component comprises the C flow lost through mortality (i.e. by constrained predation and/or natural death) and does not equal each of the residual C flows as listed in Table 6.

Heterotrophic component (modeled)	Ingestion (C demand) ($g\ C\ m^{-2}$)	Excretion/egestion ($g\ C\ m^{-2}$)	Assimilation efficiency (%)	Respiration outflow ($g\ C\ m^{-2}$)	Net secondary production ($g\ C\ m^{-2}$)	Gross growth efficiency (%)	Bacterial growth efficiency (net) (%)
Bacterioplankton	29.9	6.9	76.9	19.5	3.5	11.7	15.2
Microzooplankton	15.6	3.8	75.9	7.9	3.9	25.2	–
Calanus hyperboreus	9.8	3.8	61.4	4.3	1.7	17.4	–
Calanus glacialis	6.2	2.1	66.0	2.6	1.5	23.6	–
Metridia longa	6.4	2.1	67.2	2.7	1.6	24.8	–
Other mesozooplankton	6.9	2.4	66.0	2.8	1.8	26.2	–
Benthos[a]	2.8	0.6	80.0	1.6	0.7	24.0	–

[a] Values calculated upon Fig. 11 and according to Brey (2001).

their maximum in May, thus supporting the match hypothesis between the growth of Arctic copepods and phytoplankton blooms (see Falk-Petersen et al., 2009 for a review). The vernal increase in the production of *C. glacialis* was less visible (Fig. 7b) because the biomass of this species was roughly twice lower in May than in July (Forest et al., 2011). Hence, the observation that the productivity of *C. glacialis* reached daily rates as high as ~38 mg C m^{-2} d^{-1} in early July (Fig. 7b) suggests a tight coupling between the development of the SCM in open water conditions and the growth of this species (cf. Søreide et al., 2010). On the other hand, the relatively low herbivory rates measured in *C. glacialis* and *M. longa* during summer can likely be explained by a diverse diet (e.g. Campbell et al., 2009) not captured by the gut fluorescence technique (Hattori and Saito, 1997). In our C flow model, 19% of the feeding mode of *C. glacialis* was carnivorous and 23% of that of *M. longa* was carnivorous and detritivorous (Table 6). In fact, stable isotope analyses revealed that only the large grazer *C. hyperboreus* could be considered a true herbivore in the Amundsen Gulf in spring-summer 2008 (Forest et al., 2011). This is in accord with the evident bimodal pattern and high rates of phytoplankton ingestion observed for this species (Fig. 7a, Table 6).

Feeding and egestion activities by copepods are increasingly known to trigger the fragmentation of large-size particles and the transfer of particulate material into the dissolved phase. Such shift in the size-spectrum of biogenic matter is due to sloppy feeding, coprophagy/chaly/rhexy behaviors (i.e. ingestion, handling and fragmentation of fecal pellets), leakage from fecal pellets, and direct excretion (e.g. Møller et al., 2003; Iversen and Poulsen, 2007). This perspective contrasts with the general view that fecal pellet production by large copepods contributes to vertical POC export since a substantial proportion (50–98%) of fecal POC material produced in the upper water column is indeed retained there (e.g. Sampei et al., 2004, 2009a; Wexels Riser et al., 2007). When focused on phytoplankton blooms, feeding activities by copepods are thus expected to release high-quality DOC that can be readily used by bacterioplankton (e.g. Titelman et al., 2008). In our food web model, the fraction of DOC egested by mesozooplankton represented on the average 53 ± 10% of their unassimilated C (Table 6). In addition, exoenzymatic activity by bacteria diverted 43% of the detrital C flow to DOC. As a result, bacterial production in our study was not only statistically linked to chl *a* concentration and water temperature (Garneau et al., 2008), but also to mesozooplankton production (see Section 3.3.3). The temporal patterns we observed and modeled convincingly show that microbial growth (Fig. 9b) was promoted by elevated phytoplankton and zooplankton production (Figs. 6c and 7). According to our time-series of DOC concentration in the upper water column (Fig. 5a), the DOC produced by local biological activities over the study period was rapidly used by bacteria, as no major accumulation could be noticed from April to early August. Interestingly, the DOC pool during the spring bloom in May did not increase, but a ~50% rise was detected simultaneously with the increase in SCM intensity. This suggests that the warm surface temperature in summer (Fig. 2b) might have played a role in enabling more efficient exoenzymatic POC degradation by bacteria in summer than in spring (Table 4). On the other hand, we cannot exclude the possibility that photodissolution of POC (Estapa and Mayer, 2010) was facilitated in early July when Z_{EU} (0.2% PAR) reached down to ~100 m depth (Fig. 2d).

Despite low production, bacteria are relatively abundant over the winter months in the Amundsen Gulf region, so they respond quickly to the onset of the productive season (Garneau et al., 2008). During the polar night, they can potentially assimilate CO_2 (Alonso-Sáez et al., 2010) and/or use refractory C sources – such as colored dissolved organic matter (CDOM) – to sustain a minimal growth that compensates for mortality (Garneau et al., 2008; Vaqué et al., 2008). In marine environments, CDOM can be generated by zooplankton and bacteria themselves (e.g. Ortega-Retuerta et al., 2009), but river inputs are possibly the main contributors to CDOM inventories at high-north latitudes (e.g. Retamal et al., 2007). In the Beaufort Sea, the Mackenzie River (ca. 300 km west of the Amundsen Gulf mouth) delivers annually a vast amount of freshwater (~330 km^3 yr^{-1}) and particulate matter (~124 Tg yr^{-1}) (Rachold et al., 2004), but almost all of the terrigenous sediments (~97%) are deposited on the shallow Mackenzie Shelf (O'Brien et al., 2006) and only 2–10% of riverine water appear to occupy the surface layer in the Amundsen Gulf (Lansard et al., submitted for publication; Thomas et al., submitted for publication). The loading of CDOM and DOC from the Mackenzie River to the Arctic Ocean is low when compared with the other Arctic rivers (Stedmon et al., 2011). In the western Arctic, the major CDOM pool lies at intermediate depths (~50–200 m) with maximum concentration in association with the cold core of the Pacific winter water mass (Guéguen et al., 2007; Benner and Amon, 2010). Such vertical layering suggests that the high baseline of DOC concentration in the Amundsen Gulf (Fig. 5a) results primarily from the influence of Pacific-origin water, which is laden with refractory dissolved compounds as a consequence of the oxidation of marine organic matter during the long transit within the global conveyor belt (Nelson et al., 2010). Further CDOM incorporation into the cold Pacific halocline appears to occur during sea ice formation when dense water from the water–sediment interface is entrained offshore (Guéguen et al., 2007). A similar input mechanism is the resuspension of detrital material from the shelf bottom and its subsequent lateral transport offshore during storm and convection events (e.g. O'Brien et al., 2006; Forest et al., 2007). All these processes feed actively the upper water column with both marine organic matter in early diagenesis and terrigenous material. In turn, the large DOC/CDOM inventory in the Beaufort Sea region sustains

an active community of bacteria (Garneau et al., 2008; Nguyen and Maranger, 2010) that might explain why the central Amundsen Gulf appears overall (i.e. surface and subsurface waters combined) to be net-heterotrophic over an annual cycle (Shadwick et al., 2011).

Production of heterotrophic protists was not measured in the field, but their *in situ* bacterivory rates from November 2007 to June 2008 were significantly correlated to bacterial production (Section 3.3.2 and Table 3). This tight fit suggests that the background of bacterial production likely fueled by refractory compounds over the winter months was able to maintain a functional population of protozoans. Such a view is consistent with the notion of an active microbial-detrital food web in the dark waters of the Arctic Ocean in winter (e.g. Garneau et al., 2008; Sampei et al., 2009a; Alonso-Sáez et al., 2010; Rokkan Iversen and Seuthe, 2011). A seasonal shift occurs however in spring when photosynthesis becomes rapidly (once again) the main determinant of organic C fluxes in Arctic marine ecosystems (see Fig. 10 in Forest et al., 2008). Assuming that bacterivory could meet only 14% of the C demand of large protozoans (>5 μm) in spring-summer (Vaqué et al., 2008), we estimated that at least ca. 10 g C m^{-2} of small phytoplankton or detrital POC was needed to fulfill the C requirement of heterotrophic protists in our study (Table 5). The inverse C flow model actually computed that 41% of the POC ingested by microzooplankton exited from the detritus compartment and that 54% of C inputs to the detritus pool entered directly from the two phototrophic components (Fig. 12 and Table 6). Hence, the break-up of freshly-produced ice algal and phytoplankton cells into small phycodetritus through mechanical burst or sloppy feeding by copepods was not only an important source of DOC for microbes, but also probably of small detrital POC for protozooplankton. Interestingly, the Amundsen Gulf ecosystem in spring-summer 2008 was dominated at ~68% by the production of large cells (mainly diatoms), but clearly, cannot be classified as an export system (*sensu* Wassmann, 1998). Such disconnection between the size-structure of phototrophic communities and food web function has been observed in other Arctic polynyas (Berreville et al., 2008) as well as in the subarctic Gulf of St-Lawrence (Rivkin et al., 1996), and is likely due to a rich set of internal trophic interactions, as exemplified by our diagram of the planktonic food web (Fig. 12).

4.3. Comparison of the central Amundsen Gulf with other Arctic ecosystems: implications for higher trophic levels and biogeochemical carbon fluxes

A persistent paradigm of Arctic shelf seas is that the pelagic–benthic coupling in these regions is tight due to a large proportion of PP left ungrazed by zooplankton and directly available to the benthos via sinking (e.g. Dunton et al., 2005; Renaud et al., 2008; Tamelander et al., 2008). This is generally the case on the shallow Barents, Chukchi and Bering shelves, where PP is high (100–400 g C m^{-2} yr^{-1}; Sakshaug, 2004), but strong pelagic–benthic coupling in other Arctic regions is patchier and typically associated with upwelling areas, marginal ice zones and polynyas (Piepenburg, 2005). Among Arctic polynyas, however, both the North Water (NOW) and Northeast Water (NEW) polynyas have been identified as retention systems because of the rich spring-summer zooplankton populations that inhabit these regions (Grebmeier and Barry, 2007). To a lesser extent, a similar functioning occurs in the northern Barents Sea where zooplankton could potentially ingest POC in the range of 22–44% of the daily PP during the spring bloom (Wexels Riser et al., 2008). According to our results, we can clearly add the Amundsen Gulf flaw lead polynya to the list of Arctic systems where vertical export is low (*e*-ratio at $Z_{EU} \approx 10\%$) as a result of high top-down regulation (as discussed above). This comparison becomes more insightful when considering similarities and contrasts in the magnitude of PP and its fate in the food web across the so-called retention systems. A convenient comparison can be made with the pelagic food web of the eastern NOW in spring-summer 1998, which was investigated by Tremblay et al. (2006a). Out of a total PP of 139 g C m^{-2} measured during this period, 79% was consumed by heterotrophs, 6% accumulated as detritus and DOC, and 15% sank below 150 m depth. Furthermore, the fractions of PP reaching the 200 and 500 m isobaths were only 7% and 1%, respectively. Functioning of the planktonic food web in the central Amundsen Gulf in 2008 thus appears similar to what has been deduced for the NOW polynya in 1998. The prompt response of the heterotrophic components to micro-algal production and the significant prey-predator relationships found in our study are further evidence for similarities between the two environments. What differs is presumably the absolute quantity of energy transferred to higher trophic levels and available for the development of vertebrate populations.

In the NOW polynya, the planktonic food web supports large biomasses of seabirds and marine mammals, whereas the density of top predators in the Amundsen Gulf region is known to be much lower (Stirling, 1997). The most striking example concerns the seabird population, as literally millions of seabirds, mainly of the copepod-specialist species dovekie (*Alle alle*), migrate every year to the NOW polynya to feed and breed (Karnovsky et al., 2007). The average C flux to dovekies in the NOW is estimated to be ~1 g C m^{-2} yr^{-1}, or ~0.5% of the annual PP of 250 g C m^{-2} (Karnovsky and Hunt, 2002). By contrast, only one colony of <1000 seabirds, dominated by thick-billed murres (*Uria lomvia*), appears to settle in the Amundsen Gulf at Cape Parry (Fig. 1). This is despite the existence of suitable nesting cliffs along Banks Island, in particular at Nelson Head at the southern tip of the island (Johnson and Ward, 1985; Stirling, 1997; Dickson and Gilchrist, 2002). Dickson and Gilchrist (2002) suggested that the lack of pelagic seabirds nesting at Nelson Head was indicative of the relatively low productivity of the offshore Beaufort Sea area, when compared for example with the Bering Sea or the eastern Canadian Arctic. The only substantial population of marine birds in the Amundsen Gulf region (>100,000 individuals) appears to occur nearshore and to coincide with the spring migration of eiders (*Somateria* spp.) and long-tailed ducks that feed mainly on bottom-dwelling invertebrates within the <50 m isobath contour (Dickson and Gilchrist, 2002). Hence, in the absence of notable seabird predation pressure, the organic matter derived from mesozooplankton production in the central Amundsen Gulf would thus be expected to be transferred toward larger planktivores, such as carnivorous zooplankton, fishes or whales.

Carnivorous macrozooplankton (e.g. chaetognaths, amphipods, cnidarians) in the Amundsen Gulf polynya represents ca. 12% of the zooplankton biomass (Darnis et al., 2008), yielding a mean seasonal estimate of 0.6 g C m^{-2} during CFL 2008 when assuming a 40% C-content in zooplankton dry weight. This conservative value is at least one order of magnitude lower than the average biomass (~11.6 g C m^{-2}) of polar cod (*Boreogadus saida*) as estimated during the CFL expedition in 2007–2008 with the ship-mounted Simrad EK60 echosounder (Geoffroy et al., 2011) and when assuming a C-content of 12.6% in the wet weight of Gadidae (Crabtree, 1995). In the Beaufort Sea, polar cod feeds primarily on copepods, with the three calanoids *C. hyperboreus*, *C. glacialis* and *M. longa* as the most frequent preys (Benoit et al., 2010), and serves as a key link in the transfer of energy to seals, belugas and polar bears (Loseto et al., 2008). Hence most of the residual C flow resulting from the net production of large calanoid copepods in our model (~4.4 g C m^{-2}, Table 7) would be directed toward this simple and short food chain. The southeastern Beaufort Sea is also the summer feeding ground (June–September) for migrating bowhead whales (*Balaena mysticetus*) of the Bering–Chukchi–Beaufort population

(COSEWIC, 2009). Bowhead whales spend the summer across a vast territory (>200,000 km^2) that spans from the western Mackenzie Shelf up to the eastern Amundsen Gulf, mostly in waters shallower than 200 m depth (COSEWIC, 2009). Bowhead whales are filter-feeders specialized in the harvest of any available zooplankton in the water column and so occupy the same trophic level as polar cod (e.g. Hoekstra et al., 2002). Their population was evaluated at 8100–13,500 individuals in 2001, with an annual rate of increase of 3.4% (George et al., 2004). Unfortunately, the trophic coupling dynamics and the predation pressure exerted by bowhead whales on their prey in the Amundsen Gulf are unknown, making it impossible to evaluate their role in the top-down control of zooplankton.

Despite the successful partitioning of PP into key food web components in the NOW polynya, the fraction of C returned back to the water column by pelagic respiration remained unknown there (Tremblay et al., 2006b). In the central Amundsen Gulf in 2008, we estimated that the planktonic community respired 43.1 g C m^{-2} (82% of the initial GPP), of which 92% was mediated by heterotrophs (Fig. 12). By comparison, less than 1% of the PP in Arctic marine ecosystems is estimated to be respired by upper trophic predators (e.g. Karnovsky and Hunt, 2002 and references therein; see also Wassmann et al., 2006). Such a high respiration flux by plankton in our study was constrained by the different field and literature values (Table 5) and is reflected in the physiological efficiencies of the heterotrophic food web components computed by the inverse analysis (Table 7). Interestingly, the bacterial growth efficiency (BGE) and microzooplankton gross growth efficiency (GGE) corresponded to the mean typical percentages as seen in the literature: ~15% for BGE (del Giorgio and Cole, 2000; Kirchman et al., 2009b) and ~25% for microzooplankton GGE (Straile, 1997). Concerning bacteria, our analysis indeed contrasts with Kirchman et al. (2009a) who measured a mean BGE of only 6.9% through a dataset obtained in the Chukchi and Beaufort seas in summer 2004. Such a low BGE was, however, not statistically different than the typical value of ~15% reported for oceanic systems by del Giorgio and Cole (2000). Given the oligotrophic regime of the Canadian Beaufort Shelf (e.g. Carmack et al., 2004), we were expecting our model to compute low GGE for microorganisms (e.g. <10% BGE; del Giorgio and Cole, 2000). Our results thus suggest that the production efficiencies of bacteria and microzooplankton reflected the state of the southeast Beaufort Sea ecosystem in 2007–2008, which was richer in nutrients and more productive than in previous years (Tremblay et al., submitted for publication). Except for *C. hyperboreus*, the GGE for mesozooplankton were also close to the usual value of ~25% used in global biogeochemical models (Straile, 1997; Frangoulis et al., 2010). Low GGE in copepods (<20%) may be induced by low food levels, but are also possible at high food concentrations (e.g. during phytoplankton blooms) as a result of superfluous feeding (Straile, 1997). Hence, it is difficult to conclude on the exact mechanisms driving the relatively low GGE of 17.4% obtained for *C. hyperboreus* in our analysis. Because *C. hyperboreus* has been considered as a strict herbivore, a combination of low vs. high food regimes alternating during the study period as consequence of pulses in PP flanked by low-productivity phases (Fig. 2d) can most probably explain the low GGE in this species.

Results from our inverse analysis (as calculated upon Table 6) also showed that the net secondary production (i.e. residual C flux + mortality by predation and/or natural death) summed for microzooplankton and bacteria (7.4 g C m^{-2}) was slightly higher than the one cumulated for mesozooplankton (6.6 g C m^{-2}), thus representing 53% of the total secondary production (Table 7). However, bacteria and microzooplankton contributed little to the residual C flow (~10%) because they were subjected to strong top-down control within the planktonic food web (Table 6 and Fig. 12). Our model calculated that 55% of bacterial production was diverted to microzooplankton, 9% to virus and 6% to mucous-feeders (for a total of 70%, Table 6). Similarly, 75% of microzooplankton production was redirected toward carnivorous mesozooplankton. Nevertheless, if we sum up the net production of bacteria and microzooplankton to what accumulated in the model as detrital POC and DOC (Table 6), it appears that ~22% of the residual C flow resulting from plankton production in spring-summer 2008 ended up within microbial and detrital pathways. Hence, our results support the emerging view that the contribution of micro-heterotrophs to marine C cycling in the Arctic Ocean is higher than previously assumed (e.g. Garneau et al., 2008; Rokkan Iversen and Seuthe, 2011; Seuthe et al., 2011), but still lower than at sub-polar latitudes – at least during the productive season (cf. Kirchman et al., 2009b; Sherr et al., 2009; Calbet et al., 2011). For example, the grazing impact of microzooplankton on PP in temperate and tropical waters usually exceeds that of mesozooplankton, with consumption rates reaching 60–70% of the PP flow (Calbet, 2008). In our study, the direct ingestion of phototrophic cells by microzooplankton accounted for only 14% of the net PP, consistent with the envelope of 22 ± 26% found by Sherr et al. (2009) in the western Beaufort Sea in summer. By contrast, Seuthe et al. (2011) found that protozoans in Kongsfjorden (Svalbard Archipelago) could have grazed 100% of the daily PP in April when assuming complete herbivory, which is obviously an over-simplification of the trophic interactions. Here, it is possible that the C flow through microzooplankton has been underestimated as the field dataset of microzooplankton was not as exhaustive as the one of mesozooplankton (Appendix A). However, our model took into account a minimum grazing bound consistent with the literature (Vaqué et al., 2008; Sherr et al., 2009) as well as the alternative feeding modes of microzooplankton (Table 5). Nevertheless, our analysis indicated that mesozooplankton (mainly large copepods) ingested directly 52% of the net PP through herbivory in spring-summer 2008, whereas 18% of the phototrophic C flow was directed to the detritus pool (Table 6). At first glance, such a proportion of "ungrazed" PP channeled into detritus might imply a large potential for vertical POC export in the central Amundsen Gulf, or at least larger than the small 3% of the initial GPP computed upon our field measurements. However, the degradation of POC to DOC by bacterial exoenzymes (Kellogg et al., 2011) combined with intense detritivory by protozoans, omnivorous copepods and unselective filter-feeders (e.g. appendicularians) recycled ~87% of detritus back in the food web (Table 6), which stresses the importance of the detritus hub as a major trophic link in the pelagic system of the Amundsen Gulf.

5. Summary and concluding remarks

The central Amundsen Gulf in 2008 can be defined as a retention system (*e*-ratio at $Z_{EU} \approx 10\%$) within which: (1) the structure of phototrophic communities, characterized by the dominance of large cells at 68% and a high seasonal *f*-ratio of 0.64 at the Z_{CM}, was decoupled from the typical export function that would be expected under these conditions; (2) relatively large populations of zooplankton (mainly copepods) yielded an exploitation efficiency of ~66% and took advantage of increased GPP to sustain their development, consistent with the traditional view that the offshore Beaufort Sea is oligotrophic; (3) allochthonous DOC inputs associated with the Pacific-derived water masses maintained an active microbial food web over the dark season, allowing a quick response of bacteria and protozoans to pulses in the availability of labile C at the onset of the productive season; (4) sedimentation and

benthic C demand at ca. 400 m depth remained low since feeding and degradation by heterotrophs retained nearly all (97%) of the primary-produced C in the water column; and (5) the residual C flow as a result of net community production, dilution and accumulation was modest (7.7 g C m^{-2}) because most of the GPP-derived organic C (82%) was respired by the planktonic community and released as CO_2.

The depth at which CO_2 is released by planktonic respiration dictates whether the initial GPP-derived C could potentially return back to the atmosphere within a year or be stored for at least a decade or even hundred of years. This is because the average residence time of Pacific water (~50–200 m depth) in the Beaufort Sea is estimated to be 11 years (Yamamoto-Kawai et al., 2008) and that of Atlantic and deep waters (>250 m depth) from approximately 30 to 300 years (Gregor et al., 1998). Unfortunately, discrepancies in the sampling depth or incomplete coverage of the water column in the various datasets, as well as uncertainties related to zooplankton diel vertical migration (e.g. Fortier et al., 2001) prevented the conception of a multi-layer C flow model in the present study. The intermittent on-shelf upwellings of Amundsen Gulf intermediate waters (~33 salinity) during spring and summer 2008 (Tremblay et al., submitted for publication) – which are supersaturated with respect to atmospheric CO_2 – might complicate assessments of the ultimate fate of the C respired during our sampling period. However, measurements of surface water CO_2 concentrations (0–50 m depth) and subsequent air–sea flux computations confirmed that the central Amundsen Gulf acted as a sink for atmospheric CO_2 at the annual scale in 2007–2008 (Shadwick et al., 2011). Future studies of C fluxes in the region should thus aim at using a finer vertical resolution, especially since plankton respiration rates are expected to increase in response to Arctic warming in spring-summer (Vaquer-Sunyer et al., 2010).

A yet unresolved issue concerns the fate of the residual C flow in the Amundsen Gulf ecosystem. Much uncertainty remains on the trophic transfer of organic matter from zooplankton to higher trophic levels, in particular through the key species polar cod. Here, it was difficult to calculate an average ecological efficiency for the planktonic system (i.e. secondary production divided by net PP) as the set of internal trophic interactions was rich and involved links between consumers and decomposers (Fig. 12). If we exclude bacteria, the pelagic secondary production constrained by the inverse analysis amounted to 10.5 g C m^{-2} (Table 7), which yields an ecological efficiency of 21.4%, a fraction as high as in productive upwelling systems (Ryther, 1969). However, the actual residual C flow resulting from zooplankton growth (including nauplii and protozoans) after accounting for trophic interactions rather suggests that vertebrates had access to a maximum of 6.6 g C m^{-2} (i.e. 13.4% ecological efficiency). This transfer efficiency is presumably in the upper range of "environmentally possible" values for the central Amundsen Gulf region since it was obtained during a year of low ice coverage, warm sea surface temperature and enhanced new PP. Nevertheless, it is much lower than the absolute production required for sustaining commercial fish catches (15–130 g C m^{-2} yr^{-1}) as recorded throughout large marine ecosystems (Conti and Scardi, 2010). It is therefore unlikely that the increase in zooplankton productivity caused by more favorable physical and biological conditions, such as the ones observed in 2008, could foster a substantial increase in new harvestable resources in the offshore Beaufort Sea domain. The relatively simple Arctic pelagic food web in its present structure (e.g. see Fig. 9 in Welch et al., 1992) would conversely benefit from such a relaxed situation (cf. Tremblay et al., 2006a), at least if other threats like the loss of sea ice habitats, ocean acidification or increased stratification do not stress it. Less is known on the possible effects of the sea ice decline on benthic processes (Piepenburg, 2005) and their feedback to the pelagic system.

The apparent increase in pelagic productivity as inferred from our analysis needs obviously to be confirmed by the inclusion of an extensive multi-year dataset in order to account for the intrinsic system variability. To achieve this goal, the time-series of physical and biological measurements that began in the Canadian Beaufort Sea since the CASES program should be maintained and further developed. Moreover, given that our inverse C flow model was the most parsimonious solution out of many food web possibilities (e.g. Soetaert and van Oevelen, 2009) and that numerous environmental changes might affect Arctic marine systems in the coming years (see Section 1), future work should focus on the design of a fully-coupled 3D model for the Beaufort Sea ecosystem in order to decipher its future state under various climate scenarios (cf. Lavoie et al., 2010). Such a model is indispensable for understanding the probable consequences of shifts in physical forcing mechanisms for Arctic marine food webs (Carmack and Wassmann, 2006; Wegner et al., 2010; Carmack and McLaughlin, 2011; Wassmann et al., 2011) and their impacts on biogeochemical cycling and biological productivity. An unprecedented ecosystem modeling effort is now underway at the pan-Arctic scale (e.g. Popova et al., 2010; Zhang et al., 2010; Slagstad et al., 2011), but current models rely on many unverified assumptions due to a lack of *in situ* ecological data. Our synthesis of field measurements and inverse analyses contributed to close this gap in knowledge and provided detailed information on food web structure, biological processes and predator–prey interactions in the offshore Beaufort Sea region.

Acknowledgments

We express gratitude to the officers and crew of the research icebreaker CCGS *Amundsen* for professional and enthusiastic assistance at sea. We thank all the following IPY–CFL colleagues and friends for their essential help at sea and/or in the laboratory: L. Létourneau, L. Michaud, P. Massot, S. Blondeau, S. Gagné, J. Michaud, M. Ringuette, C. Bouchard, J. Gagné, S. Thanassekos, H. Cloutier, B. Robineau, C. Lalande, M. Berrouard, K. Simpson, S. Pineault, C.J. Mundy, J. Ferland, M. Simard, R. St-Louis, M. Thaler, R. Terrado, C. Evans, T. Tamelander, and M. Estrada. We gratefully acknowledge V. Galindo, M.-C. Perreault and A. Aubert for part of the zooplankton counts. Special thanks to M. Blais for the *f*-ratio dataset of late summer and to B. Philippe for the ice algal dataset. Thanks to V. Lago, M.E. Rail, P. Guillot and D. Boisvert for the processing of CTD cast data. We thank the leaders and coordinators of the CFL system study: D. Barber, G. Stern, D. Leitch and M. Pucko for the organization of the fieldwork and workshops. We are highly grateful to G. Jackson, T. Richardson, A. Burd, and N. Niquil for making available the initial code for the inverse food web model. The CFL system study is a project of the International Polar Year 2007–2008 funded by the Government of Canada (IPY #96). AF benefited from postdoctoral scholarships from the Fonds québécois de la recherche sur la nature et les technologies, and from the Natural Sciences and Engineering Research Council of Canada. The early data analyses conducted for this work have been made during a postdoctoral stay at the University of Tromsø, Norway, and AF would like to thank the Hyperboreum-Sedimentation Group for the hospitality. This synthesis is a joint contribution to the research programs of IPY–CFL, Québec-Océan, ISMER, CHONe, ArcticNet Network of Centres of Excellence of Canada, and to the Canada Research Chair on the response of marine Arctic ecosystems to climate warming.

Appendix A. List of stations and meta-data

Station information					Water column profiles and variables							Ice algae	Phytoplankton			Mesozooplankton			Micro-zooplankton		Bacterio-plankton		Vertical fluxes		Benthos	
Station ID	Date (±24 h) (month-day)	Latitude (°N)	Longitude (°W)	Bottom (m)	CTD-Fluo.	Nitrate	Silicic acid	Ammonium	DIC	TPC	DOC	Biomass	Biomass	Production	*f*-ratio	Biomass	Calanoid herbivory	Community respiration	Cop. nauplii biomass	HNF biomass/ bacterivory	Production	Enzymatic activity (EEA)	Short-term samplings	Long-term mooring	C-demand	POC
19D	2-4	71° 4.63′	124° 49.02′	348	X	X	X		X				X			X		X	X		X				← Actual station	
19D	2-8	71° 4.61′	124° 48.94′	347	X	X	X		X																locations may vary	
19D	2-11	71° 4.55′	124° 48.12′	361	X	X	X		X				X					X							(see Figure 11)	←
22D	2-18	71° 19.33′	124° 31.86′	267	X	X	X		X				X					X		X						
26D	2-25	70° 55.96′	123° 56.16′	361	X	X	X		X				X			X		X	X		X					
26D	2-29	70° 50.74′	123° 36.78′	435	X	X	X		X																	
27D	3-2	70° 45.61′	123° 27.48′	550	X	X	X		X				X					X		X						
29D	3-8	71° 0.94′	123° 46.5′	312	X	X	X																			
29D	3-11	71° 1.99′	123° 53.82′	321	X	X	X					X	X					X			X					
D29	3-18	70° 54.48′	123° 28.62′	401	X	X	X					X	X			X		X	X	X	X					
D36	4-7	71° 16.43′	124° 23.04′	274	X	X	X		X			X	X			X		X	X		X					
D37	4-10	71° 15.04′	124° 36.84′	278	X	X	X	X	X			X	X							X	X				X	
D40	4-16	70° 47.63′	122° 28.32′	477	X	X	X	X	X	X	X	X	X			X			X		X				X	
D41	4-18	70° 37.06′	121° 54.84′	503	X	X	X	X	X			X	X					X								
D41	4-21	70° 41.68′	121° 42.6′	486	X	X	X	X	X				X													
D42	4-23	70° 36.05′	122° 13.44′	483	X	X	X	X	X																	
D43a	4-26	70° 35.24′	122° 26.16′	558	X	X	X		X			X	X			X	X		X		X					
D43b	4-28	70° 41.57′	123° 4.92′	510	X	X	X	X	X			X	X		X											
D43c	5-1	70° 49.16′	124° 16.5′	418	X	X	X	X	X			X	X		X											
D43d	5-4	71° 0.91′	125° 55.86′	408	X	X	X		X				X			X		X	X							
1020A	5-6	71° 1.59′	126° 57.9′	276	X	X	X	X	X	X	X		X		X										X	X
405b	5-19	70° 40.27′	122° 49.86′	590	X	X	X	X	X	X	X		X		X	X	X			X	X				X	X
1011	5-21	70° 43.81′	123° 59.94′	429	X	X	X	X	X				X						X							
D46	5-30	71° 34.18′	125° 17.58′	289	X	X	X	X	X				X													
D47	5-31	71° 12.46′	124° 41.04′	273	X	X	X		X																	
405	6-1	70° 37.78′	123° 10.38′	490	X	X	X	X		X	X		X		X	X	X		X	X						
405b	6-10	70° 39.51′	122° 59.88′	590	X	X	X	X	X	X	X		X		X	X		X	X	X	X	X	X		X	X
1204	6-28	71° 18.31′	125° 11.7′	312	X	X	X								X										X	X
1208	6-28	71° 3.85′	126° 2.88′	400	X	X	X	X	X	X	X		X	X		X	X	X	X	→	X	X	X		X	X
1212	6-29	71° 49.28′	126° 54.24′	279	X	X	X																			
410	7-8	71° 41.93′	126° 28.98′	400	X	X	X	X	X	X	X		X	X	X	X		X	X		X	X	X			
412	7-9	71° 33.82′	126° 55.38′	413	X	X	X																			
414	7-9	71° 25.26′	127° 21.84′	305	X	X	X																			
1901	7-10	71° 37.81′	125° 53.82′	349	X	X	X														X					
1903	7-11	71° 29.8′	125° 26.46′	328	X	X	X																			
1907	7-11	71° 13.17′	124° 32.64′	276	X	X	X																			
1911	7-11	70° 57.17′	123° 37.92′	350	X	X	X																			
1100	7-11	71° 2.74′	123° 15.66′	268	X	X	X	X	X	X	X		X			X		X	X	Actual station locations may vary (see Table 3)	X					
1106	7-12	70° 36.77′	124° 12.84′	438	X	X	X																			
1104	7-12	70° 45.26′	123° 53.46′	424	X	X	X																			
1102	7-12	70° 54.01′	123° 34.74′	390	X	X	X																			
1913	7-12	70° 53.96′	123° 4.86′	470	X	X	X																			
1915	7-12	70° 54′	122° 27.42′	405	X	X	X																			
1917	7-13	70° 54.05′	121° 49.86′	387	X	X	X																		X	X
1919	7-13	70° 53.99′	121° 13.68′	303	X	X	X																			
403	7-20	70° 5.47′	120° 5.61′	411	X	X	X	X	X	X			X			X			X							
404	7-20	70° 20.99′	121° 36.25′	479	X	X	X																			
405	7-21	70° 42.12′	122° 56.29′	600	X	X	X	X	X	X			X		X	X	X	X	X				X		X	X
1901	7-22	71° 13.46′	124° 42.18′	274	X	X	X																			
437	7-23	71° 41.63′	126° 36.01′	441	X	X	X	X	X	X	X		X	X	X	X										
412	7-24	71° 33.86′	126° 55.03′	416	X	X	X																			
414	7-24	71° 25.35′	127° 21.96′	305	X	X	X																			
1300	7-26	71° 16.81′	127° 4.41′	304	X	X	X																			
407	7-26	70° 59.4′	126° 2.58′	398	X											X		X					X		X	X
2006	8-1	71° 18.95′	127° 15.53′	273	X	X	X																			
2008	8-2	71° 19.99′	126° 13.16′	442	X	X	X	X	X	X	X		X			X			X							
2009	8-2	71° 20.37′	125° 42.39′	434	X	X	X																		X	X
405	8-3	70° 42.12′	122° 56.29′	598	X								X	X	X	X	X		X							

Sequential sediment trap Technicap PPS3/3 (0.125 m^2 aperture, 24 cups) deployed at mooring station CA08-07 (=sampling station 407), coordinates: 71° 3.24′ N, 126° 1.38′W, bottom depth 397 m, sampling depth 104 m, deployed 30-Oct-07, recovered 28-Jul-08.

Appendix B. Model rationale and components

Our inverse plankton model constructed for the central Amundsen Gulf for spring-summer 2008 (Fig. 12 and Table 6) contains 11 compartments (small phototrophs <5 μm, large phototrophs >5 μm, bacteria, microzooplankton (i.e. protozoans and copepod nauplii), *C. glacialis*, *M. longa*; *C. hyperboreus*, other mesozooplankton, detrital POC, DOC, and a residual C flow). Please note that the contribution of both phytoplankton (93.6%) and ice algae (6.4%) to GPP is somehow included in the two phototroph components as our mean GPP value was derived from the drawdown of DIC and NO_3^- in the upper water column (Figs. 4a and 6a), a seasonal *f*-ratio (Fig. 6b) and further divided in two size fractions according to chl *a* biomass (Fig. 6c). The model encompasses the spatial domain from 120 to 128°W within the isobath >250 m (Fig. 1) and extends vertically from the surface to a depth of 395 m (average bottom depth of all stations, see Appendix A). We did not directly include a benthic compartment in the model given the variability in the timescale of C cycling in the sediment when compared to the pelagic realm (e.g. Rysgaard and Nielsen, 2006); and because of the uncertainties related to resuspension and lateral transport within the bottom boundary layer in trough-like environments such as Amundsen Gulf where cascading particles from shallower depths can occur (cf. Thomsen, 1999). Instead, the benthos dataset was used as a validation of the vertical POC output.

We considered possible the flow of small phototrophs (<5 μm) to micro- and mesozooplankton, but the flow of large phototrophs (>5 μm) was only possible to mesozooplankton. The mesozooplankton were divided into four sub-categories to take into account the species-specific feeding strategies. *Calanus hyperboreus* was considered a strict herbivore (Falk-Petersen et al., 2009; Forest et al., 2011), *C. glacialis* was considered both herbivore and carnivore (Campbell et al., 2009; Forest et al., 2011), and *M. longa* was considered omnivore (i.e. herbivory, carnivory and detritivory) (Sampei et al., 2009a; Forest et al., 2011). The compartment named "other mesozooplankton" comprised all other copepod species >200 μm length as well as the pteropod, appendicularian and ostracod species considered in the budget (Section 2.4.1). Other mesozooplankton were considered omnivore and a flow from bacteria was also allowed as mucous-feeders are able to use bacteria as food source (Deibel, 1998). Only the respiration rates of mesozooplankton measured in the field during the productive period (late March–early August) were considered in the analysis. We further assumed that an average of 10% of the zooplankton production was diverted to the detritus pool through natural mortality (Elliott et al., 2010). The partitioning of ingested C by planktonic heterotrophs was assessed using standard equations (Tremblay et al., 2006a) binding ingestion (I) to respiration (R_e), egestion/excretion (e), secondary production (P_s), assimilation efficiency (AE), gross growth efficiency (GGE), and exploitation efficiency (EE). These equations can be solved in different manners:

$$I = P_s + R_e + e \quad (1)$$

$$GGE = P_s/I \quad (2)$$

$$AE = (P_s + R_e)/I \quad (3)$$

$$R_e = I \cdot (AE - GGE) \quad (4)$$

$$e = I \cdot (1 - AE) \quad (5)$$

$$EE = I/P_s \quad (6)$$

For bacteria, we further used net bacterial growth efficiency (BGE) as physiological constraint:

$$BGE = P_s/(P_s + R_e) \quad (7)$$

The cumulative net community production (NCP) rate for the whole study period (Table 1) was used to estimate the residual C flow as an outlet from other compartments (to provide a steady state). Only the mean GPP as well as the fraction of large and small phototrophs were used as fixed constraints in the inverse model, whereas the 95% confidence interval limits associated with every other parameters measured in the field were used as lower and upper bounds. In the absence of any confidence interval associated with a given parameter, the standard deviation or the same coefficient of variation as GPP was used for consistency across the food web. Supplementary physiological constraints were obtained from the appropriate literature, with an emphasis on studies from the Beaufort Sea (Table 5).

References

ACIA, 2005. Arctic Climate Impact Assessment – Scientific Report. Cambridge University Press, Cambridge, 1046 pp.

Alonso-Sáez, L., Galand, P.E., Casamayor, E.O., Pedros-Alio, C., Bertilsson, S., 2010. High bicarbonate assimilation in the dark by Arctic bacteria. The International Society for Microbial Ecology Journal 4, 1581–1590. doi:10.1038/ismej.2010.69.

Archambault, P., Snelgrove, P.V.R., Fisher, J.A.D., Gagnon, J.-M., Garbary, D.J., Harvey, M., Kenchington, E.L., Lesage, V., Levesque, M., Lovejoy, C., Mackas, D.L., McKindsey, C.W., Nelson, J.R., Pepin, P., Piché, L., Poulin, M., 2010. From sea to sea: Canada's three oceans of biodiversity. PLoS ONE 5, e12182. doi:10.1371/journal.pone.0012182.

Arrigo, K.R., van Dijken, G.L., 2004. Annual cycles of sea ice and phytoplankton in Cape Bathurst polynya, southeastern Beaufort Sea, Canadian Arctic. Geophysical Research Letters 31, L08304. doi:10.1029/2003GL018978.

Arrigo, K.R., van Dijken, G., Pabi, S., 2008. Impact of a shrinking Arctic ice cover on marine primary production. Geophysical Research Letters 35, L19603. doi:10.1029/2008GL035028.

Båmstedt, U., 2000. A new method to estimate respiration rate of biological material based on the reduction of tetrazolium violet. Journal of Experimental Marine Biology and Ecology 251, 239–263, doi:10.1016/S0022-0981(00)00217-3.

Barange, M., Field, J.G., Harris, R.P., Hofmann, E.E., Perry, R.I., Werner, F., 2010. Marine Ecosystems and Global Change. Oxford University Press, Oxford, 412 pp.

Barber, D.G., Massom, R.A., 2007. The role of sea ice in Arctic and Antarctic polynyas. In: Smith, W.O., Barber, D.G. (Eds.), Polynyas: Windows to the World. Elsevier, Amsterdam, pp. 1–43.

Barber, D., Asplin, M., Gratton, Y., Lukovich, J., Galley, R.J., Raddatz, R.L., Leitch, D., 2010. The International Polar Year (IPY) Circumpolar Flaw Lead (CFL) system study: overview and the physical system. Atmosphere-Ocean 48, 225–243. doi:10.3137/OC317.2010.

Bates, N.R., Mathis, J.T., 2009. The Arctic Ocean marine carbon cycle: evaluation of air–sea CO_2 exchanges, ocean acidification impacts and potential feedbacks. Biogeosciences 6, 2433–2459, doi: 10.5194/bg-6-2433-2009.

Benner, T., Amon, R., 2010. Biogeochemistry of dissolved organic matter in the southeast Beaufort Sea. In: Malina Plenary Meeting, Villefranche-sur-Mer, France, 6–7 May 2010.

Benoit, D., Simard, Y., Gagné, J., Geoffroy, M., Fortier, L., 2010. From polar night to midnight sun: photoperiod, seal predation, and the diel vertical migrations of polar cod (*Boreogadus saida*) under landfast ice in the Arctic Ocean. Polar Biology 33, 1505–1520, doi:10.1007/s00300-010-0840-x.

Berreville, O., Vézina, A., Thompson, K., Klein, B., 2008. Exploratory data analysis of the interactions among physics, food web structure, and function in two Arctic polynyas. Canadian Journal of Fisheries and Aquatic Sciences 65, 1036–1046. doi:10.1139/F08-016.

Brey, T., http://hdl.handle.net/10013/epic.15243, 2001. Population Dynamics in benthic invertebrates. A virtual handbook. Alfred Wegener Institute for Polar and Marine Research, Bremerhaven, Germany.

Brown, T.A., Belt, S.T., Philippe, B., Mundy, C.J., Massé, G., Poulin, M., Gosselin, M., 2011. Temporal and vertical variations of lipid biomarkers during a bottom ice diatom bloom in the Canadian Beaufort Sea: further evidence for the use of the IP_{25} biomarker as a proxy for spring Arctic sea ice. Polar Biology, doi:10.1007/s00300-010-0942-5.

Brugel, S., Nozais, C., Poulin, M., Tremblay, J.E., Miller, L.A., Simpson, K.G., Gratton, Y., Demers, S., 2009. Phytoplankton biomass and production in the southeastern Beaufort Sea in autumn 2002 and 2003. Marine Ecology Progress Series 377, 63–77. doi:10.3354/meps07808.

Buesseler, K.O., Antia, A.N., Chen, M., Fowler, S.W., Gardner, W.D., Gustafsson, O., Harada, K., Michaels, A.F., van der Loeff, M., Sarin, M., 2007. An assessment of the use of sediment traps for estimating upper ocean particle fluxes. Journal of Marine Research 65, 345–416.

Burdige, D.J., Homstead, J., 1994. Fluxes of dissolved organic carbon from Chesapeake Bay sediments. Geochimica et Cosmochimica Acta 58, 3407–3424, doi:10.1016/0016-7037(94)90095-7.

Calbet, A., 2008. The trophic roles of microzooplankton in marine systems. ICES Journal of Marine Science 65, 325–331. doi:10.1093/icesjms/fsn013.

Calbet, A., Saiz, E., Almeda, R., Movilla, J.I., Alcaraz, M., 2011. Low microzooplankton grazing rates in the Arctic Ocean during a Phaeocystis pouchetii bloom (Summer 2007): fact or artifact of the dilution technique? Journal of Plankton Research 33, 687–701. doi:10.1093/plankt/fbq142.

Campbell, R.G., Sherr, E.B., Ashjian, C.J., Plourde, S., Sherr, B.F., Hill, V., Stockwell, D.A., 2009. Mesozooplankton prey preference and grazing impact in the Western Arctic Ocean. Deep Sea Research Part II: Topical Studies in Oceanography 56, 1274–1289. doi:10.1016/j.dsr2.2008.10.027.

Carmack, E., McLaughlin, F., 2011. Towards recognition of physical and geochemical change in Subarctic and Arctic Seas. Progress in Oceanography 90, 90–104. doi:10.1016/j.pocean.2011.02.007.

Carmack, E., Wassmann, P., 2006. Food webs and physical–biological coupling on pan-Arctic shelves: unifying concepts and comprehensive perspectives. Progress in Oceanography 71, 446–477. doi:10.1016/j.pocean.2006.10.004.

Carmack, E.C., Macdonald, R.W., Jasper, S., 2004. Phytoplankton productivity on the Canadian Shelf of the Beaufort Sea. Marine Ecology Progress Series 277, 37–50. doi:10.3354/meps277037.

CIS, <http://ice-glaces.ec.gc.ca/content_contenu/anim/amundsen_animation.gif>, 2007. Amundsen Gulf Animation 1980–2007. Canadian Ice Service Archives.

Conlan, K.E., Kvitek, R.G., 2005. Recolonization of soft-sediment ice scours on an exposed Arctic coast. Marine Ecology Progress Series 286, 21–42. doi:10.3354/meps286021.

Conover, R.J., Huntley, M., 1991. Copepods in ice-covered seas – distribution, adaptations to seasonally limited food, metabolism, growth patterns and life cycle strategies in polar seas. Journal of Marine Systems 2, 1–41.

Conti, L., Scardi, M., 2010. Fisheries yield and primary productivity in large marine ecosystems. Marine Ecology Progress Series 410, 233–244. doi:10.3354/meps08630.

COSEWIC, <http://www.sararegistry.gc.ca/status/status_e.cfm>, 2009. COSEWIC Assessment and Update Status Report on the Bowhead Whale *Balaena mysticetus*, Bering–Chukchi–Beaufort Population and Eastern Canada-West Greenland Population, Canada. Committee on the Status of Endangered Wildlife in Canada, Ottawa.

Crabtree, R., 1995. Chemical composition and energy content of deep-sea demersal fishes from tropical and temperate regions of the western North Atlantic. Bulletin of Marine Science 56, 434–449.

Crease, J., 1988. The Acquisition, Calibration and Analysis of CTD Data. UNESCO Technical Papers in Marine Science No. 54. A Report of SCOR Working Group 51, Division of Marine Sciences, UNESCO, Paris, 105 pp.

Daly, K.L., 1997. Flux of particulate matter through copepods in the Northeast water polynya. Journal of Marine Systems 10, 319–342, doi:10.1016/S0924-7963(96)00062-0.

Dam, H., Peterson, W., 1988. The effect of temperature on the gut clearance rate constant of planktonic copepods. Journal of Experimental Marine Biology and Ecology 123, 1–14, doi:10.1016/0022-0981(88)90105-0.

Darnis, G., Barber, D.G., Fortier, L., 2008. Sea ice and the onshore–offshore gradient in pre-winter zooplankton assemblages in south-eastern Beaufort Sea. Journal of Marine Systems 74, 994–1011. doi:10.1016/j.jmarsys.2007.09.003.

Degerlund, M., Eilertsen, H., 2010. Main species characteristics of phytoplankton spring blooms in NE Atlantic and Arctic Waters (68–80°N). Estuaries and Coasts 33, 242–269. doi:10.1007/s12237-009-9167-7.

Deibel, D., 1998. Feeding and metabolism of Appendicularia. In: Bone, Q. (Ed.), The Biology of Pelagic Tunicates. Oxford University Press, New York, pp. 139–159.

del Giorgio, P., Cole, J., 2000. Bacterial energetics and growth efficiency. In: Kirchman, D.L. (Ed.), Microbial Ecology of the Oceans. Wiley-Liss, New York, pp. 289–325.

Dickson, D., Gilchrist, H., 2002. Status of marine birds of the southeastern Beaufort Sea. Arctic 55, 46–58.

Dmitrenko, I.A., Polyakov, I.V., Kirillov, S.A., Timokhov, L.A., Frolov, I.E., Sokolov, V.T., Simmons, H.L., Ivanov, V.V., Walsh, D., 2008. Toward a warmer Arctic Ocean: spreading of the early 21st century Atlantic Water warm anomaly along the Eurasian Basin margins. Journal of Geophysical Research: Oceans 113, C05023. doi:10.1029/2007jc004158.

Dugdale, R.C., Goering, J.J., 1967. Uptake of new and regenerated forms of nitrogen in primary productivity. Limnology and Oceanography 12, 196–206.

Dunton, K.H., Goodall, J.L., Schonberg, S.V., Grebmeier, J.M., Maidment, D.R., 2005. Multi-decadal synthesis of benthic–pelagic coupling in the western arctic: role of cross-shelf advective processes. Deep Sea Research Part II: Topical Studies in Oceanography 52, 3462–3477. doi:10.1016/j.dsr2.2005.09.007.

Dunton, K.H., Weingartner, T., Carmack, E.C., 2006. The nearshore western Beaufort Sea ecosystem: circulation and importance of terrestrial carbon in arctic coastal food webs. Progress in Oceanography 71, 362–378. doi:10.1016/j.pocean.2006.09.011.

Elliott, D., Harris, C., Tang, K., 2010. Dead in the water: the fate of copepod carcasses in the York River estuary, Virginia. Limnology and Oceanography 55, 1821–1834.

Estapa, M.L., Mayer, L.M., 2010. Photooxidation of particulate organic matter, carbon/oxygen stoichiometry, and related photoreactions. Marine Chemistry 122, 138–147, 10.1016/j.marchem.2010.06.003.

Falk-Petersen, S., Mayzaud, P., Kattner, G., Sargent, J.R., Fenchel, T., 2009. Lipids and life strategy of Arctic Calanus. Marine Biology Research 5, 18–39. doi:10.1080/17451000802512267.

Feder, H., Naidu, A., Jewett, S., Hameedi, J., Johnson, W., Whitledge, T., 1994. The northeastern Chukchi Sea: benthos–environmental interactions. Marine Ecology Progress Series 111, 171–190.

Forest, A., Sampei, M., Hattori, H., Makabe, R., Sasaki, H., Fukuchi, M., Wassmann, P., Fortier, L., 2007. Particulate organic carbon fluxes on the slope of the Mackenzie Shelf (Beaufort Sea): physical and biological forcing of shelf-basin exchanges. Journal of Marine Systems 68, 39–54. doi:10.1016/j.jmarsys.2006.10.008.

Forest, A., Sampei, M., Makabe, R., Sasaki, H., Barber, D., Gratton, Y., Wassmann, P., Fortier, L., 2008. The annual cycle of particulate organic carbon export in Franklin Bay (Canadian Arctic): environmental control and food web implications. Journal of Geophysical Research: Oceans 113, C03S05. doi:10.1029/2007JC004262.

Forest, A., Bélanger, S., Sampei, M., Sasaki, H., Lalande, C., Fortier, L., 2010. Three-year assessment of particulate organic carbon fluxes in Amundsen Gulf (Beaufort Sea): satellite observations and sediment trap measurements. Deep Sea Research Part I: Oceanographic Research Papers 57, 125–142. doi:10.1016/j.dsr.2009.10.002.

Forest, A., Galindo, V., Darnis, G., Lalande, C., Pineault, S., Tremblay, J.E., Fortier, L., 2011. Carbon biomass, elemental ratios (C:N) and stable isotopic composition ($\delta^{13}C$, $\delta^{15}N$) of dominant calanoid copepods during the winter-to-summer transition in the Amundsen Gulf (Arctic Ocean). Journal of Plankton Research 33, 161–178. doi:10.1093/plankt/fbq103.

Fortier, M., Fortier, L., Hattori, H., Saito, H., Legendre, L., 2001. Visual predators and the diel vertical migration of copepods under Arctic sea ice during the midnight sun. Journal of Plankton Research 23, 1263–1278. doi:10.1093/plankt/23.11.1263.

Frangoulis, C., Carlotti, F., Eisenhauer, L., Zervoudaki, S., 2010. Converting copepod vital rates into units appropriate for biogeochemical models. Progress in Oceanography 84, 43–51. doi:10.1016/j.pocean.2009.09.005.

Frey, K.E., McClelland, J.W., 2009. Impacts of permafrost degradation on arctic river biogeochemistry. Hydrological Processes 23, 169–182. doi:10.1002/hyp.7196.

Frost, B.W., 1974. *Calanus marshallae*, a new species of calanoid copepod closely allied to the sibling species *C. finmarchicus* and *C. glacialis*. Marine Biology 26, 77–99.

Fuhrman, J.A., Steele, J.A., Hewson, I., Schwalbach, M.S., Brown, M.V., Green, J.L., Brown, J.H., 2008. A latitudinal diversity gradient in planktonic marine bacteria. Proceedings of the National Academy of Science 105, 7774–7778. doi:10.1073/pnas.0803070105.

Galley, R.J., Key, E., Barber, D.G., Hwang, B.J., Ehn, J.K., 2008. Spatial and temporal variability of sea ice in the southern Beaufort Sea and Amundsen Gulf: 1980–2004. Journal of Geophysical Research: Oceans 113, C05S95. doi:10.1029/2007JC004553.

Gardner, W., 2000. Sediment trap sampling in surface waters. In: Hanson, R.B., Ducklow, H.W., Field, J.G. (Eds.), The Changing Ocean Carbon Cycle: A Midterm Synthesis of the Joint Global Ocean Flux Study. IGBP Book Series, vol. 5. Cambridge University Press, pp. 240–280.

Garneau, M., Gosselin, M., Klein, B., Tremblay, J., Fouilland, E., 2007. New and regenerated production during a late summer bloom in an Arctic polynya. Marine Ecology Progress Series 345, 13–26. doi:10.3354/meps06965.

Garneau, M.E., Roy, S., Pedrós-Alió, C., Lovejoy, C., Gratton, Y., Vincent, W.F., 2008. Seasonal dynamics of bacterial biomass and production in a coastal arctic ecosystem: Franklin Bay, western Canadian Arctic. Journal of Geophysical Research: Oceans 113, C07S91. doi:10.1029/2007JC004281.

Geoffroy, M., Robert, D., Darnis, G., Fortier, L., 2011. The aggregation of polar cod (*Boreogadus saida*) in the deep Atlantic layer of ice-covered Amundsen Gulf (Beaufort Sea) in winter. Polar Biology. doi:10.1007/s00300-011-1019-9.

George, J., Zeh, J., Suydam, R., Clark, C., 2004. Abundance and population trend (1978–2001) of western Arctic bowhead whales surveyed near Barrow, Alaska. Marine Mammal Science 20, 755–773, doi: 10.1111/j.1748-7692.2004.tb01191.

Gosselin, M., Levasseur, M., Wheeler, P.A., Horner, R.A., Booth, B.C., 1997. New measurements of phytoplankton and ice algal production in the Arctic Ocean. Deep Sea Research Part II: Topical Studies in Oceanography 44, 1623–1644, doi:10.1016/S0967-0645(97)00054-4.

Gradinger, R., Bluhm, B., Hopcroft, R., Gebruk, A., Kosobokova, K., Sirenko, B., Weslawski, J., 2010. Marine life in the Arctic. In: McIntyre, A. (Ed.), Life in the World's Oceans: Diversity, Distribution and Abundance. Wiley-Blackwell, Oxford, pp. 183–202.

Grami, B., Niquil, N., Sakka Hlaili, A., Gosselin, M., Hamel, D., Hadj Mabrouk, H., 2008. The plankton food web of the Bizerte Lagoon (South-western Mediterranean): II. Carbon steady-state modelling using inverse analysis. Estuarine, Coastal and Shelf Science 79, 101–113. doi:10.1016/j.ecss.2008.03.009.

Grasshoff, K., Ehrhardt, M., Kremling, K., 1999. Methods of Seawater Analysis, third ed. Wiley-VCH, Weinheim, New York, p. 600.

Grebmeier, J., Barry, J., 2007. Benthic processes in polynyas. In: Smith, W.O., Barber, D.G. (Eds.), Polynyas: Windows to the World. Elsevier, Amsterdam, pp. 363–390.

Gregor, D.J., Loeng, H., Barrie, L., 1998. The influence of physical and chemical processes on contaminant transport into and within the arctic. In: AMAP (Ed.), Assessment Report: Arctic Pollution Issues. Arctic Monitoring and Assessment Programme, Oslo, Norway, pp. 25–116 (Chapter 3).

Guéguen, C., Guo, L., Yamamoto-Kawai, M., Tanaka, N., 2007. Colored dissolved organic matter dynamics across the shelf-basin interface in the western Arctic Ocean. Journal of Geophysical Research: Oceans 112, C05038. doi:10.1029/2006jc003584.

Hattori, H., Saito, H., 1997. Diel changes in vertical distribution and feeding activity of copepods in ice-covered Resolute Passage, Canadian Arctic, in spring 1992. Journal of Marine Systems 11, 205–219, doi: 10.1016/S0924-7963(96)00039-5.

Hirst, A.G., Bunker, A.J., 2003. Growth of marine planktonic copepods: global rates and patterns in relation to chlorophyll *a*, temperature, and body weight. Limnology and Oceanography 48, 1988–2010.

Hoegh-Guldberg, O., Bruno, J.F., 2010. The impact of climate change on the world's marine ecosystems. Science 328, 1523–1528. doi:10.1126/science.1189930.
Hoekstra, P., Dehn, L., George, J., Solomon, K., Muir, D., O'Hara, T., 2002. Trophic ecology of bowhead whales (*Balaena mysticetus*) compared with that of other arctic marine biota as interpreted from carbon-, nitrogen-, and sulfur-isotope signatures. Canadian Journal of Zoology 80, 223–231. doi:10.1139/z01-229.
Holmes, R., 1970. The Secchi disk in turbid coastal waters. Limnology and Oceanography 15, 688–694.
Holmes, R., Aminot, A., Kerouel, R., Hooker, B.A., Peterson, J.B., 1999. A simple and precise method for measuring ammonium in marine and freshwater ecosystems. Canadian Journal of Fisheries and Aquatic Sciences 56, 1801–1808.
Hopcroft, R.R., Clarke, C., Nelson, R.J., Raskoff, K.A., 2005. Zooplankton communities of the Arctic's Canada Basin: the contribution by smaller taxa. Polar Biology 28, 198–206. doi:10.1007/s00300-004-0680-7.
Hoppema, M., Goeyens, L., Fahrbach, E., 2000. Intense nutrient removal in the remote area off Larsen Ice Shelf (Weddell Sea). Polar Biology 23, 85–94. doi:10.1007/s003000050012.
Hovelsrud, G.K., McKenna, M., Huntington, H.P., 2008. Marine mammal harvests and other interactions with humans. Ecological Applications 18, S135–S147. doi:10.1890/06-0843.1.
Huntley, M., Lopez, M., 1992. Temperature-dependent production of marine copepods: a global synthesis. American Naturalist 140, 201–242.
Iversen, M., Poulsen, L., 2007. Coprorhexy, coprophagy, and coprochaly in the copepods *Calanus helgolandicus, Pseudocalanus elongatus*, and *Oithona similis*. Marine Ecology Progress Series 350, 79–89, doi:10.3354/meps07095.
Jackson, J., Allen, S., Carmack, E., McLaughlin, F., 2010. Suspended particles in the Canada Basin from optical and bottle data, 2003–2008. Ocean Science 6, 799–813. doi:10.5194/os-6-799-2010.
Johnson, S.R., Ward, J.G., 1985. Observations of thick-billed murres (*Uria lomvia*) and other seabirds at Cape Parry, Amundsen Gulf, N. W. T. Arctic 38, 112–115.
Jones, B.M., Arp, C.D., Jorgenson, M.T., Hinkel, K.M., Schmutz, J.A., Flint, P.L., 2009. Increase in the rate and uniformity of coastline erosion in Arctic Alaska. Geophysical Research Letters 36, L03503. doi:10.1029/2008gl036205.
Juul-Pedersen, T., Michel, C., Gosselin, M., Seuthe, L., 2008. Seasonal changes in the sinking export of particulate material under first-year sea ice on the Mackenzie Shelf (western Canadian Arctic). Marine Ecology Progress Series 353, 13–25. doi:10.3354/meps07165.
Juul-Pedersen, T., Michel, C., Gosselin, M., 2010. Sinking export of particulate material from the euphotic zone in the eastern Beaufort Sea. Marine Ecology Progress Series 410, 55–70. doi:10.3354/meps08608.
Kaleschke, L., Lüpkes, C., Vihma, T., Haarpaintner, J., Bochert, A., Hartmann, J., Heygster, G., 2001. SSM/I sea ice remote sensing for mesoscale ocean–atmosphere interaction analysis. Canadian Journal of Remote Sensing 27, 526–537.
Karnovsky, N., Hunt, G., 2002. Estimation of carbon flux to dovekies (*Alle alle*) in the North Water. Deep Sea Research Part II: Topical Studies in Oceanography 49, 5117–5130, doi:10.1016/S0967-0645(02)00181-9.
Karnovsky, N., Ainley, D., Lee, P., 2007. The impact and importance of production in polynyas to top-trophic predators: three case histories. In: Smith, W.O., Barber, D.G. (Eds.), Polynyas: Windows to the World. Elsevier, Amsterdam, pp. 391–410.
Kellogg, C., Deming, J.W., 2009. Comparison of free-living, suspended particle, and aggregate-associated bacterial and archaeal communities in the Laptev Sea. Aquatic Microbial Ecology 57, 1–18. doi:10.3354/ame01317.
Kellogg, C., Carpenter, S., Renfro, A., Sallon, A., Michel, C., Cochran, J., Deming, J., 2011. Evidence for microbial attenuation of particle flux in the Amundsen Gulf and Beaufort Sea: elevated hydrolytic enzyme activity on sinking aggregates. Polar Biology. doi:10.1007/s00300-011-1015-0.
Kirchman, D.L., Hill, V., Cottrell, M.T., Gradinger, R., Malmstrom, R.R., Parker, A., 2009a. Standing stocks, production, and respiration of phytoplankton and heterotrophic bacteria in the western Arctic Ocean. Deep Sea Research Part II: Topical Studies in Oceanography 56, 1237–1248. doi:10.1016/j.dsr2.2008.10.018.
Kirchman, D.L., Morán, X.A.G., Ducklow, H., 2009b. Microbial growth in the polar oceans—role of temperature and potential impact of climate change. Nature Reviews Microbiology 7, 451–459. doi:10.1038/nrmicro2115.
Klein, B., LeBlanc, B., Mei, Z.-P., Beret, R., Michaud, J., Mundy, C.J., von Quillfeldt, C.H., Garneau, M.-È., Roy, S., Gratton, Y., Cochran, J.K., Bélanger, S., Larouche, P., Pakulski, J.D., Rivkin, R.B., Legendre, L., 2002. Phytoplankton biomass, production and potential export in the North Water. Deep Sea Research Part II: Topical Studies in Oceanography 49, 4983–5002, doi:10.1016/S0967-0645(02)00174-1.
Knap, A., Michaels, A., Close, A., Ducklow, H., Dickson, A., 1996. Protocols for the Joint Global Ocean Flux Study (JGOFS) Core Measurements. JGOFS Report, Nr. 19, pp. 155–162.
Kosobokova, K., Hirche, H.-J., 2009. Biomass of zooplankton in the eastern Arctic Ocean – a base line study. Progress in Oceanography 82, 265–280. doi:10.1016/j.pocean.2009.07.006.
Lanos, R., 2009. Circulation régionale, masses d'eau, cycles d'évolution et de transports entre la mer de Beaufort et le Golfe d'Amundsen (Ph.D Thesis, in French). Québec, Canada. Institut National de la Recherche Scientifique – Eau Terre Environnement, Université du Québec, 272 pp.
Lansard, B., Mucci, A., Miller, L.A., Macdonald, R.W., Gratton, Y., submitted for publication. Seasonal variability of water mass distribution in the southeastern Beaufort Sea determined by total alkalinity and $\delta^{18}O$. Journal of Geophysical Research: Oceans.
Lavoie, D., Denman, K.L., Macdonald, R.W., 2010. Effects of future climate change on primary productivity and export fluxes in the Beaufort Sea. Journal of Geophysical Research: Oceans 115, C04018. doi:10.1029/2009jc005493.
Lean, D., Burnison, B., 1979. An evaluation of errors in the delta^{14}C method of primary production measurement. Limnology and Oceanography 24, 917–928.
Lee, S.H., Whitledge, T.E., Kang, S.-H., 2008. Spring time production of bottom ice algae in the landfast sea ice zone at Barrow, Alaska. Journal of Experimental Marine Biology and Ecology 367, 204–212.
Legendre, L., Demers, S., Yentsch, C.M., Yentsch, C.S., 1983. The ^{14}C method: patterns of dark CO_2 fixation and DCMU correction to replace the dark bottle. Limnology and Oceanography 28, 996–1003.
Li, W.K.W., McLaughlin, F.A., Lovejoy, C., Carmack, E.C., 2009. Smallest algae thrive as the Arctic Ocean freshens. Science 326, 539. doi:10.1126/science.1179798.
Link, H., Archambault, P., Tamelander, T., Renaud, P.E., Piepenburg, D., 2011. Spring-to-summer changes and regional variability of benthic processes in relation to sea ice cover dynamics in the western Canadian Arctic. Polar Biology. doi:10.1007/s00300-011-1046-6.
Loseto, L.L., Stern, G.A., Deibel, D., Connelly, T.L., Prokopowicz, A., Lean, D.R.S., Fortier, L., Ferguson, S.H., 2008. Linking mercury exposure to habitat and feeding behaviour in Beaufort Sea beluga whales. Journal of Marine Systems 74, 1012–1024. doi:10.1016/j.jmarsys.2007.10.004.
Lovejoy, C., Vincent, W.F., Bonilla, S., Roy, S., Martineau, M.J., Terrado, R., Potvin, M., Massana, R., Pedrós-Alió, C., 2007. Distribution, phylogeny, and growth of cold adapted picoprasinophytes in Arctic Seas. Journal of Phycology 43, 78–89, doi:10.1111/j.1529-8817.2006.00310.x.
Magen, C., Chaillou, G., Crowe, S.A., Mucci, A., Sundby, B., Gao, A., Makabe, R., Sasaki, H., 2010. Origin and fate of particulate organic matter in the southern Beaufort Sea – Amundsen Gulf region, Canadian Arctic. Estuarine, Coastal and Shelf Science 86, 31–41. doi:10.1016/j.ecss.2009.09.009.
Markus, T., Stroeve, J.C., Miller, J., 2009. Recent changes in Arctic sea ice melt onset, freezeup, and melt season length. Journal of Geophysical Research: Oceans 114, C12024. doi:10.1029/2009jc005436.
Martin, J., Tremblay, J.E., Gagnon, J., Tremblay, G., Lapoussière, A., Jose, C., Poulin, M., Gosselin, M., Gratton, Y., Michel, C., 2010. Prevalence, structure and properties of subsurface chlorophyll maxima in Canadian Arctic waters. Marine Ecology Progress Series 42, 69–84. doi:10.3354/meps08666.
Maslanik, J., Stroeve, J.C., http://nsidc.org/data/nsidc-0081.html, 1999. Near-real-time DMSP SSM/I daily polar gridded sea ice concentrations (February–August 2008), National Snow and Ice Data Center, Boulder, Colorado, USA.
Menden-Deuer, S., Lessard, E.J., 2000. Carbon to volume relationships for dinoflagellates, diatoms, and other protist plankton. Limnology and Oceanography 45, 569–579.
Møller, E.F., Thor, P., Nielsen, T.G., 2003. Production of DOC by *Calanus finmarchicus*, *C. glacialis* and *C. hyperboreus* through sloppy feeding and leakage from fecal pellets. Marine Ecology Progress Series 262, 185–191. doi:10.3354/meps262185.
Moore, S.E., Huntington, H.P., 2008. Arctic marine mammals and climate change: impacts and resilience. Ecological Applications 18, 157–165.
Morata, N., Renaud, P., Brugel, S., Hobson, K., Johnson, B., 2008. Spatial and seasonal variations in the pelagic–benthic coupling of the southeastern Beaufort Sea revealed by sedimentary biomarkers. Marine Ecology Progress Series 371, 47–63. doi:10.3354/meps07677.
Mundy, C.J., Gosselin, M., Ehn, J., Gratton, Y., Rossnagel, A., Barber, D.G., Martin, J., Tremblay, J.-É., Palmer, M., Arrigo, K.R., Darnis, G., Fortier, L., Else, B., Papakyriakou, T., 2009. Contribution of under-ice primary production to an ice-edge upwelling phytoplankton bloom in the Canadian Beaufort Sea. Geophysical Research Letters 36, L17601. doi:10.1029/2009gl038837.
Mundy, C., Gosselin, M., Starr, M., Michel, C., 2010. Riverine export and the effects of circulation on dissolved organic carbon in the Hudson Bay system, Canada. Limnology and Oceanography 55, 315–323. doi:10.4319/lo.2010.55.1.0315.
Mustapha, S., Larouche, P., 2008. Evaluation of MODIS and SeaWiFS ocean color algorithms in the Canadian arctic waters: the Cape Bathurst polynya. In: Geoscience and Remote Sensing Symposium, Boston, MA, 7–11 July 2008. doi:10.1109/IGARSS.2008.4779872.
Nelson, N., Siegel, D., Carlson, C., Swan, C., 2010. Tracing global biogeochemical cycles and meridional overturning circulation using chromophoric dissolved organic matter. Geophysical Research Letters 37, L03610. doi:10.1029/2009GL042325.
Nguyen, D., Maranger, R., 2010. Microbial Community Respiration in Amundsen Gulf of the Arctic Ocean. In: Joint AGU-ASLO 2010 Ocean Sciences Meeting, Abstract BO15E-4.
Niquil, N., Bartoli, G., Urabe, J., Jackson, J., Legendre, L., Dupuy, C., 2006. Carbon steady-state model of the planktonic food web of Lake Biwa, Japan. Freshwater Biology 51, 1570–1585, doi:10.1111/j.1365-2427.2006.01595.x.
Nozais, C., Gosselin, M., Michel, C., Tita, G., 2001. Abundance, biomass, composition and grazing impact of the sea-ice meiofauna in the North Water, northern Baffin Bay. Marine Ecology Progress Series 217, 235–250. doi:10.3354/meps217235.
NSIDC, http://nsidc.org/arcticseaicenews/index.html, 2011. National Snow and Ice Data Center. Arctic Sea Ice News and Analysis (Updated Frequently).
O'Brien, M.C., Macdonald, R.W., Melling, H., Iseki, K., 2006. Particle fluxes and geochemistry on the Canadian Beaufort Shelf: implications for sediment transport and deposition. Continental Shelf Research 26, 41–81. doi:10.1016/j.csr.2005.09.007.
Olli, K., Wassmann, P., Reigstad, M., Ratkova, T.N., Arashkevich, E., Pasternak, A., Matrai, P.A., Knulst, J., Tranvik, L., Klais, R., Jacobsen, A., 2007. The fate of production in the central Arctic Ocean – top-down regulation by zooplankton expatriates? Progress in Oceanography 72, 84–113. doi:10.1016/j.pocean.2006.08.002.

Ortega-Retuerta, E., Frazer, T., Duarte, C., Ruiz-Halpern, S., Tovar-Sánchez, A., Arrieta, J., Rechea, I., 2009. Biogeneration of chromophoric dissolved organic matter by bacteria and krill in the Southern Ocean. Limnology and Oceanography 54, 1941–1950. doi:10.4319/lo.2009.54.6.1941.

Parsons, T., Maita, Y., Lalli, C., 1984. A Manual of Chemical and Biological Methods for Seawater Analysis. Pergamon Press, Toronto, p. 173.

Perovich, D., Richter Menge, J., Jones, K., Light, B., 2008. Sunlight, water, and ice: extreme Arctic sea ice melt during the summer of 2007. Geophysical Research Letters 35, L11501. doi:10.1029/2008GL034007.

Piepenburg, D., 2005. Recent research on Arctic benthos: common notions need to be revised. Polar Biology 28, 733–755. doi:10.1007/s00300-005-0013-5.

Polyakov, I.V., Alexeev, V.A., Ashik, I.M., Bacon, S., Beszczynska-Möller, A., Carmack, E.C., Dmitrenko, I.A., Fortier, L., Gascard, J.C., Hansen, E., Hölemann, J., Ivanov, V.V., Kikuchi, T., Kirillov, S., Lenn, Y.-D., McLaughlin, F.A., Piechura, J., Repina, I., Timokhov, L.A., Walczowski, W., Woodgate, R., 2011. Fate of early-2000's Arctic warm water pulse. Bulletin of the American Meteorological Society. doi:10.1175/2010BAMS2921.1.

Popova, E.E., Yool, A., Coward, A.C., Aksenov, Y.K., Alderson, S.G., de Cuevas, B.A., Anderson, T.R., 2010. Control of primary production in the Arctic by nutrients and light: insights from a high resolution ocean general circulation model. Biogeosciences 7, 3569–3591. doi:10.5194/bg-7-3569-2010.

Primeau, F., 2006. On the variability of the exponent in the power law depth dependence of POC flux estimated from sediment traps. Deep Sea Research Part I: Oceanographic Research Papers 53, 1335–1343. doi:10.1016/j.dsr.2006.06.003.

Proshutinsky, A., Krishfield, R., Timmermans, M., Toole, J., Carmack, E., McLaughlin, F., Williams, W., Zimmermann, S., Itoh, M., Shimada, K., 2009. Beaufort Gyre freshwater reservoir: state and variability from observations. Journal of Geophysical Research: Oceans 114, C00A10. doi:10.1029/2008JC005104.

Rachold, V., Eicken, H., Gordeev, V.V., Grigoriev, M.N., Hubberten, H.W., Lisitzin, A.P., Shevchenko, V.P., Schirrmeister, L., 2004. Modern terrigenous organic carbon input to the Arctic Ocean. In: Stein, R., MacDonald, R.W. (Eds.), The Organic Carbon Cycle in the Arctic Ocean. Springer, New-York, pp. 33–54.

Renaud, P.E., Morata, N., Ambrose Jr., W.G., Bowie, J.J., Chiuchiolo, A., 2007. Carbon cycling by seafloor communities on the eastern Beaufort Sea shelf. Journal of Experimental Marine Biology and Ecology 349, 248–260. doi:10.1016/j.jembe.2007.05.021.

Renaud, P.E., Morata, N., Carroll, M.L., Denisenko, S.G., Reigstad, M., 2008. Pelagic–benthic coupling in the western Barents Sea: processes and time scales. Deep Sea Research Part II: Topical Studies in Oceanography 55, 2372–2380. doi:10.1016/j.dsr2.2008.05.017.

Retamal, L., Vincent, W., Martineau, C., Osburn, C., 2007. Comparison of the optical properties of dissolved organic matter in two river-influenced coastal regions of the Canadian Arctic. Estuarine, Coastal and Shelf Science 72, 261–272. doi:10.1016/j.ecss.2006.10.022.

Richardson, T.L., Jackson, G.A., Ducklow, H.W., Roman, M.R., 2006. Spatial and seasonal patterns of carbon cycling through planktonic food webs of the Arabian Sea determined by inverse analysis. Deep Sea Research Part II: Topical Studies in Oceanography 53, 555–575. doi:10.1016/j.dsr2.2006.01.015.

Rivkin, R.B., Legendre, L., Deibel, D., Tremblay, J.-E., Klein, B., Crocker, K., Roy, S., Silverberg, N., Lovejoy, C., Mesplé, F., Romero, N., Anderson, M.R., Matthews, P., Savenkoff, C., Vézina, A., Therriault, J.-C., Wesson, J., Bérubé, C., Ingram, R.G., 1996. Vertical flux of biogenic carbon in the ocean: is there food web control? Science 272, 1163–1166. doi:10.1126/science.272.5265.1163.

Rokkan Iversen, K., Seuthe, L., 2011. Seasonal microbial processes in a high-latitude fjord (Kongsfjorden, Svalbard): I. Heterotrophic bacteria, picoplankton and nanoflagellates. Polar Biology 34, 731–749. doi:10.1007/s00300-010-0929-2.

Rysgaard, S., Glud, R.N., 2007. Carbon Cycling in Arctic Marine Ecosystems: Case Study Young Sound. Meddelelser om Grønland, Bioscience, Copenhagen.

Rysgaard, S., Nielsen, T.G., 2006. Carbon cycling in a high-arctic marine ecosystem-Young Sound, NE Greenland. Progress in Oceanography 71, 426–445. doi:10.1016/j.pocean.2006.09.004.

Ryther, J., 1969. Photosynthesis and fish production in the sea. Science 166, 72–76.

Sakshaug, E., 2004. Primary and secondary production in the Arctic seas. In: Stein, R., MacDonald, R.W. (Eds.), The Organic Carbon Cycle in the Arctic Ocean. Springer-Verlag, New-York, pp. 57–81.

Sallon, A., Michel, C., Gosselin, M., in press. Summertime primary production and carbon export in the southeastern Beaufort Sea during the low ice year of 2008. Polar Biology.

Sampei, M., Sasaki, H., Hattori, H., Fukuchi, M., Hargrave, B.T., 2004. Fate of sinking particles, especially fecal pellets, within the epipelagic zone in the North Water (NOW) polynya of northern Baffin Bay. Marine Ecology Progress Series 278, 17–25.

Sampei, M., Forest, A., Sasaki, H., Hattori, H., Makabe, R., Fukuchi, M., Fortier, L., 2009a. Attenuation of the vertical flux of copepod fecal pellets under Arctic sea ice: evidence for an active detrital food web in winter. Polar Biology 32, 225–232. doi:10.1007/s00300-008-0523-.

Sampei, M., Sasaki, H., Hattori, H., Forest, A., Fortier, L., 2009b. Significant contribution of passively sinking copepods to downward export flux in Arctic waters. Limnology and Oceanography 54, 1894–1900. doi:10.4319/lo.2009.54.6.1894.

Sampei, M., Sasaki, H., Makabe, R., Forest, A., Hattori, H., Tremblay, J.-É., Gratton, Y., Fukuchi, M., Fortier, L., 2011. Production and retention of biogenic matter in the southeast Beaufort Sea during 2003–2004: insights from annual vertical particle fluxes of organic carbon and biogenic silica. Polar Biology 34, 501–511. doi:10.1007/s00300-010-0904-.

Sejr, M.K., Nielsen, T.G., Rysgaard, S., Risgaard-Petersen, N., Sturluson, M., Blicher, M.E., 2007. Fate of pelagic organic carbon and importance of pelagic–benthic coupling in a shallow cove in Disko Bay, West Greenland. Marine Ecology Progress Series 341, 75–88. doi:10.3354/meps341075.

Seuthe, L., Darnis, G., Riser, C.W., Wassmann, P., Fortier, L., 2007. Winter–spring feeding and metabolism of Arctic copepods: insights from faecal pellet production and respiration measurements in the southeastern Beaufort Sea. Polar Biology 30, 427–436. doi:10.1007/s00300-006-0199-1.

Seuthe, L., Rokkan Iversen, K., Narcy, F., 2011. Microbial processes in a high-latitude fjord (Kongsfjorden, Svalbard): II. Ciliates and dinoflagellates. Polar Biology 34, 751–766. doi:10.1007/s00300-010-0930-9.

Shadwick, E.H., Thomas, H., Chierici, M., Else, B., Fransson, A., Michel, C., Miller, L.A., Mucci, A., Niemi, A., Papakyriakou, T., Tremblay, J.-É., 2011. Seasonal variability of the inorganic carbon system in the Amundsen Gulf region of the southeastern Beaufort Sea. Limnology and Oceanography 56, 303–322. doi:10.4319/lo.2011.56.1.0303.

Sherr, E., Sherr, B., Hartz, A., 2009. Microzooplankton grazing impact in the Western Arctic Ocean. Deep Sea Research Part II: Topical Studies in Oceanography 56, 1264–1273. doi:10.1016/j.dsr2.2008.10.036.

Shimada, K., Kamoshida, T., Itoh, M., Nishino, S., Carmack, E., McLaughlin, F., Zimmermann, S., Proshutinsky, A., 2006. Pacific Ocean inflow: influence on catastrophic reduction of sea ice cover in the Arctic Ocean. Geophysical Research Letters 33, L08605. doi:10.1029/2005gl025624.

Simpson, K., Tremblay, J.E., Price, N.M., 2007. Nutrient dynamics in the Amundsen Gulf and Cape Bathurst Polynya: 1. New production in spring inferred from nutrient draw-down. In: Simpson, K. (Ed.), Nutrient Dynamics and Nitrogen-based Production in the Western Canadian Arctic Ocean, Master Degree Thesis, Department of Biology, McGill University, Montreal, pp. 52–82.

Simpson, K., Tremblay, J.-É., Gratton, Y., Price, N.M., 2008. An annual study of inorganic and organic nitrogen and phosphorus, and silicic acid, in the southeastern Beaufort Sea. Journal of Geophysical Research: Oceans 113, C07016. doi:10.1029/2007JC004462.

Slagstad, D., Ellingsen, I., Wassmann, P., 2011. Evaluating primary and secondary production in a future Arctic Ocean void of summer sea ice: an experimental simulation approach. Progress in Oceanography 90, 117–131. doi:10.1016/j.pocean.2011.02.009.

Smith, D., Azam, F., 1992. A simple, economical method for measuring bacterial protein synthesis rates in seawater using super ^{3}H-leucine. Marine Microbial Food Webs 6, 107–114.

Soetaert, K., van Oevelen, D., 2009. Modeling food web interactions in deep-sea ecosystems. Oceanography 22, 128–143.

Søreide, J.E., Leu, E., Berge, J., Graeve, M., Falk-Petersen, S., 2010. Timing of blooms, algal food quality and *Calanus glacialis* reproduction and growth in a changing Arctic. Global Change Biology 16, 3154–3163, doi:10.1111/j.1365-2486.2010.02175.x.

Stedmon, C.A., Amon, R.M.W., Rinehart, A.J., Walker, S.A., 2011. The supply and characteristics of colored dissolved organic matter (CDOM) in the Arctic Ocean: Pan Arctic trends and differences. Marine Chemistry. doi:10.1016/j.marchem.2010.1012.1007.

Steele, M., Ermold, W., Zhang, J., 2008. Arctic Ocean surface warming trends over the past 100 years. Geophysical Research Letters 35, L02614. doi:10.1029/2007gl031651.

Steinacher, M., Joos, F., Frölicher, T.L., Plattner, G.K., Doney, S.C., 2009. Imminent ocean acidification in the Arctic projected with the NCAR global coupled carbon cycle-climate model. Biogeosciences 6, 515–533. doi:10.5194/bg-6-515-2009.

Steinberg, D., Van Mooy, B., Buesseler, K., Boyd, P., Kobari, T., Karl, D., 2008. Bacterial vs. zooplankton control of sinking particle flux in the ocean's twilight zone. Limnology and Oceanography 53, 1327–1338. doi:10.4319/lo.2008.53.4.1327.

Stirling, I., 1997. The importance of polynyas, ice edges, and leads to marine mammals and birds. Journal of Marine Systems 10, 9–21, doi:10.1016/S0924-7963(96)00054-1.

Straile, D., 1997. Gross growth efficiencies of protozoan and metazoan zooplankton and their dependence on food concentration, predator–prey weight ratio, and taxonomic group. Limnology and Oceanography 42, 1375–1385.

Tamelander, T., Reigstad, M., Hop, H., Carroll, M.L., Wassmann, P., 2008. Pelagic and sympagic contribution of organic matter to zooplankton and vertical export in the Barents Sea marginal ice zone. Deep Sea Research Part II: Topical Studies in Oceanography 55, 2330–2339. doi:10.1016/j.dsr2.2008.05.019.

Thomas, H., Friederike Prowe, A.E., van Heuven, S., Bozec, Y., de Baar, H.J.W., Schiettecatte, L.-S., Suykens, K., Kone, M., Borges, A.V., Lima, I.D., Doney, S.C., 2007. Rapid decline of the CO_2 buffering capacity in the North Sea and implications for the North Atlantic Ocean. Global Biogeochemical Cycles 21, GB4001. doi:10.1029/2006gb002825.

Thomas, H., E. H. Shadwick, F. Dehairs, B. Lansard, A. Mucci, J. Navez, Y. Gratton, F. A. E. Prowe, M. Chierici, A. Fransson, T. Papakyriakou, E. Sternberg, L. A. Miller, J.-E. Tremblay, and C. Monnin, 2011, Barium and Carbon fluxes in the Canadian Arctic Archipelago, Journal of Geophysical Research C (Oceans), in press, doi:10.1029/2011JC007120.

Thomsen, L., 1999. Processes in the benthic boundary layer at continental margins and their implication for the benthic carbon cycle. Journal of Sea Research 41, 73–86, doi:10.1016/S1385-1101(98)00039-2.

Titelman, J., Riemann, L., Holmfeldt, K., Nilsen, T., 2008. Copepod feeding stimulates bacterioplankton activities in a low phosphorus system. Aquatic Biology 2, 131–141. doi:10.3354/ab00042.

Tremblay, G., Belzile, C., Gosselin, M., Poulin, M., Roy, S., Tremblay, J.É., 2009. Late summer phytoplankton distribution along a 3500 km transect in Canadian

Arctic waters: strong numerical dominance by picoeukaryotes. Aquatic Microbial Ecology 54, 55–70.
Tremblay, J.-É., Gagnon, J., 2009. The effects of irradiance and nutrient supply on the productivity of Arctic waters: a perspective on climate change. In: Nihoul, J.C.J., Kostianoy, A.G. (Eds.), Influence of Climate Change on the Changing Arctic and Sub-Arctic Conditions. Proceedings of the NATO Advanced Research Workshop, Liège, Belgium, 8–10 May 2008. Springer Verlag, Dordrecht, The Netherlands, pp. 73–94.
Tremblay, J.-É., Hattori, H., Michel, C., Ringuette, M., Mei, Z.-P., Lovejoy, C., Fortier, L., Hobson, K.A., Amiel, D., Cochran, K., 2006a. Trophic structure and pathways of biogenic carbon flow in the eastern North Water Polynya. Progress in Oceanography 71, 402–425. doi:10.1016/j.pocean.2006.10.006.
Tremblay, J.-É., Michel, C., Hobson, K.A., Gosselin, M., Price, N.M., 2006b. Bloom dynamics in early opening waters of the Arctic Ocean. Limnology and Oceanography 51, 900–912.
Tremblay, J.-É., Simpson, K., Martin, J., Miller, L.A., Gratton, Y., Price, N.M., 2008. Vertical stability and the annual dynamics of nutrients and chlorophyll fluorescence in the coastal, southeast Beaufort Sea. Journal of Geophysical Research: Oceans 113, C07S90. doi:10.1029/2007JC004547.
Tremblay, J.-., S. Blanger, D. G. Barber, M. Asplin, J. Martin, G. Darnis, L. Fortier, Y. Gratton, H. Link, P. Archambault, A. Sallon, C. Michel, W. J. Williams, B. Philippe, and M. Gosselin, 2011, Geophysical Research Letters., 38, L18604, doi:10.1029/2011GL048825.
Vaqué, D., Guadayol, Ò., Peters, F., Felipe, J., Angel-Ripoll, L., Terrado, R., Lovejoy, C., Pedrós-Alió, C., 2008. Seasonal changes in planktonic bacterivory rates under the ice-covered coastal Arctic Ocean. Limnology and Oceanography 53, 2427–2438. doi:10.4319/lo.2008.53.6.2427.
Vaquer-Sunyer, R., Duarte, C., Santiago, R., Wassmann, P., Reigstad, M., 2010. Experimental evaluation of planktonic respiration response to warming in the European Arctic Sector. Polar Biology 33, 1661–1671. doi:10.1007/s00300-010-0788-.
Vézina, A., Platt, T., 1988. Food web dynamics in the ocean. 1. Best-estimates of flow networks using inverse methods. Marine Ecology Progress Series 42, 269–287.
Wang, M., Overland, J.E., 2009. A sea ice free summer Arctic within 30 years? Geophysical Research Letters 36, L07502. doi:10.1029/2009GL037820.
Wassmann, P., 1998. Retention versus export food chains: processes controlling sinking loss from marine pelagic systems. Hydrobiologia 363, 29–57. doi:10.1023/A:1003113403096.
Wassmann, P., 2006. Structure and function of contemporary food webs on arctic shelves: a pan-arctic comparison. Progress in Oceanography 71, 123–128. doi:10.1016/j.pocean.2006.09.008.
Wassmann, P., 2011. Arctic marine ecosystems in an era of rapid climate change. Progress in Oceanography 90, 1–17. doi:10.1016/j.pocean.2011.02.002.
Wassmann, P., Reigstad, M., Haug, T., Rudels, B., Carroll, M., Hop, H., Gabrielsen, G., Falk-Petersen, S., Denisenko, S., Arashkevich, E., 2006. Food webs and carbon flux in the Barents Sea. Progress in Oceanography 71, 232–287. doi:10.1016/j.pocean.2006.10.003.
Wassmann, P., Duarte, C.M., Agusti, S., Sejr, M.K., 2011. Footprints of climate change in the Arctic marine ecosystem. Global Change Biology 17, 1235–1249, doi:10.1111/j.1365-2486.2010.02311.x.
Wegner, C., Frey, K., Forest, A., Forwick, M., Mathis, J.T., Michel, C., Nikolopoulos, A., O'Regan, M., Peeken, I., Reigstad, M., <http://aosb.arcticportal.org/art.html>, 2010. Arctic in Rapid Transition (ART) Science Plan. Arctic Ocean Sciences Board/International Arctic Science Committee (AOSB/IASC), 34 pp.
Welch, H., Bergmann, M., Siferd, T., Martin, K., Curtis, M., Crawford, R., Conover, R., Hop, H., 1992. Energy flow through the marine ecosystem of the Lancaster Sound region, Arctic Canada. Arctic 45, 343–357.
Wexels Riser, C., Reigstad, M., Wassmann, P., Arashkevich, E., Falk-Petersen, S., 2007. Export or retention? Copepod abundance, faecal pellet production and vertical flux in the marginal ice zone through snap shots from the northern Barents Sea. Polar Biology 30, 719–730. doi:10.1007/s00300-006-0229-.
Wexels Riser, C., Wassmann, P., Reigstad, M., Seuthe, L., 2008. Vertical flux regulation by zooplankton in the northern Barents Sea during Arctic spring. Deep Sea Research Part II: Topical Studies in Oceanography 55, 2320–2329. doi:10.1016/j.dsr2.2008.05.006.
White, D., Hinzman, L., Alessa, L., Cassano, J., Chambers, M., Falkner, K., Francis, J., Gutowski Jr., W.J., Holland, M., Holmes, R.M., Huntington, H., Kane, D., Kliskey, A., Lee, C., McClelland, J., Peterson, B., Rupp, T.S., Straneo, F., Steele, M., Woodgate, R., Yang, D., Yoshikawa, K., Zhang, T., 2007. The arctic freshwater system: changes and impacts. Journal of Geophysical Research: Biogeosciences 112, G04S54. doi:10.1029/2006jg000353.
Whitehead, R., de Mora, S., Demers, S., Gosselin, M., Monfort, P., Mostajir, B., 2000. Interactions of ultraviolet-B radiation, mixing, and biological activity on photobleaching of natural chromophoric dissolved organic matter: a mesocosm study. Limnology and Oceanography 45, 278–291. doi:10.4319/lo.2000.45.2.0278.
Wilhelm, S., Suttle, C., 1999. Viruses and nutrient cycles in the sea. Bioscience 49, 781–788. doi:10.1525/bisi.1999.49.10.781.
Williams, W.J., Carmack, E.C., 2008. Combined effect of wind-forcing and isobath divergence on upwelling at Cape Bathurst, Beaufort Sea. Journal of Marine Research 66, 645–663. doi:10.1357/002224008787536808.
Wu, Y., Ting, M., Seager, R., Huang, H.-P., Cane, M., 2010. Changes in storm tracks and energy transports in a warmer climate simulated by the GFDL CM2.1 model. Climate Dynamics. doi:10.1007/s00382-00010-00776-00384, doi:10.1007/s00382-010-0776-4.
Yamamoto-Kawai, M., McLaughlin, F.A., Carmack, E.C., Nishino, S., Shimada, K., 2008. Freshwater budget of the Canada Basin, Arctic Ocean, from salinity, $\delta^{18}O$, and nutrients. Journal of Geophysical Research: Oceans 113, C01007. doi:10.1029/2006jc003858.
Zhang, J., Spitz, Y.H., Steele, M., Ashjian, C., Campbell, R., Berline, L., Matrai, P., 2010. Modeling the impact of declining sea ice on the Arctic marine planktonic ecosystem. Journal of Geophysical Research: Oceans 115, C10015. doi:10.1029/2009JC005387.